IMPACT BEHAVIOR OF THE ACTIVE ZONE WITHIN A FROZEN SOIL PROFILE

STUDY DAAL03 - 90 - G - 0196

FINAL REPORT
FOR
THE ARMY RESEARCH OFFICE

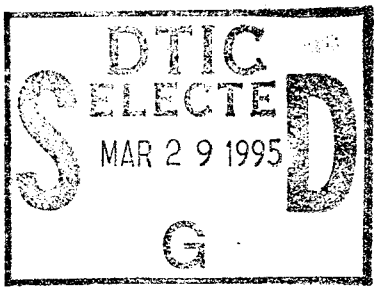

FEBRUARY 1995

CENTER FOR GEOTECHNICAL & HIGHWAY MATERIALS RESEARCH
THE UNIVERSITY OF TEXAS AT EL PASO
EL PASO, TEXAS 79968
(915)747-5464

REPORT DOCUMENTATION PAGE

1a. REPORT SECURITY CLASSIFICATION: Unclassified	1b. RESTRICTIVE MARKINGS
2a. SECURITY CLASSIFICATION AUTHORITY	3. DISTRIBUTION / AVAILABILITY OF REPORT: Approved for public release; distribution unlimited.
2b. DECLASSIFICATION / DOWNGRADING SCHEDULE	
4. PERFORMING ORGANIZATION REPORT NUMBER(S)	5. MONITORING ORGANIZATION REPORT NUMBER(S): ARO 28201.1-GS-SAH
6a. NAME OF PERFORMING ORGANIZATION: University of Texas at El Paso; 6b. OFFICE SYMBOL (If applicable)	7a. NAME OF MONITORING ORGANIZATION: U. S. Army Research Office
6c. ADDRESS (City, State, and ZIP Code): 500 W. University Avenue, El Paso, Tx 79968-0516	7b. ADDRESS (City, State, and ZIP Code): P. O. Box 12211, Research Triangle Park, NC 27709-2211
8a. NAME OF FUNDING / SPONSORING ORGANIZATION: U. S. Army Research Office; 8b. OFFICE SYMBOL (If applicable)	9. PROCUREMENT INSTRUMENT IDENTIFICATION NUMBER: DAAL03-90-G-0196
8c. ADDRESS (City, State, and ZIP Code): P. O. Box 12211, Research Triangle Park, NC 27709-2211	10. SOURCE OF FUNDING NUMBERS: PROGRAM ELEMENT NO. / PROJECT NO. / TASK NO. / WORK UNIT ACCESSION NO.

11. TITLE (Include Security Classification)

Impact Behavior of the Active Zone within a Frozen Soil Profile

12. PERSONAL AUTHOR(S)

Drs. Miguel Picornell and Soheil Nazarian

13a. TYPE OF REPORT	13b. TIME COVERED	14. DATE OF REPORT (Year, Month, Day)	15. PAGE COUNT
Final	FROM 9/90 TO 8/94	1995, February, 28	144

16. SUPPLEMENTARY NOTATION

The view, opinions and/or findings contained in this report are those of the author(s) and should not be construed as an official Department of the Army position, policy, or decision, unless so designated by other documentation.

17. COSATI CODES		
FIELD	GROUP	SUB-GROUP

18. SUBJECT TERMS (Continue on reverse if necessary and identify by block number)

Pavements, Freeze/Thaw, Tomography, Backcalculation of Layer Moduli

19. ABSTRACT (Continue on reverse if necessary and identify by block number)

The report describes a lab experiment with a pavement profile subject to a freeze/thaw cycle. The 5 x 5 x 5 ft lab specimen was instrumented with thermocouples, resistivity sensors, and 48 embedded geophones. The records of these sensors were used to delineate the progress of a freezing front through the soil profile and to implement a tomographic survey.

At selected intervals, a 550-lb impulse, lasting 15 milliseconds, was imparted on a circular plate placed on the surficial asphalt layer, and the records at all geophone locations were recorded. The surface deflection bowl was used to backcalculate the moduli of all pavement layers present using a computer code: WESDEF. Then, the two sets of moduli from WESDEF and those found from the tomographic survey were used to

20. DISTRIBUTION / AVAILABILITY OF ABSTRACT: ☐ UNCLASSIFIED/UNLIMITED ☐ SAME AS RPT. ☐ DTIC USERS	21. ABSTRACT SECURITY CLASSIFICATION: Unclassified
22a. NAME OF RESPONSIBLE INDIVIDUAL	22b. TELEPHONE (Include Area Code) / 22c. OFFICE SYMBOL

predict the deflections at all geophone locations. The report describes the comparison of the measured with the predicted deflections to evaluate the capabilities of the backcalculation procedure in the presence of frozen and thawed soil layers.

1. Foreword

The loads imposed on soils and pavements by land-transport vehicles are known to be dynamic in nature; that is, they are larger than the static loads involved. In areas experiencing seasonal frost, subsurface soils can exist in three distinct states: frozen, thawed and mostly liquid, and intermediate, having characteristics of both frozen and semi-thawed soil. The response of such a system to dynamic loads is quite complicated because of extreme differences in rigidity among the soil layers.

This research report addresses the interaction of three soil layers in determining the response of the soil profile to dynamic loads. This was accomplished by artificially freezing soil in the lab with an array of embedded sensors to establish soil conditions and record the response. Specific measurements included temperature and resistivity profiles. The extent of the three soil zones was assessed from temperature, resistivity, and tomography based on strategically placed geophones. Vertical and horizontal displacements at several depths were determined from specially calibrated and located geophones.

A soil susceptible to freeze-thaw was compacted inside an insulated circular tank. At ten stages of a freezing and thawing cycle, impact tests were performed. The dynamic load was imparted on the soil surface with a pulse of a servo-controlled hydraulic actuator. The measurements at each stage were used to evaluate the capabilities of existing multi-layered computer models to predict the response of the soil profile.

Table of Contents

Report Documentation Page i

1. Foreword 1

2. Table of Contents 2

3. List of Figures 3

4. Body of Report 4
   - 4A. Statement of Problem Studied 4
   - 4B. Summary of the Most Important Results 11
   - 4C. List of All Publications 17
   - 4D. List of Participating Scientific Personnel 18

5. Bibliography 19

6. Appendices
   - Appendix A - Thesis by Jeffrey Lynn Williams 21
     - Table of Contents 22
     - List of Figures 24
   - Appendix B - Soil Resistivity Profiles on the Test Dates within the Subgrade Soils 75
   - Appendix C - Soil Temperature Profiles on the Test Dates within the Subgrade Soils 84
   - Appendix D - Contour Maps of Vertical Deflections Measured 93
   - Appendix E - Comparison of Measured and Predicted Deflections 109
   - Appendix F - Copies of Existing/Proposed Publications 140

3. List of Figures

1. Variation of Moduli of the Different Layers Over the Freeze/Thaw Cycle 12

2. Percentage of Mismatch in the Fitting of the Bowl of Surface Deflections 14

3. Percentage of Mismatch in the Fitting of the Deflections at all Geophone Positions 15

4. BODY OF REPORT

4.A. Statement of Problem Studied

The dynamic response of a frozen soil profile is affected by a number of factors. Among these are temperature, the frequency and duration of a dynamic load's impact, and the state of stress and strain (Vinson, 1978).

A frozen soil profile is a multi-layered system consisting of three main soil zones, one of which is made up of the frozen soil itself. In this zone, the stiffness of the material is greatly influenced by temperature but is nearly independent of the confining pressure, as was shown by Vinson *et al* (1986).

The second soil zone represents a transition from the upper frozen soil to the thawed soil underneath. Its water is only partially frozen. The water that moves by capillarity from the water table freezes and forms ice lenses that are reflected on a soil surface heave.

The soil of the third zone is thawed and decreases in moisture content with depth. In layers two and three, the confining pressures have a definite influence on soil behavior. However, the soil of these two zones sometimes becomes saturated with an excess of moisture. Because the behavior of such soil closely resembles that of a liquid, its resilient modulus is ill defined (Chamberlain *et al*, 1989).

A number of analytical models have been proposed to represent the behavior of multi-layered systems under dynamic loads. However, most of these suffer from limitations (White, 1989). Thus, there has been a recent move to use pavement designs which are more mechanistic in nature: ones that require a lot more information than has traditionally been gathered (Berg, 1989). Specifically, the stresses and strains induced within the layers of a multi-layered system are of paramount importance (Ullidtz *et al*, 1989).

A method that is presently receiving a lot of attention is deflection testing done with the Falling Weight Deflectometer (Eartman *et al*, 1981). This type of test minimizes problems with calibration and the durability of field sensors. The device itself has been used during spring thaw to detect large decreases in resilient moduli within thawed layers (Ullidtz *et al*, 1989). Nevertheless, under these conditions, the resilient modulus of the thawed layer might vary by as much as a factor of 4, causing it to be ill defined (Chamberlain *et al*, 1989).

These facts suggest that an understanding of soil behavior during periods of thaw is essential to choosing the appropriate method for predicting the dynamic behavior of a multi-layered system. Presently, the capabilities of continuum mechanics to predict frozen soil behavior are in question (Ullidtz *et al*, 1989).

The ultimate goal of this study was to obtain data related to the behavior of a frozen soil profile, particularly its frozen, transition, and thawed zones. The data, which were acquired in a controlled laboratory environment, allowed for the capabilities of available computer models to predict responses during freezing and thawing cycles to be evaluated.

This was accomplished through the construction of a laboratory model made up of freeze-thaw susceptible soil. As part of the process, geophones were embedded in the soil and placed in vertical and horizontal directions so as to permit tomography of the relative thicknesses of layers to be performed. Displacements experienced on the soil surface and within the soil mass were determined from measurements made using properly calibrated and special geophones (Nazarian and Bush, 1989).

The soil was compacted inside an insulated metal tank measuring 5 feet in depth and 5 feet in diameter. The tank was placed under a frame onto which a 5.5 kip actuator was mounted. In order to simulate field conditions and anchor frozen layers, clips were placed

through the tank's wall. Access holes were drilled in the bottom of the tank, and capillary water was added to the soil during freezing cycles.

The temperature of the soil mass was measured with thermocouples (copper - constantan) calibrated to determine the relation between microvolt output and temperature. The resistivity sensors were manufactured in-house. Stacks of temperature sensors and copper electrodes used in measuring resistivity were arranged in intervals and in a manner similar to that proposed by Berg (1989). Three stacks were manufactured, calibrated, and installed at a 120 degree angular spacing in the vicinity of the tank's wall.

A total of 48 geophones were purchased and calibrated in-house. An existing vibrator was used to measure the natural frequency, transductivity, and damping of each geophone.

The vertically oriented geophones were embedded within the soil mass in stacks of six. Horizontal geophones oriented along the same two diameters were placed at depths of 1, 2, and 3 ft and at a distance of one foot from the tank's centerline. All were kept in the vicinity of the four stacks of vertical geophones.

For the purpose of performing tomography, four access plastic pipes used to generate P- and S-waves were embedded in the soil. The signals were detected by the geophones and captured by a data acquisition system that was manufactured in-house. To avoid problems with reflections on tank walls, it was necessary to use a data acquisition system capable of achieving the appropriate sampling rates. An analysis of the signals, which accurately represented contours of equal moduli materials with depth, was performed with standard software (PROMAX). In comparing the results with the temperature and resistivity profiles, it was possible to develop a precise layer model to represent the test tank.

Two major concerns of this study were the potential effects of placing (rigid) geophones in the soil mass and the interference of the test tank's side walls with the propagation of waves. Suddhiprakarn (1983) extensively addressed both of these concerns. He concluded that, in determining the propagation velocity of shear and compression waves, these two factors have little or no effect. In determining the amplitude of vibration, the filtering and backscattering effects for relatively long wavelengths (such as those produced during the impulse tests presented herein) are minimal and, for all practical purposes, may be neglected.

Due to unforeseeable circumstances, only the freeze-thaw cycle was completed. The freezing of the soil was accomplished by placing crushed dry ice on the pavement surface. The thawing was moderated by placing a cooling plate on the pavement surface kept at a constant temperature of 4° C. This was intended to permit enough time to collect several points during the thawing part of the cycle.

The test sequence consisted of ten sets of measurements made over a period of about three months. The temperature and resistivity data were collected on nearly a daily basis to monitor the progress of freezing or thawing of the soil and select the appropriate times for testing. For each testing date, two groups of measurements were performed:

1) Tomography data were gathered by lowering a seismic source into the access holes and at several depths. For each impact, the responses of all geophones were recorded.

2) A circular plate was placed on the pavement, and an impact (a haversine of 15 milliseconds and 550-pound peak force) was imparted. Again, the responses of all geophones were recorded.

Both groups of measurements were performed on either the same day or on consecutive days. The tests were performed from February 1994 through August 1994 on the following dates:

1) February 28 . . . . . Baseline Data
2) March 9
3) March 18 . . . . . Frozen Condition
4) March 22
5) March 25
6) March 27
7) March 29 . . . . . Thawed Condition
8) April 14
9) June 2
10)August 11

The recorded data and the appropriate analysis of the tomography studies are presented in Appendix A. This appendix also includes a more detailed description of the testing setup. The resistivity and temperature records for the test dates are shown in graphical form in Appendices B and C, respectively.

In the second set of tests, a circular plate was placed on the asphalt concrete, and a 15-ms haversine with a 550-lb peak was imparted on the plate. The data acquisition was triggered, and records were kept for all properly working geophones. The record of velocity was used in conjunction with the calibration of each geophone to determine the vertical or radial displacement at the point of the embedment of the geophone. These displacements are referred to as "measured" in the remainder of this report. The data were used to draw contour lines of displacements at several depths inside the tank. Presented in Appendix D are the specific contour plots obtained for the following days:

1) February 28, 1994 . . . . . .Baseline
2) March 18, 1994 . . . . . Frozen Condition
3) April 14, 1994 . . . . . Thawed Condition

Each plot represents the vertical displacements on a horizontal section at the depth indicated.

The analysis and integration of all the results consisted of the evaluation of the capabilities of typical backcalculation programs. The following three types of analyses were implemented using the tomography and dynamic test data:

1) The pavement soil profile in the tank was reduced to a number of presumed homogeneous layers in the following fashion:

   a) For the baseline and thawed conditions, the following layers were adopted:

      a.1) asphalt layer
      a.2) base layer
      a.3) subgrade layer

   b) For the frozen condition, the following layers were adopted:

      b.1) asphalt layer
      b.2) base layer
      b.3) frozen subgrade layer
      b.4) thawed subgrade layer

   The deflections "measured" with the geophones placed on the surface of the asphalt layer were used as input for the program WESDEF (Van Cauwelaert *et al*, 1989), together with the corresponding number and thicknesses of the layers required to backcalculate the moduli of the layers and explain the surface deformations "measured." This is the backcalculation procedure typically used in practice with the Falling Weight Deflectometer.

2) The moduli obtained in this first analysis, together with the assumed layers, were used as input for the program WESLEA (Van Cauwelaert *et al*, 1989). This step was performed to calculate the deflections at all points inside the soil/pavement profile where deflections had been "measured."

3) The third type of analysis consisted of using the "slowness" values obtained in the tomography analysis. For the same layers, these values were averaged for all of

the blocks comprised in the layer. This average was inverted to obtain velocity. Then, the velocity was converted to moduli, with an assumed density of the material. These moduli were then fed into WESLEA, and deflection predictions were obtained for all geophone locations.

In Appendix E, a summary of all the deflections "measured" or predicted at all depths is given for the following three dates:

1) February 28, 1994
2) March 18, 1994
3) April 14, 1994

The results of two dynamic tests are presented along either line A-C or B-D in these plots. These are two perpendicular diameters whose locations are illustrated in Appendix A. The data shown for the distance from the center of the tank to points A, B, C, and D were obtained using four different tests. A result of these tests was that the geophone located at the center of the tank was recorded twice for each line and, in most instances, the deflections recorded were not identical.

Another salient feature of these plots is that for larger depths, the number of geophones is considerably reduced due to the malfunctioning of some units.

4B. Summary of the Most Important Results

The surface deflections measured along lines A-C and B-D were used by WESDEF to backfigure the moduli of the different layers. The results obtained from this analysis are summarized in Figure 1, where the moduli of each layer and their changes with time during the freeze/thaw cycle are shown.

Some of the limitations of the analysis are apparent in the figure, including that caused by the program's minimum modulus requirement of 200,000 psi for the asphalt layer. The backcalculation of the moduli did not come to an end because a good fit was obtained but because the limits of the band of values allowed by the program were reached.

The second limitation is apparent for the modulus of the base material. In Figure 1, it is shown to have been constant at 150,000 psi from day 10 to about day 30. However, because the base was frozen during this period, the modulus may have been larger than the value indicated; nevertheless, WESDEF limits moduli to a maximum value of 150,000 psi.

The results of the moduli obtained for the base material indicate that the material underwent dramatic deterioration as thawing progressed. The modulus of the base at the baseline time was approximately equal to 125,000 psi and 5,000 psi following completion of the thawing process. These values were confirmed during the subsequent and fairly easy excavation of the base from the tank.

Following compaction, the subbase material reached a modulus of approximately 10,000 psi. This modulus increased to more than 40,000 psi in the frozen subbase layer. After thawing, the material retained a modulus of about 1,000 psi.

A comparison of the vertical deflections "measured" along lines A-C and B-D for all of the instrumented levels is presented in Appendix E. The results show the typical problems

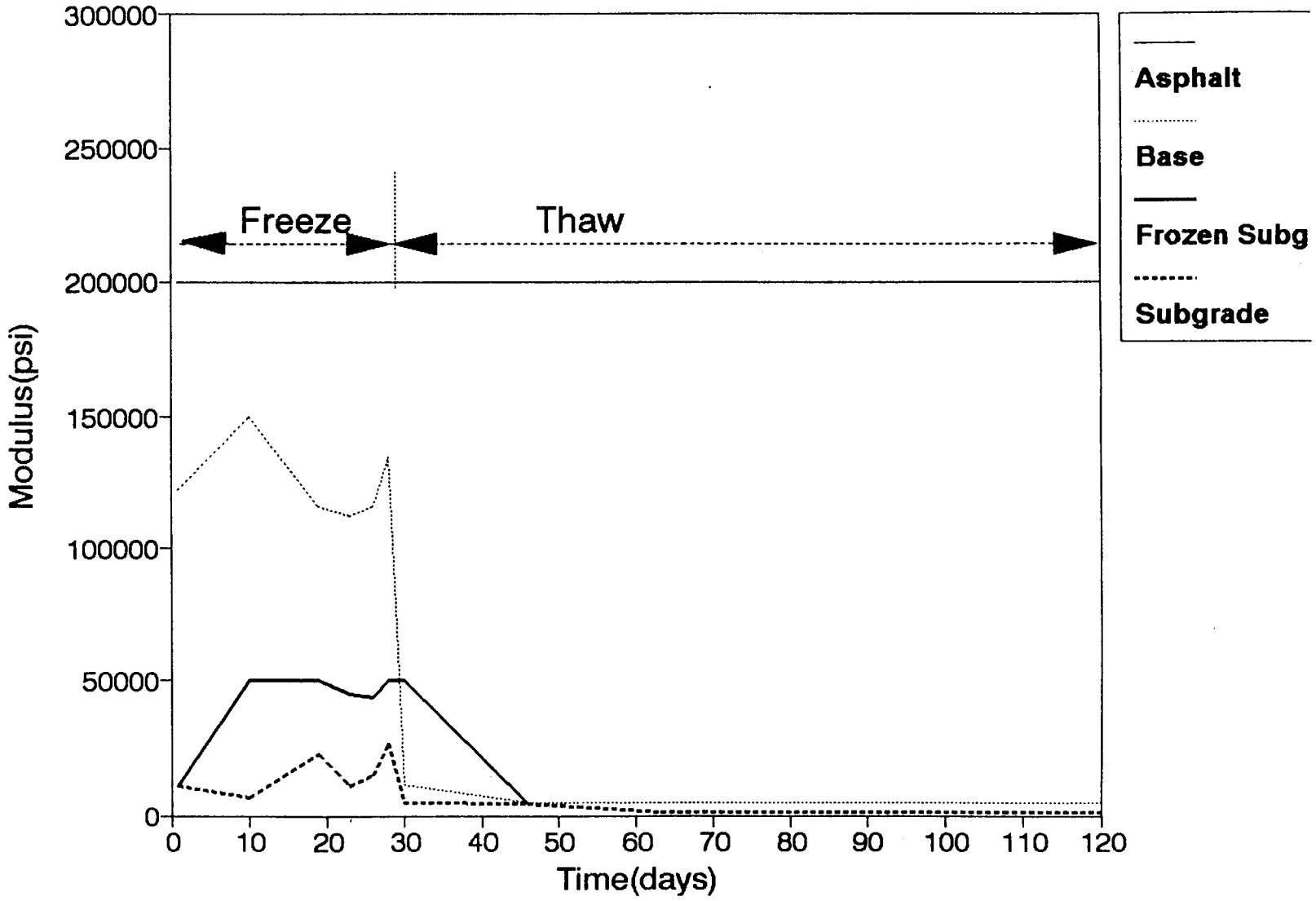

Figure 1. Variation of Moduli of the Different Layers Over the Freeze/Thaw Cycle

reported by other investigators who have attempted to match deflection bowls measured on frozen soil/pavements.

The results shown in Appendix E exhibit the following general trends:

1) The agreement between "measured" and "predicted" deflections was strongest near the center of the tank.

2) As the depth of the profile and distance between a given geophone and the center of the tank increased, the divergence of "measured" from "predicted" deformations increased.

These observations have been reported to occur in the interpretation of falling weight deflectometer data from field tests. In the presently reported lab specimen, there exist some additional factors that may have been responsible for or accentuated these effects. This is due to the fact that the boundary conditions of the test tank were not properly modelled in the computer models WEDEF and WESLEA used to reduce the data.

A summary of the errors encountered in fitting the surface deflection bowls is illustrated in Figure 2. In general, the mismatch between the "measured" deflections and those predicted by WESLEA ranged from about 40% to 80%.

When all of the geophone locations are included in the error analysis, the percentage of mismatch increases dramatically. These results are shown in Figure 3. It is important to note that the percentage is nearly identical to that for the values shown in Figure 2 for baseline and thawed conditions. However, for freezing conditions, the percentage increases dramatically. Again, these results agree with those commonly reported in the interpretation of falling weight deflectometer tests performed under frozen pavement conditions.

The predicted deflections of WESLEA, which used the slowness values obtained from

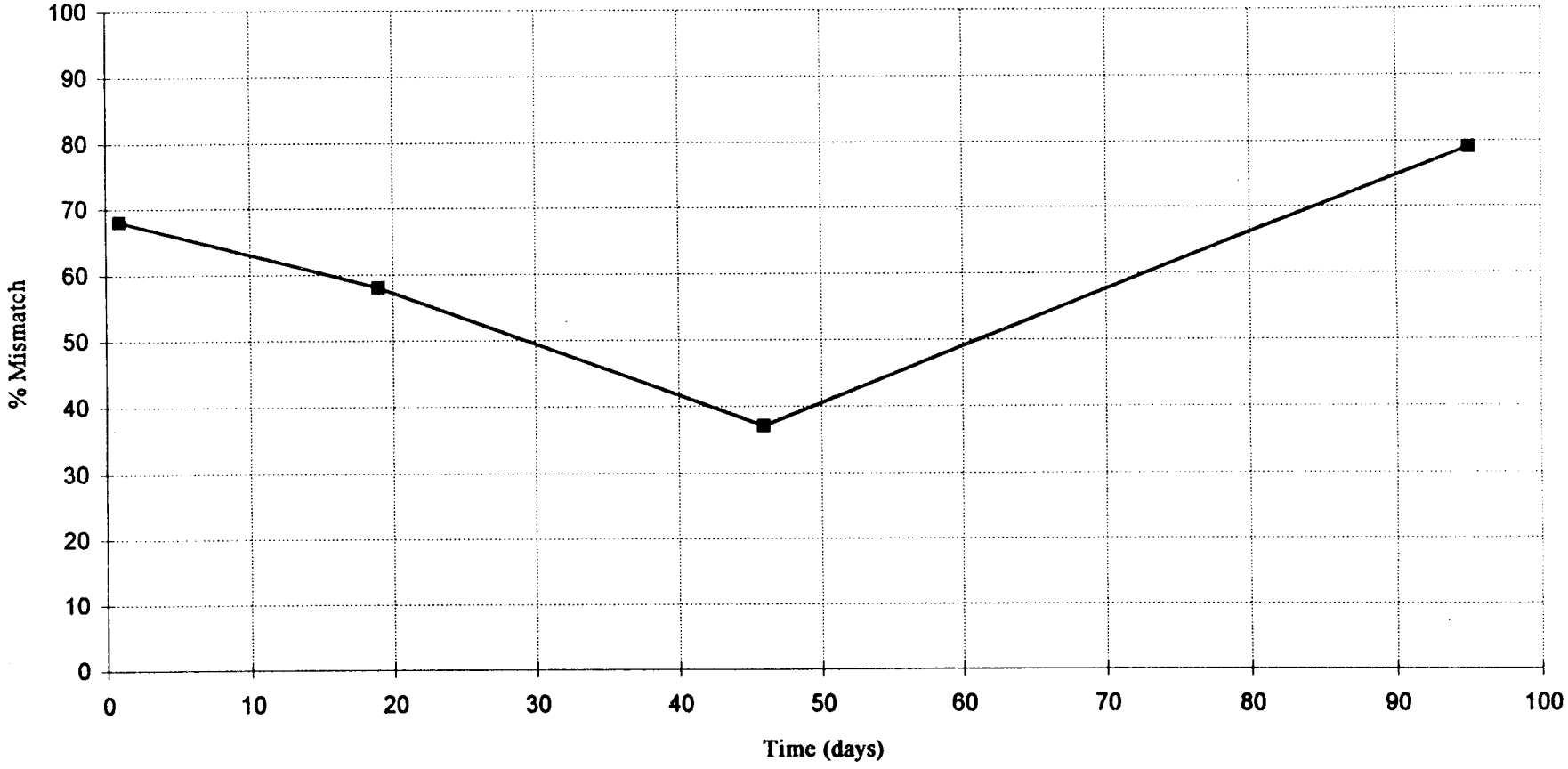

Figure 2. Percentage of Mismatch in the Fitting of the Bowl of Surface Deflections

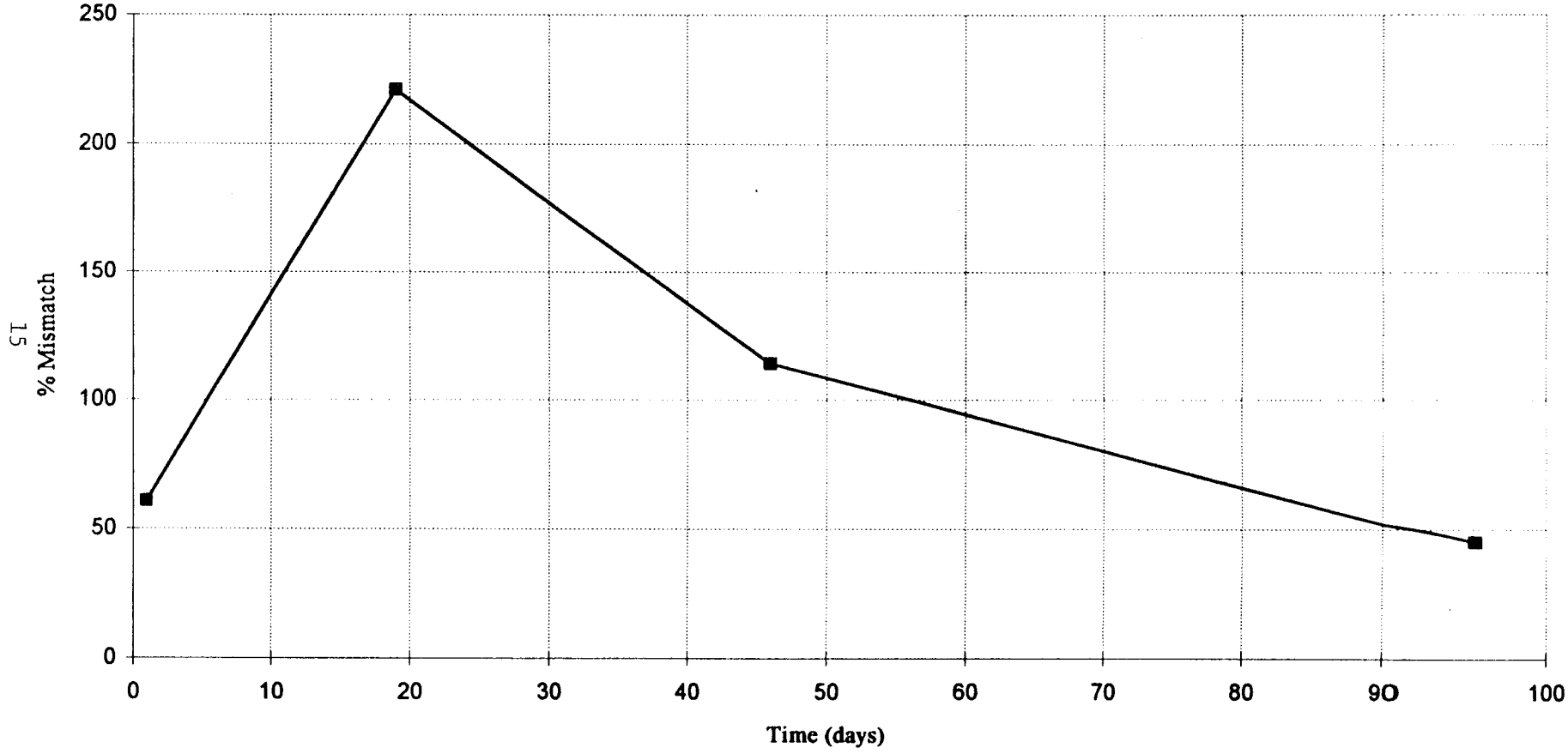

Figure 3. Percentage of Mismatch in the Fitting of the Deflections at all Geophone Positions

tomography, are consistently smaller than the "measured" deflections—usually by a factor of two to three. This finding is in general agreement with that of other researchers. However, some discrepancy may have resulted from an excessive simplification of the computer models caused by the program's consideration of only homogeneous layers in the pavement and subbase soils. Nevertheless, the results of tomography did indicate noticeable differences in moduli within the different layers.

In summary, the results obtained from this initial freeze/thaw cycle are promising, but some refinements and additional work would likely improve the resolution of the techniques used. A portion of this work will be addressed through use of the AASERT grant that was awarded to UTEP.

Specifically, it is believed that the tomography test and the interpretation analysis of the dynamic tests can be improved. The main improvements of the tomography would consist of relocating the geophone layers to shallower depths in order to provide an increase in ray coverage in the upper layers, where the highest contrasts were observed. Furthermore, the "cross-hole" surveys performed would be complemented with "downhole" surveys by impacting the surface of the pavement at an array of points and recording the signal at each geophone location. This additional survey would help increase the ray coverage and thus improve the resolution in the high contrast zone.

An improvement of the analytical models used for the interpretation of deflection data is thought to be the most needed for the dynamic tests. Such an improvement would better accomodate the boundary conditions that exist in the test tank and the variability of properties of the pavement and soil layers.

4.C List of All Publications

The project has resulted in a master's thesis for Jeffrey Williams. The thesis, to be submitted to the UTEP Graduate School, has already been defended and is in the process of being finalized. An edited copy is included as Appendix A of this report.

A poster describing the project was prepared and presented at the 1993 meeting of the American Geophysical Union in San Francisco, California. A copy of the submitted abstract is included in Appendix F, along with that of another paper which is undergoing review. If accepted, it will be presented during the Geophysical Case Histories Session of the 1996 ASCE Convention in Washington, D.C.

We also expect to submit a potential paper to the ASCE Cold Regions Research Journal before the start of the fall 1995 semester.

4.D List of Participating Scientific Personnel

Principal Investigators

Dr. Miguel Picornell, Department of Civil Engineering
Dr. Soheil Nazarian, Department of Civil Engineering

Research Associates

Dr. Rafael Pezo, Department of Civil Engineering
Dr. Diane Doser, Geophysics, Geological Sciences Department
Dr. Mark Baker, Geophysics, Geological Sciences Department

Research Assistants (major commitment)

Lin Wang, Graduate Student, Department of Civil Engineering
Jeffrey Williams, Graduate Student, Geophysics, Geological Sciences Department
Joseph Mactutis, Undergraduate Research Assistant, Department of Civil Engineering

Research Assistants (temporary commitment)

Anwar Jamal, Graduate Student, Department of Civil Engineering
Tikhe Ashish, Graduate Student, Department of Civil Engineering
Mallareddigari Ramesh Kumar, Graduate Student, Department of Civil Engineering

5. Bibliography

1. Atkins, R.F., 1979, "Determination of Frost Penetration by Soil Resistivity Measurements," USA CRREL Special Report 79-22, Hanover, N.H.

2. Berg, R.L., 1989, "Monitoring Pavement Performance in Seasonal Frost Areas," USA CRREL Special Report 89-23, Hanover, N.H.

3. Chamberlain, E.J., M.D. Cole, and G.F. Durell, 1989, "Resilient Modulus Determination for Frost Conditions," USA CRREL, Special Report 89-23, Hanover, N.H.

4. Cole D., Bently, D., Durell, L.G., and Johnson, T., 1986, "Resilient Modulus of Freeze-Thaw Affected Granular Soils for Pavement Design and Evaluation," USA CRREL Special Report 86-4, Hanover, N.H.

5. DeJong, D.L., Pentz M.G.F., and Korswagen, A.R., 1973, "Computer Program Bisar," External Report, Koninklijkel/Shell-Laboratorium, Amsterdam, the Netherlands.

6. Ertman Larsen, H.J., and Stubstad, R.N., 1982, "The Use of Non-destructive Testing in Flexible Pavement Rehabilitation Design," International Symposium on Bearing Capacity of Roads and Airfields, Trondheim.

7. Nazarian, S., and Bush, A.J., 1989, "Determination of Surface Deflection of Pavement Systems Using Velocity Transducers," presented at 68th TRB Meeting, Washington, DC (accepted for publication).

8. Selig, E.T., 1989, "*In Situ* Stress Measurements," USA CRREL, Special Report 89-23, Hanover, N.H.

9. Shadaram, M., Solehju, A., and Nazarian, S., 1990, "Application of Fiber Optic Sensors in Pavement Maintenance," SPIE 1990 International Symposium on Optical and Optoelectric Applied Science and Engineering, San Diego, California.

10. Suddhiprakarn, C., 1983, "Effects of Rigid Inclusions on Wave Propagation," Geotechnical Engineering Report 83-3, Geotechnical Engineering Center, The University of Texas at Austin, Austin, TX.

11. Ullidtz, P., and H.J. Ertman Larsen, 1989, "State-of-the-Art Stress, Strain and Deflection Measurements," USA CRREL, Special Report 89-23, Hanover, N.H.

12. Van Cauwelaert, F.J., Alexander, Don R., White, T.D., and Barker, W.R., "Multi-layer Elastic Program for Backcalculating Layer Moduli in Pavement Evaluation," Non-destructive Testing of Pavements and Backcalculation of Moduli, ASTM STP 1026, A.J. Bush III and G.Y. Baladi, Eds., American Society for Testing and Materials, Philadelphia, 1989, pp.171-188.

13. Vinson, T.S., 1978, "Response of Frozen Ground to Dynamic Loadings," Geotechnical Engineering for Cold Regions, Andersland, O.B. and Anderson, D.M., Editors, McGraw-Hill Book Co., New York.

14. Vinson, T.S., Wilson, C.R., and Bolander, P., 1986, "Dynamic Properties of Naturally Frozen Silt," Proceedings, Permafrost: Fifth International Conference, National Academy of Sciences, Washington, D.C.

15. White, T.D., 1989, "Instrumentation and Pavement Design," USA CRREL Special Report 89-23, Hanover, N.H.

Appendix A

THESIS BY JEFFREY LYNN WILLIAMS, B.A.

ON

SEISMIC TOMOGRAPHY OF FREEZING AND THAWING SOIL

Table of Contents

1. Introduction and Background 26

1.1 Motivation for Investigation 26
Geotechnical Application 26
Characterization of Ice Formation within a Freezing and Thawing Soil 28
Use of Seismic Tomography in a Controlled Laboratory Environment 30

1.2 Travel Time Inversion of Three-Dimensional Seismic Data 31
Tomographic Inversion Method 31
Use of *A Priori* Information 34

1.3 Investigation of Effect of Errors on Inversion Results 35

2. Experimental Setup and Procedures 37

2.1 Laboratory Apparatus 37
Tank, Soil, and Means of Cooling 37
Geophones, Seismic Source, and Data Acquisition System 40
Soil Resistance Probes 44
Soil Temperature Probes 45

2.2 Seismic Data Collection and Processing 45
Data Collected as Shot Gathers 45
Data Reformatted to SEGY Format for Processing in ProMax 45
Tomographic Inversion 46

2.3 Error Analysis 51
Method of Kreinovich 51

3. Results and Conclusions 52

3.1 General 52
Time Series Temperature and Resistance 52
Water and Surface Level Changes 55

3.2 Baseline Data 55
Temperature and Resistivity 55
Tomographic Results 58
Discussion 63

3.3 Freezing Soil 63
Temperature and Resistivity 63
Tomographic Results 66
Discussion 66

3.4 Thawing Soil 72

References 73

Appendix - Solving a Linear System of Equations using *A Priori* Information 73

List of Figures

Figure No.		Page No.
A.1.1	Typical Profile of Permafrost Distribution	27
A.1.2	Typical Resistance vs. Depth Curve	29
A.2.1	Grain Size Distribution of the Soil used in this Study	38
A.2.2	General Tank Layout: Vertical Section	39
A.2.3	Geophone Locations within Tank	41
A.2.4	Seismic Source	43
A.2.5	Sample Receiver Gather Data	47
A.3.1	Column B Temperature vs. Time	53
A.3.2	Column B Soil Resistance vs. Time	54
A.3.3	Water Intake vs. Time	56
A.3.4	Surface Movement vs. Time	57
A.3.5	Baseline Soil Temperature	59
A.3.6	Baseline Soil Resistance	60
A.3.7	Baseline P Velocity, Vertical Slice	61
A.3.8	Baseline P Velocity, Horizontal Slice	61
A.3.9	Baseline S Velocity, Vertical Slice	62
A.3.10	Baseline S Velocity, Horizontal Slice	62
A.3.11	Freezing Soil Temperature	64
A.3.12	Freezing Soil Resistance	65
A.3.13	Freezing Soil P Velocity, Vertical Slice	67

Figure No. Page No.

A.3.14 Freezing Soil P Velocity, Horizontal Slice 67

A.3.15 Freezing Soil S Velocity, Vertical Slice 67

A.3.16 Freezing Soil S Velocity, Horizontal Slice 67

A.3.17 Thawing Soil Temperature 70

A.3.18 Thawing Soil Resistance 71

Chapter I

1. Introduction and Background

In this first chapter, the background of the project is presented and its overall motivation explained. Included is a brief discussion of some areas in which this application of seismic tomography may be of some use, including permafrost-laden soil characterization and geotechnical use. Also included in this chapter is a general review of tomographic inversion. Finally, a scheme for assessing the effects of data and model errors on the inversion results is introduced.

1.1 Motivation for Investigation.

Geotechnical Application. Because of variations in climatic conditions and soil composition in regions of extreme latitude, a frozen region within a soil can contain both continuous and discontinuous ice layers ("permafrost") (See Fig. A.1.1) The mechanical behavior of a frozen soil region can be very different than that of a thawed region (Johnston, 1981; Janoo and Berg, 1993). Delineation of permafrost regions is important in geotechnical site investigation of structures such as foundations, roadways, and aircraft runways (Seguin and Frydecki, 1994). To properly assess the mechanical response of a layered soil system, such as a permafrost-layered region, to dynamic loads, such as those imposed on a roadway or runway, the spatial distribution of soil frozen/thawed layers must be delineated (Janoo and Berg, 1981).

Typical Frozen Soil Profile

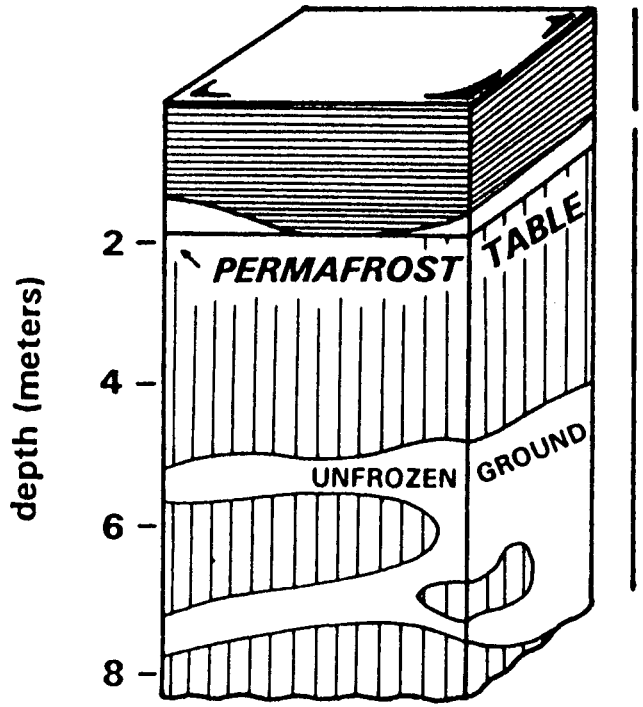

ACTIVE LAYER
Layer does not always extend to permafrost table.

DISCONTINUOUS PERMAFROST ZONE
Thickness varies from a few to tens of meters, with discontinuous lenses of unfrozen ground present.

(after Brown *et al.*, 1981)

Figure A.1.1 Typical Profile of Permafrost Distribution

Characterization of Ice Formation within a Freezing and Thawing Soil Volume. Several different approaches have been developed to effectively determine soil ice content. These methods include soil temperature, neutron density and electrical resistivity logs, ground-penetrating radar, frequency-dependent resistivity methods, gravity methods, and seismic reflection/refraction methods. Each of these methods has pitfalls, in that it is often possible to obtain only a semi-quantitative determination of the spatial distribution of ice within soil.

The most obvious choice for detection of ice within soil would seem to be soil temperature. However, such factors as freezing point depression due to impurities and near-isothermal conditions make ice-level determination difficult using temperature alone. Because of near-isothermal conditions, accurate depth determination is limited by the accuracy with which temperature can be determined (See Fig. A.1.2) (Atkins, 1979).

Soil resistance has been used previously to detect the depth of soil ice (Atkins, 1979). Despite near isothermal conditions during actual freezing, the conductance of a frozen silty soil has been observed to decrease rapidly between 0° and -3°C (32° and 26° F) (Johnston *et al*, 1981). The electrical resistance of a frozen soil has been observed to be several orders of magnitude greater than that for the same soil in the unfrozen state. For this reason, electrical resistance measurements provide an adequate means of determining soil ice conditions at probe locations. Well logs (resistivity, neutron, etc.) often provide accurate means of determining the absence or presence of ice but only near well locations. Sampling bias and limited spatial

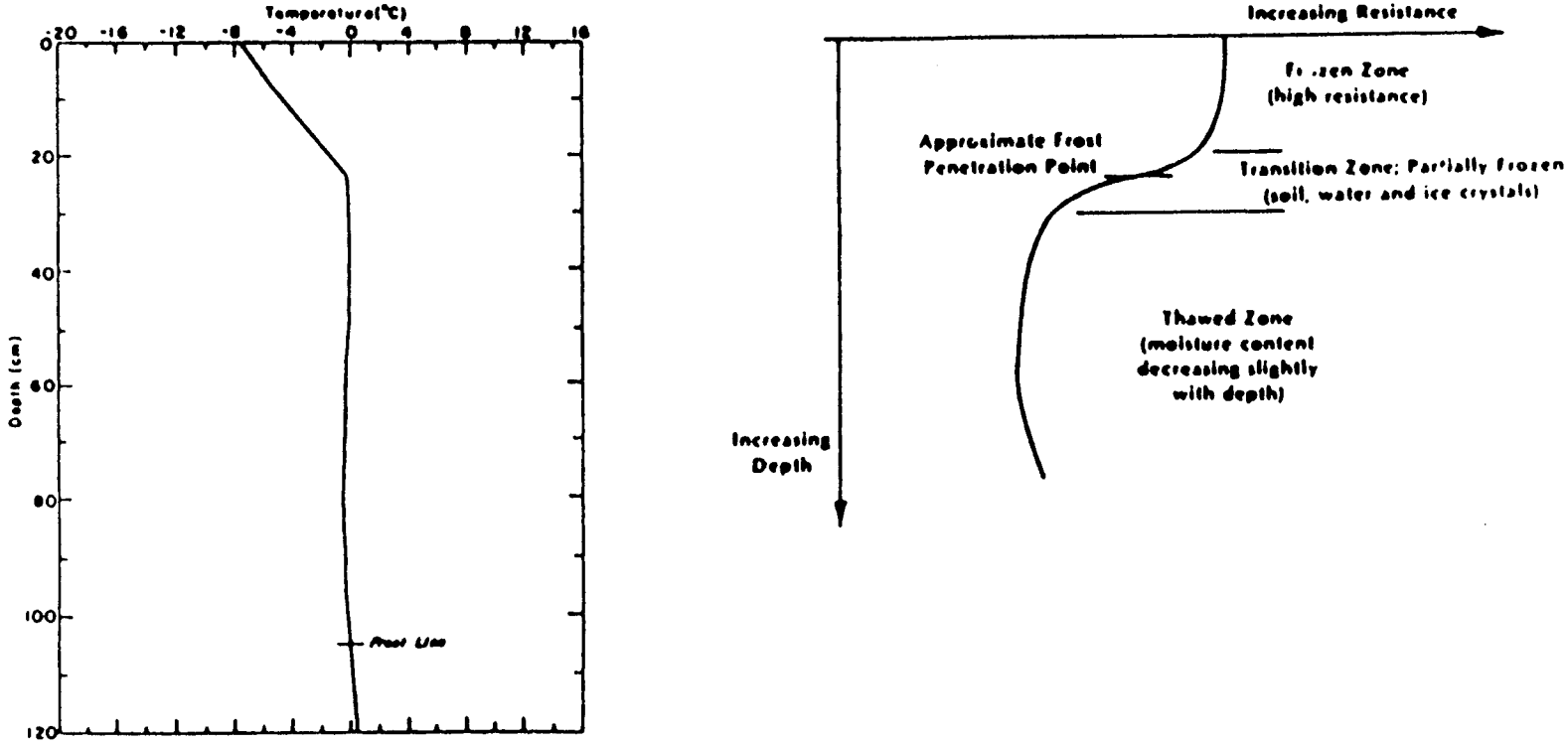

Figure A.1.2 Typical Resistance vs. Depth Curve

(Atkins, 1979)

representation limit the use of this technique. Frequency-dependent resistivity probing suffers from similar limitations (Seguin *et al*, 1988; Sinha, 1988).

Ground penetrating radar is a reliable permafrost probe, but the large attenuation of the signals due to the increased electrical conductivity of the unfrozen water absorbed by clayey particles and/or water salinity hamper this technique (Perron and Seguin, 1993; Zeng *et al*, 1993).

Seismic methods have met with mixed success. Refraction techniques often are affected by the presence of a high-velocity layer of ice above a lower velocity thawed layer; the base of the ice layer cannot be detected. Additionally, seismic wave absorption is significant in frozen clayey material, limiting the depth of penetration. Seismic reflection methods often lack sufficient resolution due to the thinness of the layers of interest (Deschastres *et al*, 1988; Seguin and Frydecki, 1994).

Use of Seismic Tomography in a Controlled Laboratory Environment. The Center for Geotechnical and Highway Materials Research, at The University of Texas at El Paso, has been conducting research to assess the response of variable frozen soil to dynamic loads (Nazarian, 1990). One aspect of this research has been the accurate determination of the extent of frozen/thawed soil layer formation. Seismic tomography was chosen as one tool that could potentially overcome many of the pitfalls of other techniques, including those described above. Source penetration limitations were countered by placing sources down-hole, within or below the ice layers. Also, use of a tomographic technique ensured that a substantial volume of soil was sampled, rather than just a selected amount. The source used was a small,

hammered one capable of producing high-enough frequencies to detect relatively thin layers, i.e. 10 cm (4 in) thick. Additionally, the build-up of ice within the soil volume could be somewhat controlled and monitored by independent means. The rate of ice formation and thawing could be tracked, and the location of ice at specific vertical locations could be determined using temperature and soil resistance measurements.

All work was performed in the laboratories of The University of Texas at El Paso. Using a large volume of soil instrumented with geophones, temperature probes, and soil resistance probes, small-scale seismic tomography experiments were carried out repeatedly as the soil volume was frozen and then thawed. Baseline data were taken before the start of freezing to assess the effectiveness of the tomographic technique at such a small scale. Then, as ice formed within the tank, additional tomography was performed to try to image the ice within the soil. In addition, the soil temperature and resistance were measured as a means of assessing the tomography results and as a source of *a priori* information on ice location.

1.2 Travel Time Inversion of Three-Dimensional Seismic Data.

Tomographic Inversion Method. Tomography is a general mathematical technique which combines information from a large number of criss-crossing rays to construct images of the medium through which rays have traversed (Anderson and Dziewonski, 1987). In seismic tomography, the rays represent seismic waves emanating from a mechanical source. The path the waves take is determined by the velocity distribution within the medium. What follows is a cursory development of

the mathematics of the tomographic technique. A more thorough derivation of the principal equation used in this study can be found in the Appendix of this thesis.

A ray travelling at a velocity v traverses a distance dl in time dt. That is,

$$dt = \frac{dl}{v(\vec{p})}, \qquad \text{(eq. 1.1)}$$

where dt is the differential travel time,

v is the ray velocity,

dl is the path length through volume element, and

p is the position vector along the raypath.

Note that we have written v as a function of position **p**. The time required for a ray to travel from source to receiver is, then, the line integral from source position to receiver position, as indicated by the following equation:

$$t = \int_{raypath} \frac{dl}{v(\vec{p})} . \qquad \text{(eq. 1.2)}$$

Here, **p** points to each point along the raypath. Note that if we knew the continuous velocity distribution v(**p**) throughout the volume, we could use Snell's law to calculate the raypath from source to receiver and then equation 1.2 to calculate the travel time from source to receiver.

Our data, however, consist only of raypath endpoints and travel times. We wish to find v(p) such that equation 1.2 is satisfied for all rays. To accomplish this, the integral equation is discretized, allowing for a large number of blocks, each with its own velocity. The integral equation then becomes

$$t_i = \sum_{j \in ray_i} \Delta_{i,j} s_j \,, \qquad \text{(eq. 1.3)}$$

where t_i is the travel time for the ith ray,

$\Delta_{i,j}$ is the path length for ray i through block j, and

s_j is the inverse velocity or *slowness* of the jth block.

The travel time from a given source to receiver is then given by a linear combination of block path lengths and slownesses. There is one equation for each observation of travel time:

$$\begin{aligned} t_1 &= \Delta_{1,1} s_1 + \Delta_{1,2} s_2 + \cdots + \Delta_{1,n} s_n \\ t_2 &= \Delta_{2,1} s_1 + \Delta_{2,2} s_2 + \cdots + \Delta_{2,n} s_n \\ &\vdots \\ t_i &= \Delta_{i,1} s_1 + \Delta_{i,2} s_2 + \cdots + \Delta_{i,n} s_n \end{aligned} \qquad \text{(eq. 1.4)}$$

Or, cast in matrix form,

$$\begin{pmatrix} t_1 \\ t_2 \\ \vdots \\ t_i \end{pmatrix} = \begin{pmatrix} \Delta_{1,1} & \Delta_{1,2} & \cdots & \Delta_{1,n} \\ \Delta_{2,1} & \Delta_{2,2} & \cdots & \Delta_{2,n} \\ \vdots & \vdots & & \vdots \\ \Delta_{i,1} & \Delta_{i,2} & \cdots & \Delta_{i,n} \end{pmatrix} \begin{pmatrix} s_1 \\ s_2 \\ \vdots \\ s_n \end{pmatrix}, \qquad \text{(eq. 1.5)}$$

from which we can write more compactly

$$\vec{t} = A\,\vec{s} \,, \qquad \text{(eq. 1.6)}$$

where **t** is a vector containing travel times,

s is a vector containing block slowness values, and

A is a matrix containing raypath lengths through all blocks.

The block slownesses are found by inverting **A** and multiplying it on both sides: The tomographic inversion is accomplished, in principle, by solving this equation.

$$\vec{s} = A^{-1}\,\vec{t} \qquad \text{(eq. 1.7)}$$

The raypath is a non-linear function of the unknown slowness (Eq. 1.2). To linearize the problem, a starting slowness model must be chosen. Travel-time residuals are then computed based on the starting model, and changes to block slownesses are calculated (Scales, 1987). Using this approach, equation 1.7 becomes

$$\Delta\vec{s} = A^{-1}\,\Delta\vec{t}\,. \qquad \text{(eq. 1.8)}$$

From these equations, three things are evident: (1) for any realistic experiment, the number of elements in **A** is equal to the product of the number of observed travel times and the number of blocks in the model; (2) **A** is likely to be sparse. That is, for a given raypath, only a relatively few blocks are actually traversed, resulting in a large number of zero elements in any row of the matrix; and (3) **A** is not necessarily a square matrix; that is, there are likely to be far more elements in the model than there are observations of travel time. Hence, the set of equations to be solved is very large, sparse, and under-determined. For all of these reasons, special precautions must be taken in solving the set of equations.

Use of *A Priori* Information. Though we are seeking to determine the velocity of the model blocks based on the observations of travel time, we do have other information with which to constrain our estimate. In this experiment, we had soil temperature and soil resistance information for three vertical columns within the soil volume. Both of these sets of observations were useful in distinguishing between areas of frozen soil and thawed soil. In addition, we had estimates of uncertainty in travel- observed times. This information was used to place uncertainties on the

velocities of our starting model. The Appendix details how this information is incorporated into the inversion.

1.3 Investigation of Effect of Errors on Inversion Results.

There were two sources of uncertainty or "error" in this experiment: error in determining travel times and error in source/receiver positioning. In addition, as we shall see, the choice of starting model greatly influenced the inversion solution in the face of uncertain data. The effect of data error on the solution uncertainty is termed *information density*. The effect of model errors is termed *resolution*. Using a method developed by Kreinovich *et al* (1994), it was possible to explore the effect of all these uncertainties on the final solution to the tomographic inversion.

We begin by assuming that the error in our ith measurement (travel time, geophone/source position, or starting model slowness) is randomly distributed, has zero mean, mean square deviation D_i, and possesses a Gaussian distribution. The quantity we want to find is the mean square deviation of block slowness. The calculated block slowness is a function of the input data; the mean square deviation of block slowness is a function of the input data's error.

Let $f(x_1,x_2,..,x_n)$ denote the solution to the inversion without error. Let ϵ be the standard deviation of the ith observation of x. $f(x_1+e_1,x_2+e_2,\ldots,x_n+e_n)$ denotes the solution with error, where the individual data x_i values have been perturbed within their uncertainty such that e_i is a normally distributed random variable with zero mean, lying on the interval $[-\epsilon,+\epsilon]$. The difference $d = f(x_1,x_2,..,x_n) - f(x_1+e_1,x_2+e_2,\ldots,x_n+e_n)$ represents the deviation of $f(x_1,x_2,..,x_n)$ realized for a

particular ensemble of data values and data error. The variable d is a linear combination of normally distributed random variables and is itself normally distributed. Using a Monte-Carlo approach, a number of d_i are computed, each with its own ensemble of $(x_1+e_1, x_2+e_2, \ldots, x_n+e_n)$. The resulting standard deviation of f is then given by

$$\sigma = \sqrt{\sum_{i=1}^{N} d_i^2} \; . \qquad \text{(eq. 1.9)}$$

The precision of this error estimate is $N^{-1/2}$. To calculate the error with a relative precision of 20%, for example, twenty computations of d would be required.

To examine the effect of travel time errors on the inversion results, only the travel time data are perturbed; the geophone and source locations are taken to be without error, as is the *a priori* model. The effects of location error and starting model uncertainty can be examined in a similar manner.

Chapter II

2. Experimental Setup and Procedures

In this chapter, the experimental apparatus, methods of data acquisition, and data processing are described. Section 2.1 details the physical model employed to investigate freezing and thawing soil and the instrumentation used. Section 2.2 describes the data collection procedures and the methods used to reduce, display, and interpret data. Included in this section is an outline of the specific tomographic inversion program used. Finally, the specific error analysis procedures are detailed.

2.1 Laboratory Apparatus.

Tank, Soil, and Means of Cooling. The physical model used in this experiment consisted of a volume of soil held within a tank whose top surface was subjected to freezing temperatures, simulating the conditions described in Chapter I. The soil volume observed was of a type susceptible to the freeze/thaw behavior previously described. Figure A.2.1 shows the grain size distribution of the soil used in relation to freeze/thaw susceptible soil. The soil's texture itself was sandy to silty.

A soil volume was contained within a cylindrical steel tank 1.5 m (5.0 ft) in diameter and 1.5 m (5.0 ft) tall. The bottom 0.46 m (1.5 ft) of the tank was filled with sand. Approximately 2.8 m^3 (99 ft^3) of soil was placed above this sand layer (Fig. A.2.2). The tank was filled by laying down 15 cm (6 in) of soil at a time and then compacting the layer. Using a hand compacting tool, each layer was uniformly compacted over its surface. This yielded a compacted surface of consistent density upon which subsequent layers were placed. The total depth of compacted soil was

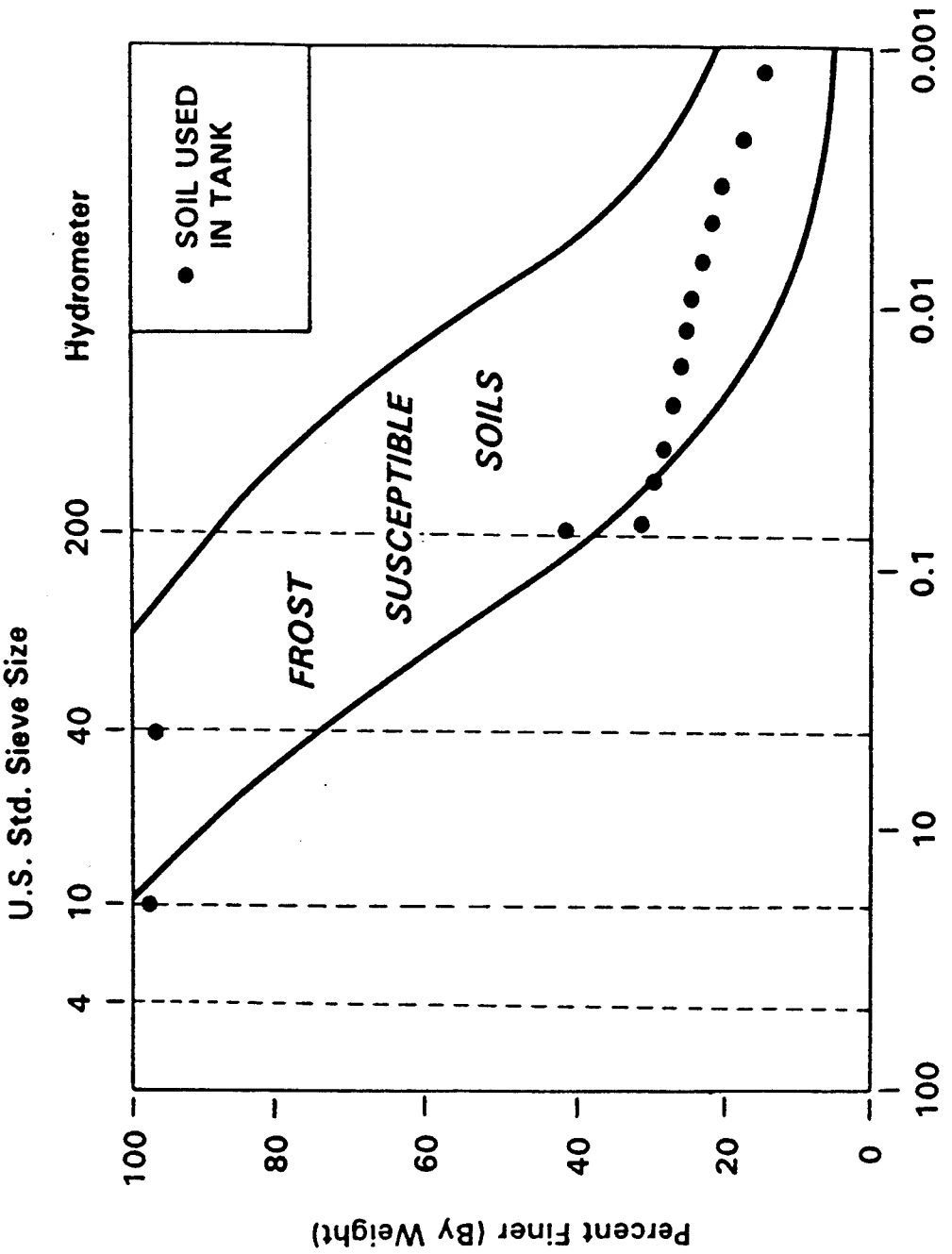

Figure A.2.1 Grain Size Distribution of the Soil Used in this Study

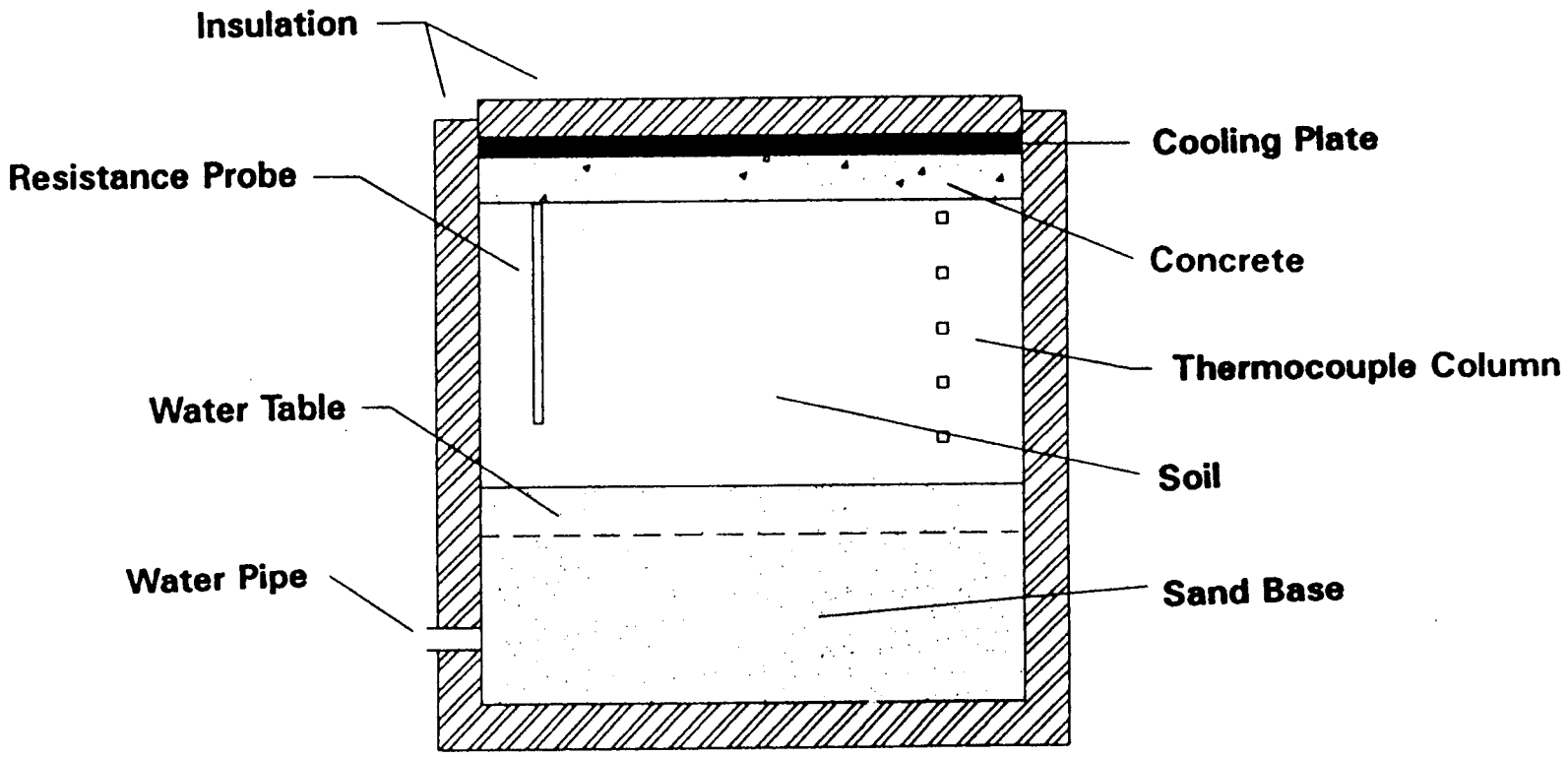

Figure A.2.2 General Tank Layout. Vertical Sections

about 0.91 m (3.0 ft). The compacted soil was topped with 13 cm (5 in) of Type B base (sandy soil mixed with coarse gravel), which itself was compacted in a manner similar to that of the soil. This compacted base was capped with 7.6 cm (3 in) of compacted asphalt mix. This base/asphalt cap was used to accommodate a related engineering study and also served as a durable layer on which dry ice could be placed to cool soil.

To cool the tank and freeze the soil, crushed dry ice was distributed over the asphalt surface. During the cooling phase of the experiment, 45.4 kg (100 lbs) of crushed dry ice provided about 24 hours of constant cooling. The exterior of the tank and the ice surface were covered in foam- and glass fiber-insulation. During the thawing stage of the experiment, a length of 1.3 cm (0.5 inch) vinyl hose was coiled on top of the asphalt surface. An anti-freeze mixture whose temperature was held a constant 4.4°C (40° F) was circulated through the hose. The surface and sides were again insulated. The cooled anti-freeze circulation slowed the thawing of the tank, allowing the temperature and resistance within the soil to be monitored. Tomographic data were collected without drastic changes in the soil conditions.

Geophones, Seismic Source, and Data Acquisition System. At selected levels within the soil volume, geophones were layed out according to the pattern shown in Figure A.2.3. The soil volume contained a total of 48 geophones, most of which were Mark Products L-28 vertical component geophones having a natural frequency of 4.5 Hz. Because the supply of L-28 geophones was limited, some L-28 horizontal component geophones and L-15 geophones were also used. Ultimately, the type of geophone did not affect the quality of data. All of the geophones were approximately

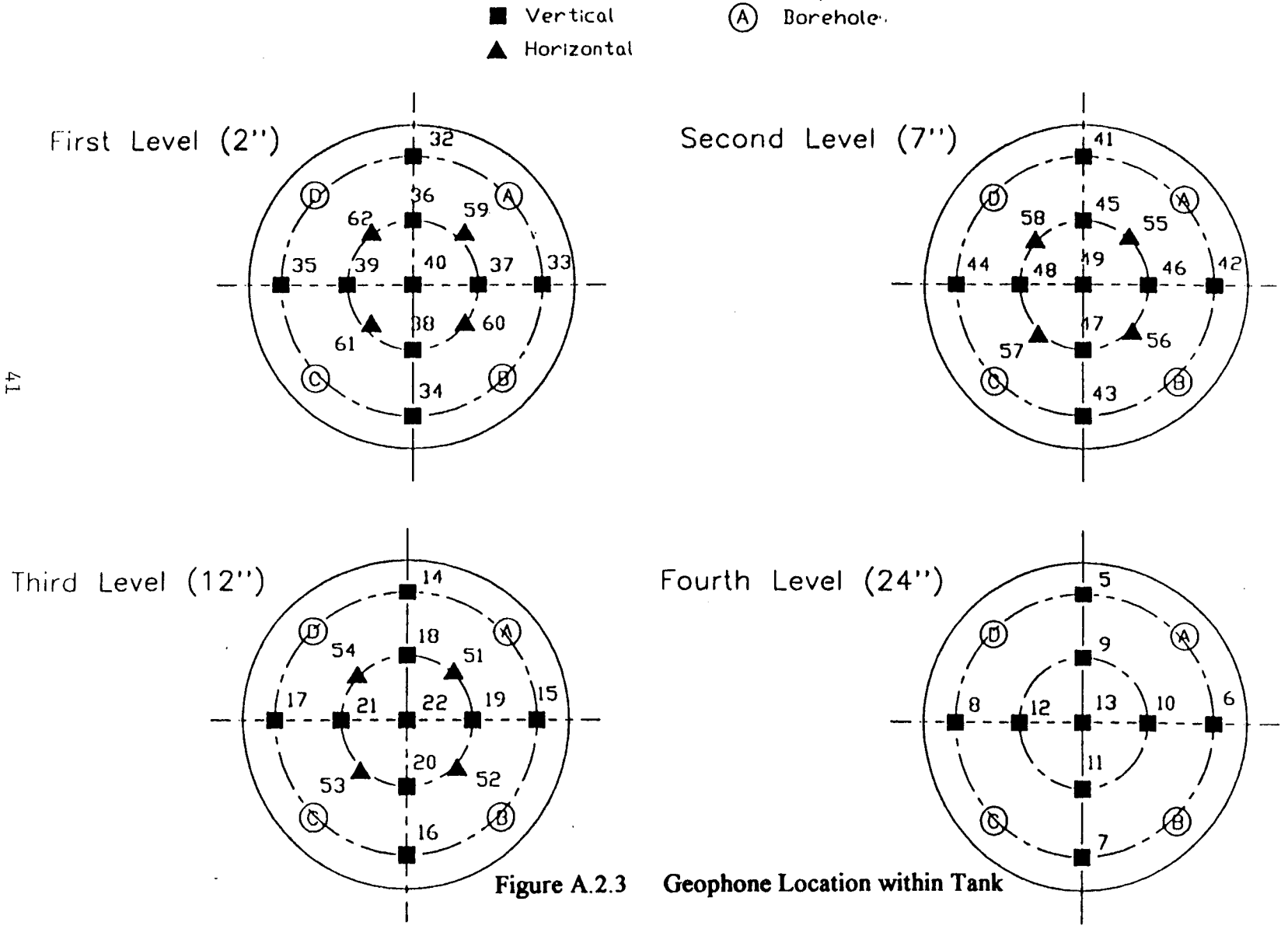

Figure A.2.3 Geophone Location within Tank

3.8 x 5.1 cm (1.5 x 2 in) in size. From each geophone level, small 30-gauge twisted-pair wires ran to a ribbon cable near the side of the tank. The ribbon cables for all levels were connected to a junction box outside the tank, which provided an integrated cable connection to a nearby amplifier and data acquisition computer. Since the data acquisition system had the capability of recording twelve channels of data at once and there was a total of forty-eight channels of data, geophone data were collected in four groups of twelve. Thus, at each source location, data were collected four consecutive times.

At four vertical locations within the tank, as shown in Figure A.2.3, 3.8 cm (1.5 in) inside diameter PVC pipe penetrated the tank to a depth of about 0.91 m (3.0 ft). These pipes served as "bore holes" into which a small seismic source was placed (Figure A.2.4). The source consisted of a 7.6 x 2.5 cm (3 x 1 in) steel cylinder cut diagonally to form two wedges. The outside of the wedges were knurled so as to provide a rough exterior capable of gripping the interior of the PVC pipes. Two rods extended from each of the wedges to the surface of the tank. To serve as a source, the wedged cylinder was placed down a PVC pipe to the desired level. Using the rods, the wedges were forced apart so as to compress against the sides of the pipe and seat securely. A small, lightweight hammer was struck against the rod connected to the top wedge, thereby creating both P- and S-waves.

The contact of the hammer with the rod acted as an electrical trigger to the analog-to-digital (A/D) boards. A simple resistor-capacitor trigger circuit which used the hammer/rod closure as a switch provided a 5-V pulse to the A/D boards which commenced the acquisition. The A/D sampling duration was 50 ms at a 50 kHz

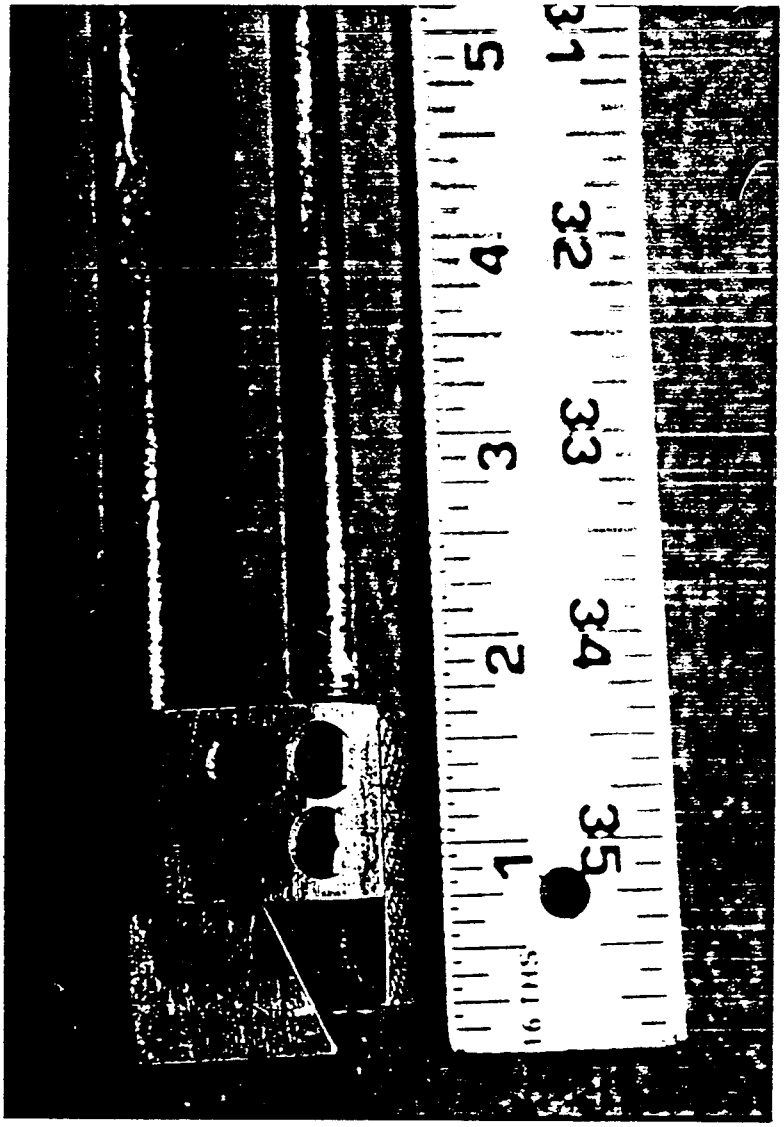

Figure A.2.4 Seismic Source

sampling rate. The A/D boards had a dynamic range of 12 bits on a scale of ± 2.5 volts. Prior to digitizing, the geophone signals were amplified by a factor of ten and low-pass filtered, with a cutoff frequency of 20 kHz.

The source was placed at depths from 0 to 61cm (0 to 24 in), every 7.6 cm (3 in), in all four holes. There was a total of 36 source locations.

Soil Resistance Probes. To monitor the ice conditions within the tank soil, resistance was measured. At three equally spaced vertical positions within the tank, an array of single-ended probes was buried. The probes were constructed of 1.3 x 0.64 cm (0.5 x 0.25 in) copper tubing pieces, soldered to the end of copper leads. The probes were located 5.1 cm (2 in) apart to a depth of 76.2 cm (30 in) (15 probes). Soil resistance was measured indirectly. A 45 Hz, 6 V_{rms} (no load) signal supplied by an HP-651B Test Oscillator was fed through a 218 Ω-fixed resistor and across two adjacent probes. For this arrangement, the apparent soil resistance between the two probes was calculated from the following expression:

$$R_{SOIL} = \frac{V_{SOIL}}{V_{FIXED}} \cdot R_{FIXED} \,, \qquad \text{(eq. 2.1)}$$

where R_{SOIL} is soil resistance,

V_{SOIL} is voltage across two adjacent resistance probes,

V_{FIXED} is voltage across the fixed resistor,

R_{FIXED} is the fixed resistor value.

Throughout the experiment, soil resistance was regularly measured for all probe locations.

Soil Temperature Probes. Soil temperature was measured by means of Type-T thermocouples embedded within the soil volume. At three equally spaced vertical columns within the tank {about 15.2 cm (6 in) adjacent to the resistance probe columns}, thermocouples were placed about 12.7 cm (5 in) apart from depths of 5.1 to 55.9 cm (2 to 22 in). The temperature was read directly by means of an Omega DP460-T-DSS Thermocouple meter. As with soil resistance, soil temperature was continually measured throughout the experiment. Soil temperature provided an indication of the extent of soil cooling and, to some degree, the location of ice within the soil volume.

2.2 Seismic Data Collection and Processing.

Data Collected as Shot Gathers. As soil ice conditions dictated, seismic data were collected from the tank. At each source location, data from each geophone were collected using the data acquisition system described in Section A.2. Since data for all geophones were collected at once for each shot location, they were recorded as *shot gathers*. For each of 36 shot locations, four sets of data were recorded, one for each 12-channel geophone group.

Data Reformatted to SEGY Format for Processing in ProMax. ProMax, a seismic data processing package, was used to display the seismic data and pick first arrivals. In order to read the data into ProMax, the separate data files were converted into SEGY format. The SEGY format is a standard binary data format developed by

the Society of Exploration Geophysicists (SEG Special Report, 19??). A program was developed to convert the 12-channel data files from ASCII data to 48-channel SEGY formatted files. The resulting SEGY formatted file could then be read directly into ProMax for further processing.

Using ProMax, the shot gather data were sorted into receiver gathers. This allowed for the viewing of a single geophone's response to all shot locations, as shown in Figure A.2.5.

Both primary (P) and secondary (S) first-arrival times were picked from these data. The data picked consisted of a "most-likely" arrival time, an "earliest-likely" arrival time, and a "latest-likely" arrival time. The earliest and latest arrival times were chosen to bracket the uncertainty in first arrival and provide a means of weighting the data within the inversion procedure. The arrival time data were collected within ProMax and exported to an external program, which reformatted the data for input into the inversion program.

Tomographic Inversion. The soil volume was modelled as a three-dimensional collection of discrete cubes. The dimensions of the individual cubes and, thus, the dimensions of the model were determined by two factors: the wavelength of the seismic source and the distribution of rays within the model. Using the seismic source described in Section 2.2 and an instrumented hammer capable of recording the impulse response of the hammer, the impulse was seen to be that of a half-sine function having a duration of 0.25 ms. (Although it was similar in weight, this was not the same hammer used in further testing.) The dominant period of this function was 0.5 ms, corresponding to a frequency of 2 kHz. Assuming a nominal seismic

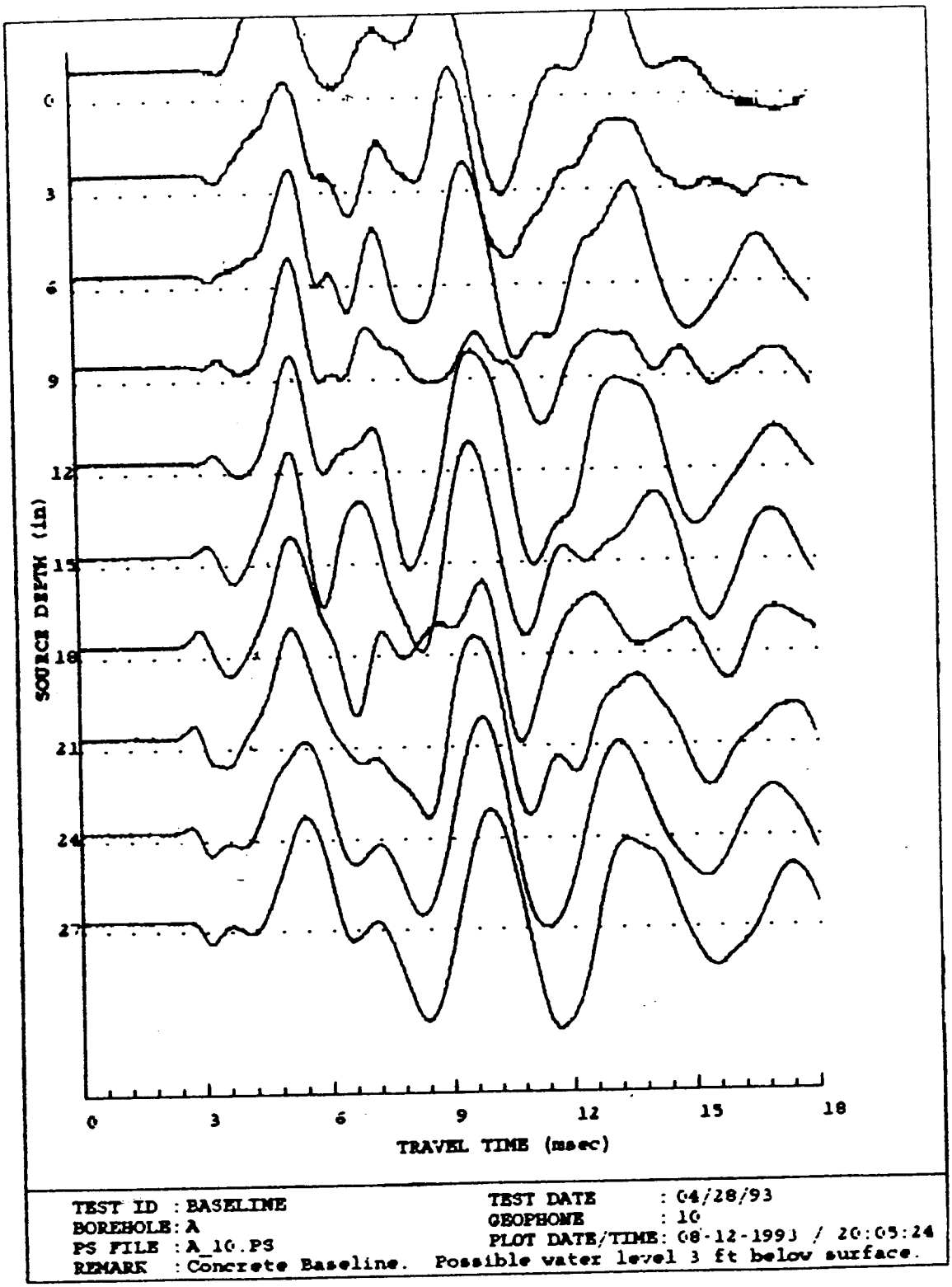

Figure A.2.5 Sample Receiver Gather Data

velocity of 200 m/s, the dominant wavelength was then 0.1 m (3.9 in). For a nominal seismic velocity of 100 m/s, the wavelength would be about 20 cm (7.9 in). Features on the order of one-half to one wavelength are adequately sampled by the seismic energy travelling through the soil. Thus, features of this size can be "detected" by a ray. Under these conditions, a reasonable block size is about 15.2 cm (6 in). A block size of 16.3 cm (6.42 in) was chosen and actually used in this analysis.

The dimension of the blocks is also dictated by the ray coverage. If the blocks are too small, a large number of them will be under-sampled, resulting in an extremely sparse system of equations. If block size is too large, velocity features within the soil will be averaged over too large of a volume. To investigate ray coverage, an initial block size is chosen. After inversion, the ray coverage is examined and adjusted, if necessary. For this experiment, the initial block size of 16.3 cm (6.42 in) provided adequate ray coverage and was not adjusted.

The soil volume within the tank was thus modeled as a cube of nine blocks on a side. In addition, the inversion program used required a "rind" of two blocks around the region to be modeled. Including these additional blocks, the inversion model consisted of 2197 blocks (13x13x13).

The inversion algorithm used for this project consisted of three steps: finite difference calculation of travel times based on the starting model, backprojection of rays from source to receiver based on the travel-time grid to determine raypaths, and inversion of the matrix equation using the conjugate-gradient algorithm to obtain a solution for the slowness of each block in the model.

The first step, calculating travel times using a finite difference method, is based on Vidale's finite difference travel-time calculation method (1988). Vidale's algorithm uses curved wavefronts to create a travel-time grid centered on a given source for every point within the model space. This algorithm, implemented by Doser *et al* (1994), is capable of taking into account anisotropy. However, only isotropic media were considered for this study.

Next, the particular raypath for a given source/receiver pair is calculated by backprojection: searching the travel-time grid for the fastest path from source to receiver. During backprojection, the path lengths through each block traversed are determined.

Finally, the matrix equation is solved using the conjugate-gradient algorithm of Scales (1986). The conjugate-gradient algorithm provides an efficient means for solving equation 1.8 without having to actually perform the matrix inversion. The conjugate-gradient algorithm uses successive approximations of the solution vector to obtain a search vector which samples the error space. From this search vector, a residual travel-time vector equal to the inverse of the norm of the gradient is calculated. This vector "points" in the direction of the solution. The search vector is updated after each iteration, and calculation continues until the residual vector meets specified error criteria.

The solution vector contains the changes to starting model slownesses. The starting model is updated with the solution vector. The "goodness" of the resulting slowness solution is indicated by two measures: the root-mean-squared (RMS) travel-time misfit and the average adjustment to block slowness (DS). The RMS misfit

indicates how well travel times obtained from the solution slowness vector match the observed travel times weighted by the travel-time uncertainties. RMS values of one indicate that the calculated slowness models fit the travel time observations to within their uncertainties. The RMS misfit is calculated using the following expression:

$$\varepsilon_{RMS} = \sqrt{\frac{1}{N}\sum_{i=1}^{N}\left(\frac{t_i - t_{pred,i}}{\varepsilon_i}\right)^2}, \qquad \text{(eq. 2.2)}$$

where ϵ_{RMS} is the RMS misfit,

t_i and $t_{pred,i}$ are the observed and predicted travel times, respectively,

ϵ_i is the travel time uncertainty for the ith observation, and

N is the total number of observations.

The average adjustment to block slowness indicates the rate of convergence of the calculations and is related to the *a priori* uncertainty. As the program converges, the adjustment to block slowness decreases. The average adjustment is calculated from the following equation:

$$DS = \frac{1}{N}\sum_{i=1}^{N}\frac{\Delta s_i}{e_i}, \qquad \text{(eq. 2.3)}$$

where DS is the average change in slowness,

Δs_i is the slowness value of the i^{th} model block,

ϵ_i is the *a priori* slowness uncertainty for the i^{th} model block, and

N is the total number of blocks whose slowness values changed.

A DS value of less than one indicates that block slownesses are being adjusted by amounts less than their uncertainty.

2.3 Error Analysis.

Method of Kreinovich. To assess the effects of data and model errors on the inversion results, a method developed by Krienovich (1993) was used. This technique allows statistical quantification of the resulting uncertainties in velocity distribution, given an uncertainty of the values of individual data. It also allows investigation of the effect of such errors as source location, geophone location, and starting model uncertainty. This Monte-Carlo technique allows estimation of both random and systematic errors in the data, although only random errors were considered here. The input data to the tomographic inversion are randomly perturbed about their expected values. The amount of pertubation is a random variable with a Gaussian distribution and standard deviation equal to the observed travel-time error. These data are then inverted, and a solution is obtained. The process is repeated a number of times, each time obtaining a solution. From the solution sets, the standard deviation is calculated. This standard deviation represents the standard error in the solution. In principle, the effect of starting model errors, termed the Information Density Matrix, could also be calculated in the same manner. However, as discussed in the next chapter, instability in the inversion process itself severely restricted the stated uncertainty of the starting model.

Chapter III

3. Results and Conclusions

In this final chapter, the experimental results for baseline, maximum ice, and thawing conditions, along with conclusions, are presented. Graphs representing soil temperature and resistance are shown, as is the *a priori* starting model. A series of graphics showing the inversion results is also provided.

3.1 General.

Time Series Temperature and Resistance. Throughout the testing period, soil temperature and resistance were monitored, as described in Chapter II. The time series plots of these data are shown below (Fig. A.3.1 and Fig. A.3.2). Note that the plotted data pertain only to probe column B. Results for the other two probe columns are comparable.

The freezing cycle lasted twenty days. The spikes representing the temperature on days 5 and 12 were produced as shown because of delays in resupplying crushed dry ice to the surface. The deepest temperature probe level did not reach zero centigrade until near the end of the freezing cycle, whereas the near-surface levels froze within three days.

A comparison of the temperature curve of Fig. A.3.1 with the soil resistance curve of Fig. A.3.2 shows that as soon as a probe level reached ice conditions, the soil resistance began to increase: first gradually, as crystals began to form and the soil turned into a semi-frozen state, and then rapidly (by several orders of magnitude).

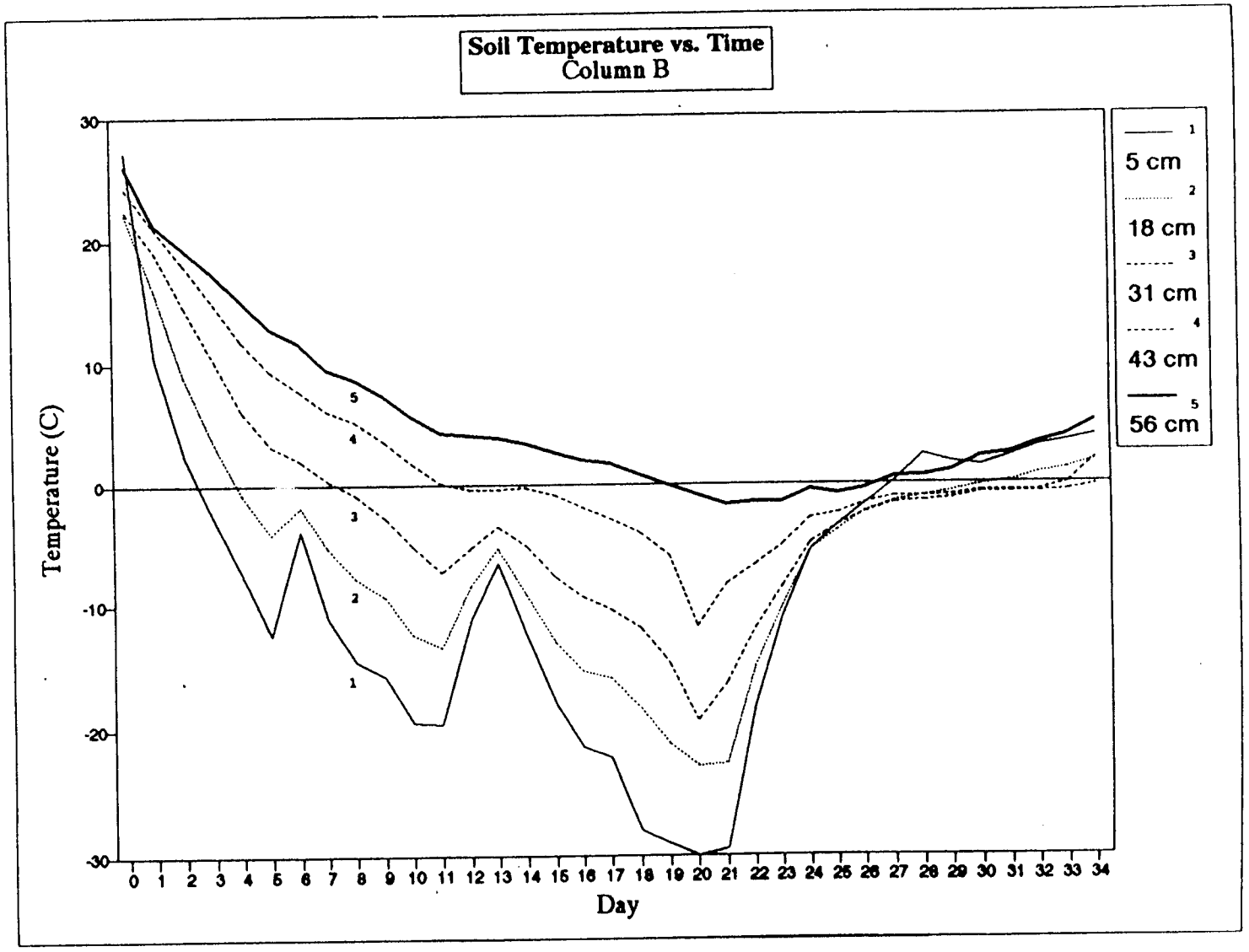

Figure A.3.1 Column B Temperature vs. Time

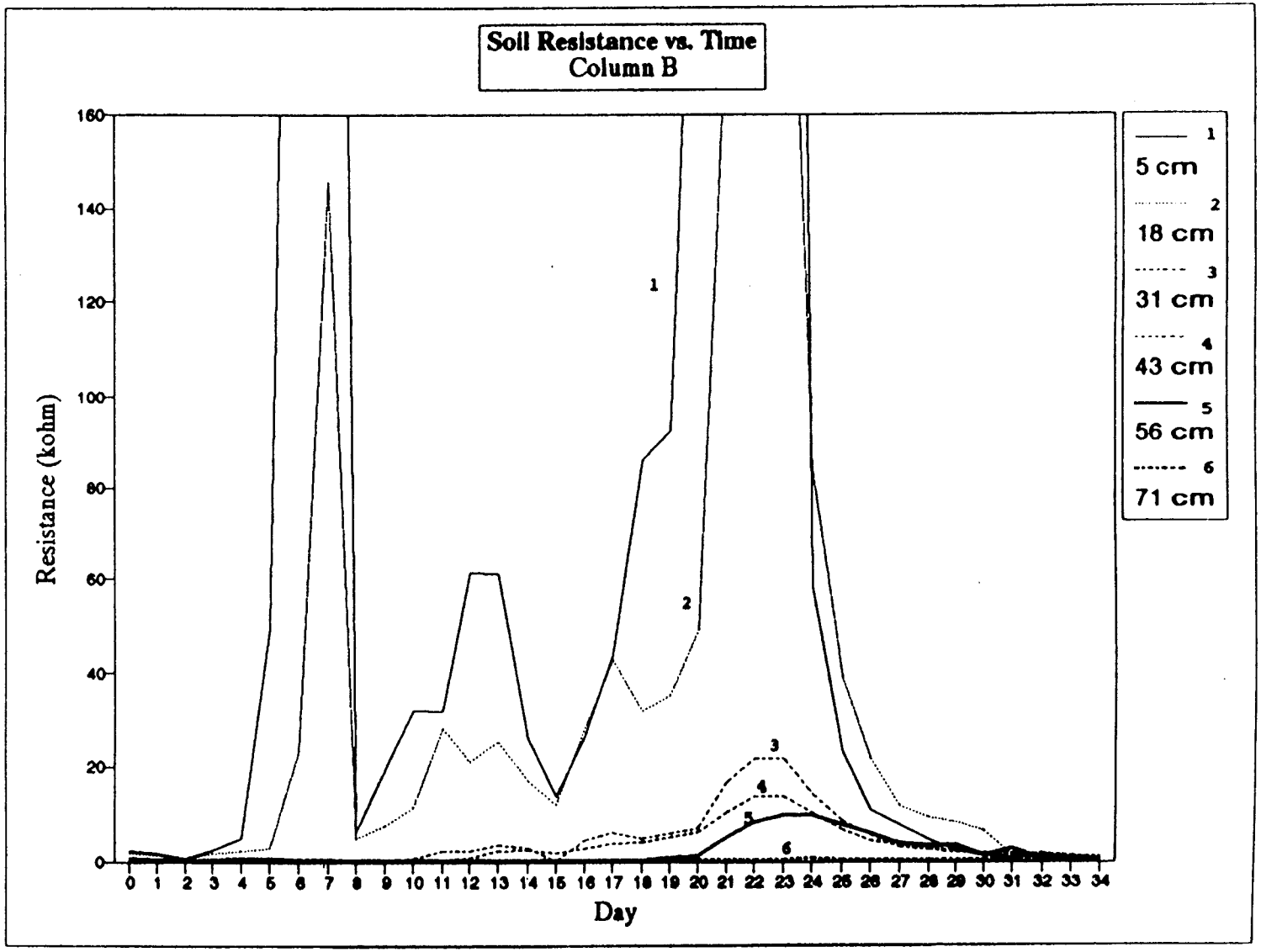

Figure A.3.2 Column B Soil Resistance vs. Time

Even though cooling of the tank's upper surface ended on day twenty, the deepest resistance probe levels showed *increases* in resistance for several days afterward. To allow thawing to take place gradually, the top surface of the tank was held near a constant 4.4°C (40°F). All temperature probe levels produced a roughly isothermal temperature curve during the thawing period, while the resistance decreased (very rapidly, in cases of shallow resistance probe levels). This suggests that although ice may have been present within the soil, the presence of any liquid water kept its level far below that of hard-frozen soil.

These preliminary data show the time series response of the tank for a fixed probe column. The following graphs show the spatial distribution of temperature and resistance for a fixed time.

Water and Surface Level Changes. The transition from unfrozen to frozen soil decreased the pore pressure within the soil and drew water up. During the thawing period, this water was recovered. The intake of water by the soil volume was monitored throughout the experiment's period (Fig. A.3.3). A malfunction in the siphon during the first eight says of freezing prevented the accurate collection of water intake amounts. However, note that on day eleven, there was an initially rapid, then fairly constant, intake of water by the soil volume, accompanied by a roughly linear increase in surface heave (Fig. A.3.4).

3.2 Baseline Data.

Temperature and Resistivity. The soil temperature and resistivity profiles prior to the start of freezing were fairly uniform (Figs. A.3.5 and A.3.6). The slight

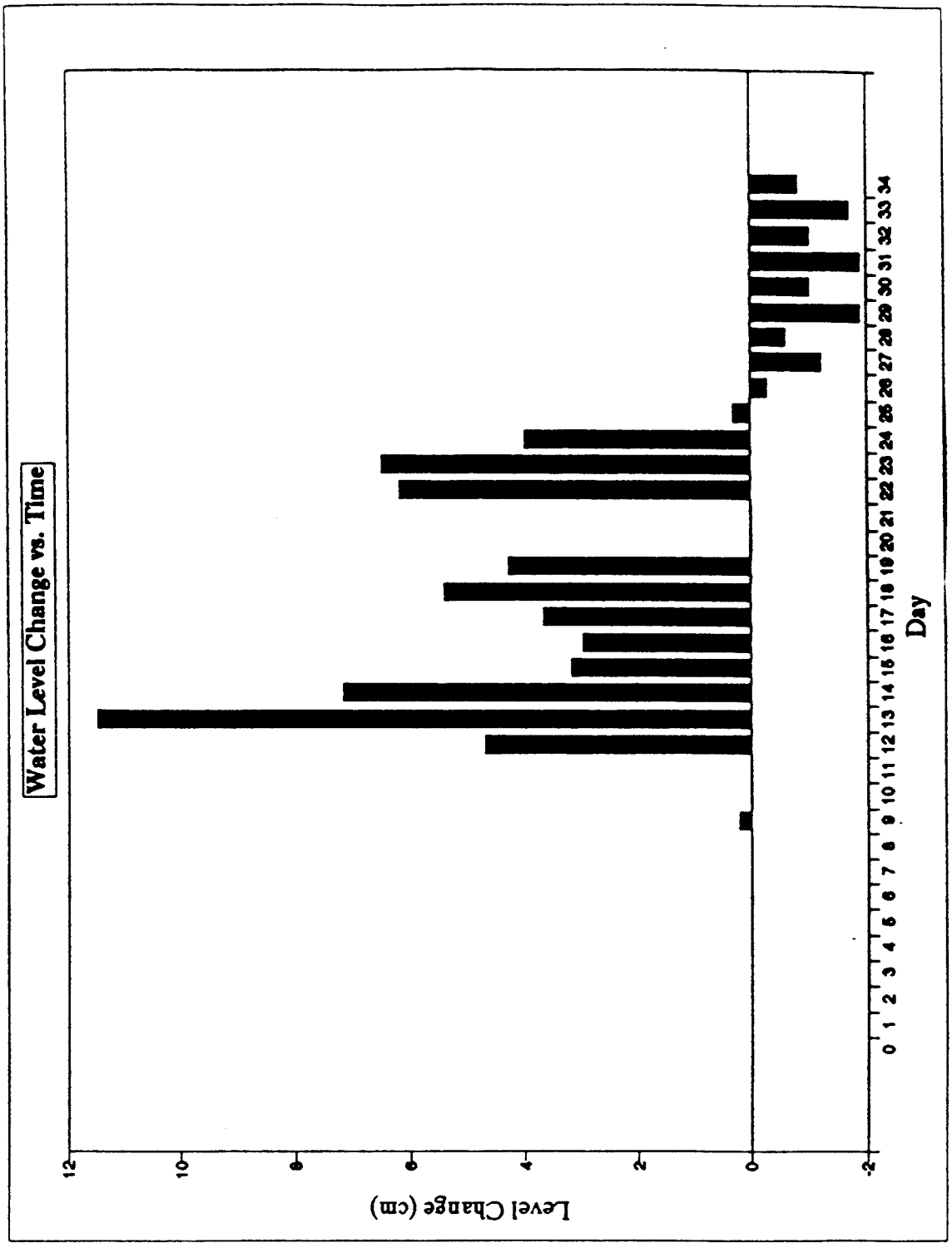

Figure A.3.3 Water Intake vs. Time

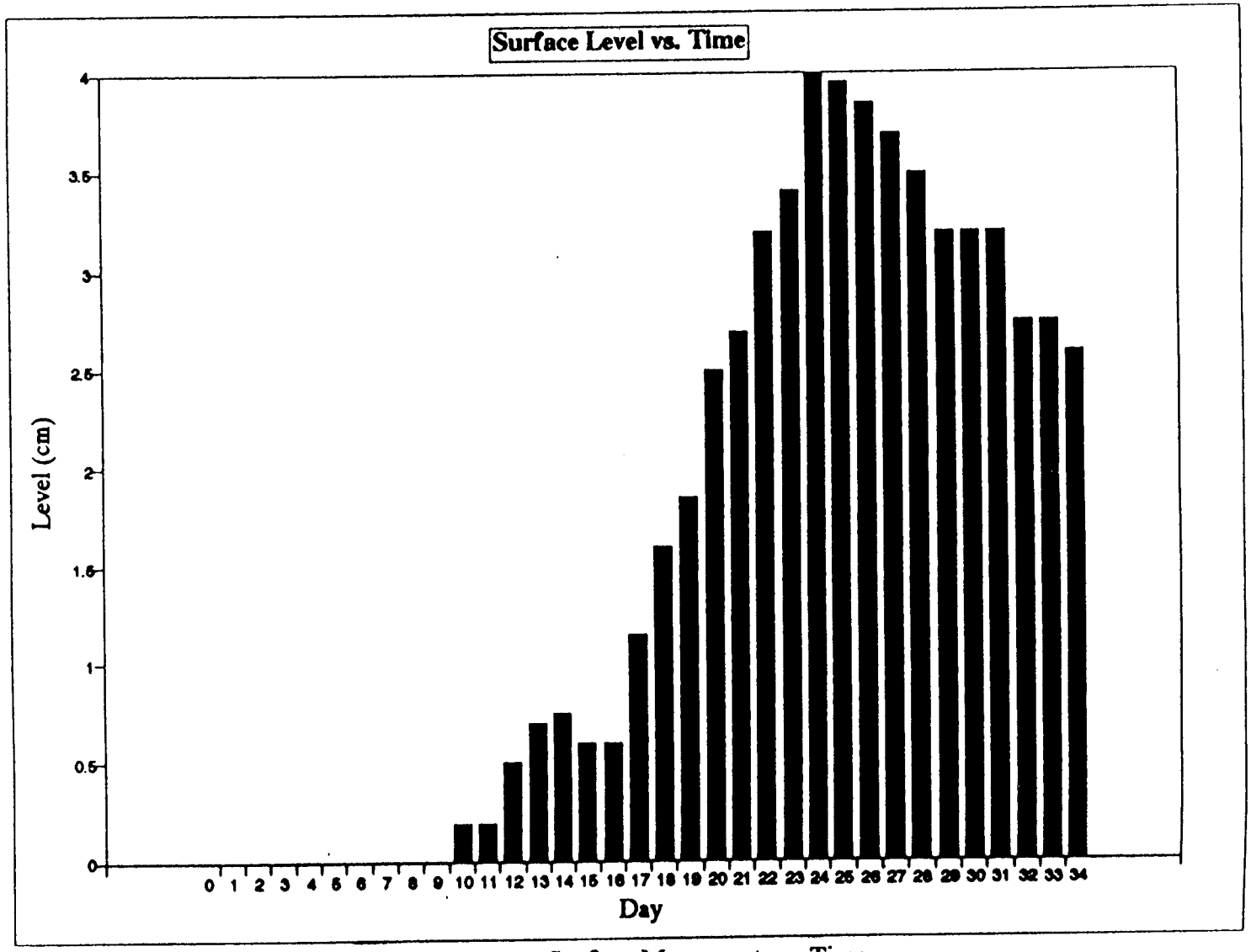

Figure A.3.4 Surface Movement vs. Time

variation of resistance with depth was probably due to a variation in soil compaction and the presence of a capillary fringe from depths of 61 cm (24 in) to the surface. The slight increase in temperature toward the surface was probably due to the residual heat produced when asphalt was placed on the tank prior to taking baseline data.

Tomographic Results. The results of the P- and S-inversions are shown in Figs. A.3.7 through A.3.10. The *a priori* model for the P-inversion consisted of a high-velocity layer atop other layers and a uniform, lower-velocity bottom layer. The high-velocity layer represented the asphalt cap. Though it was not part of the physical space modeled, it served as a refracted layer.

Fig. A.3.10 shows the gradual transition from high to low velocity in the *a priori* model. The transition occurred because of difficulties encountered in the backprojection routine of the inversion program and is not necessarily indicative of the tank's soil conditions. No such transition region was used in the S-*a priori* model.

In each of the figures, the right image represents the ray distribution within the model. The left image shows the resulting velocity solution. The baseline results show a generally homogeneous velocity distribution.

The *a priori* slowness uncertainty was required to be small (2%) for the inversion to converge. This uncertainty was, in general, smaller than travel time uncertainties, which were around 15%.

The P-inversion concluded with an RMS misfit of 4.9. The S-inversion resulted in an RMS misfit of 4.7.

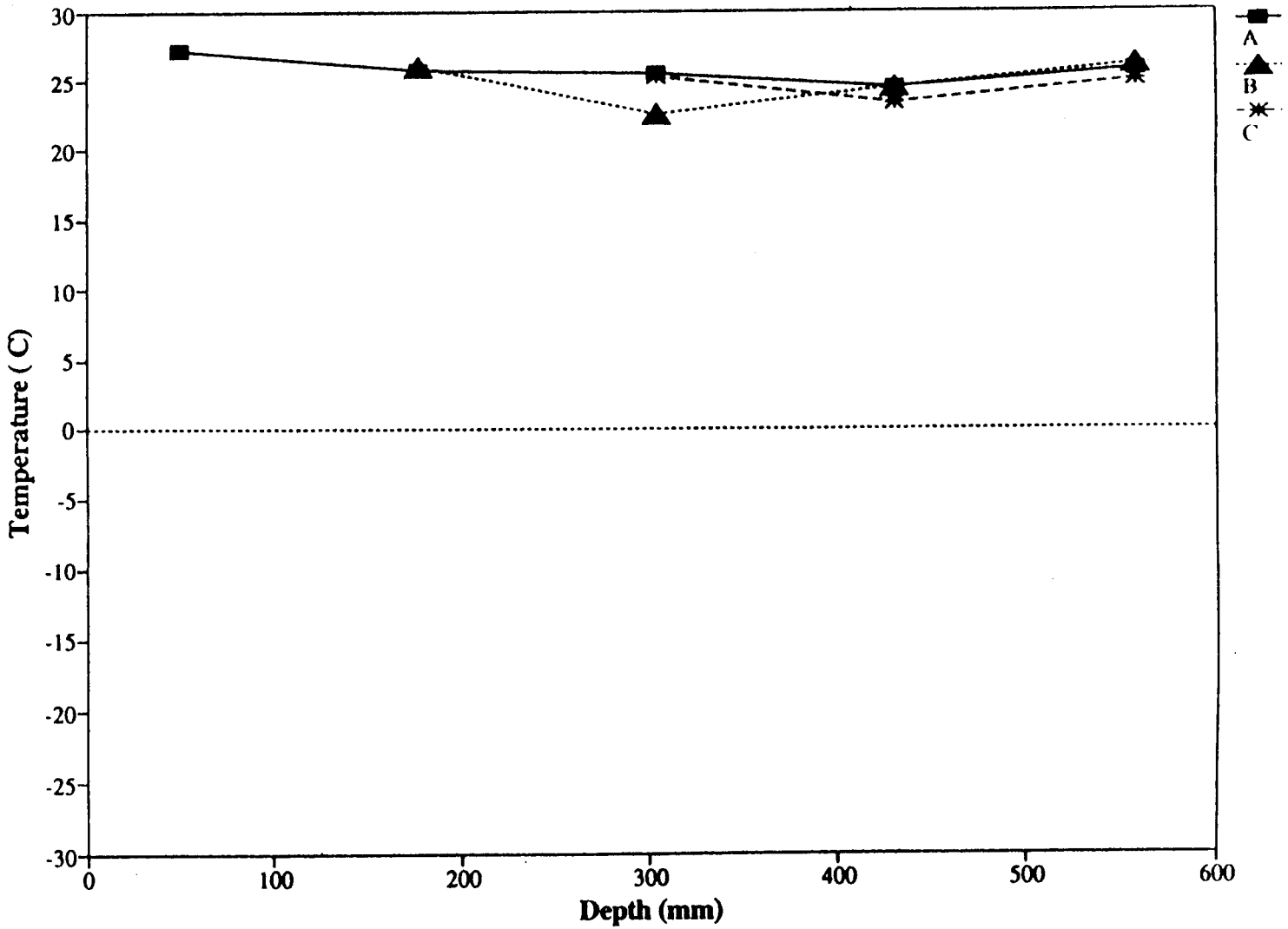

Figure A.3.5 Baseline Soil Temperature

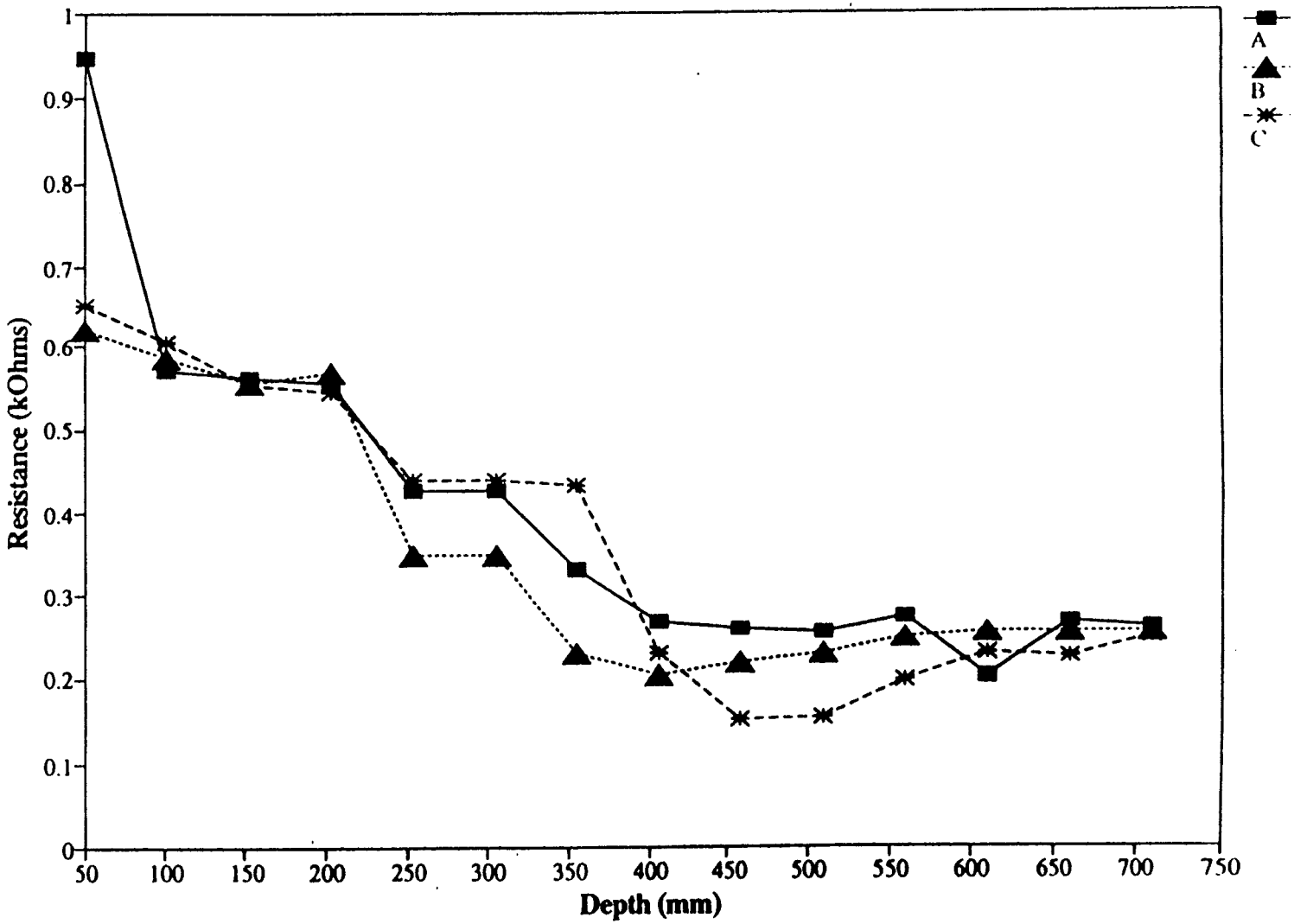

Figure A.3.6 Baseline Soil Resistance

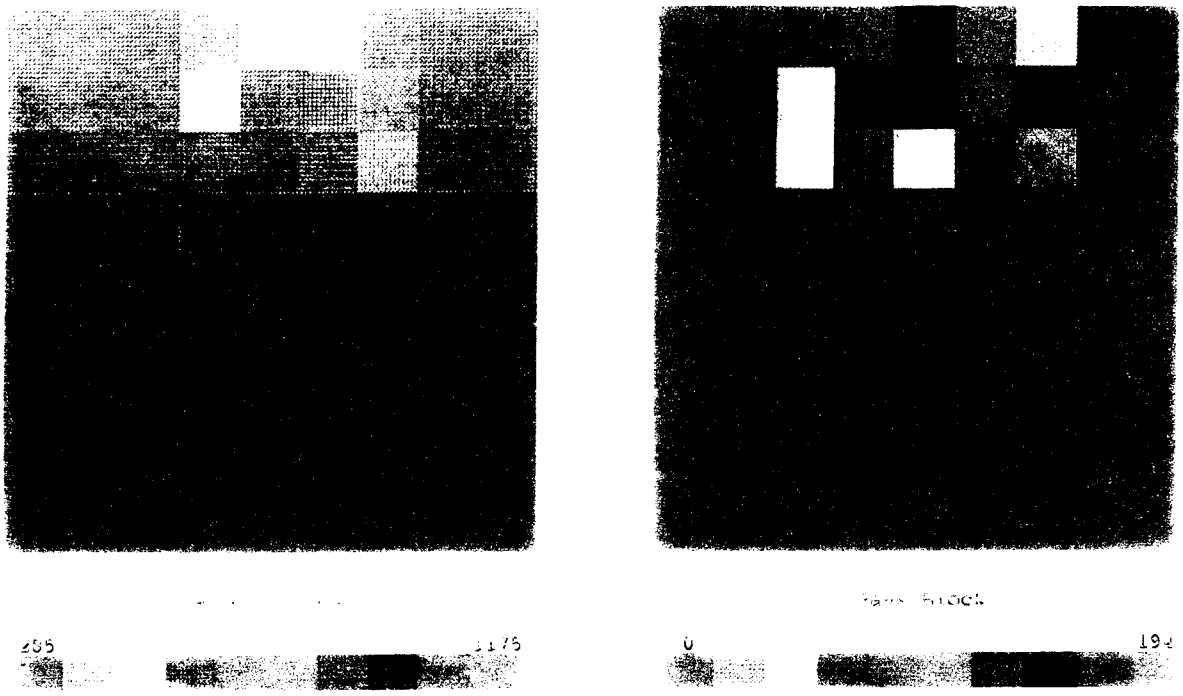

Figure A.3.7 Baseline P Velocity, Vertical Slice

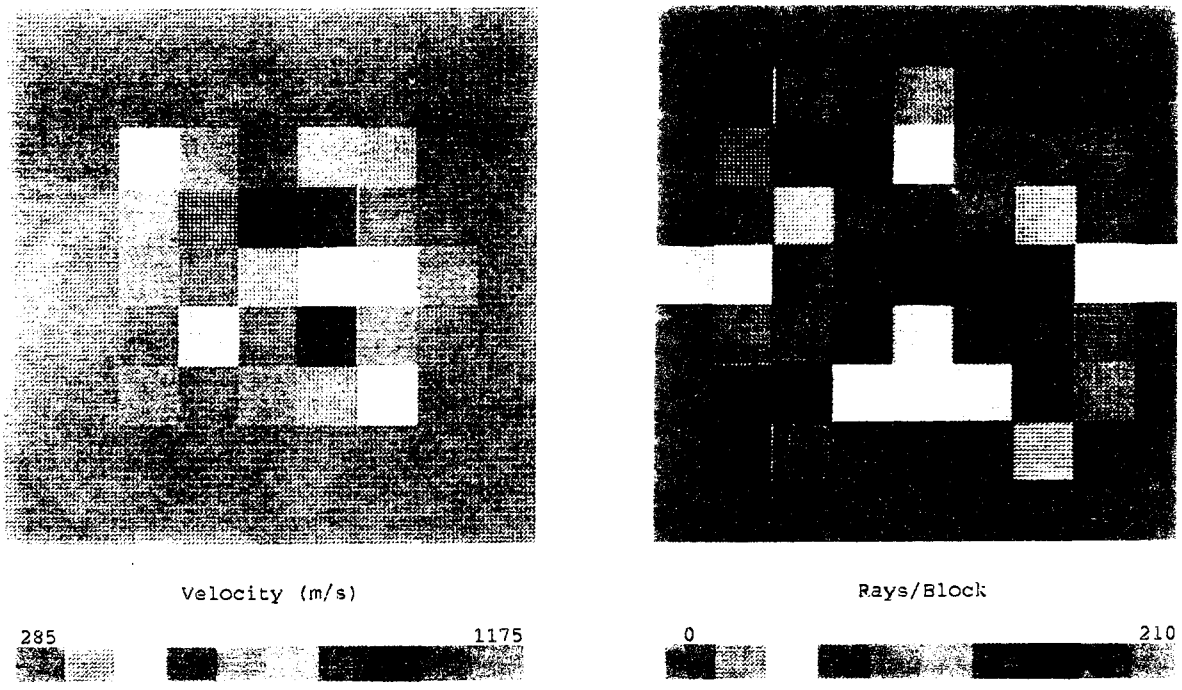

Figure A.3.8 Baseline P Velocity, Horizontal Slice

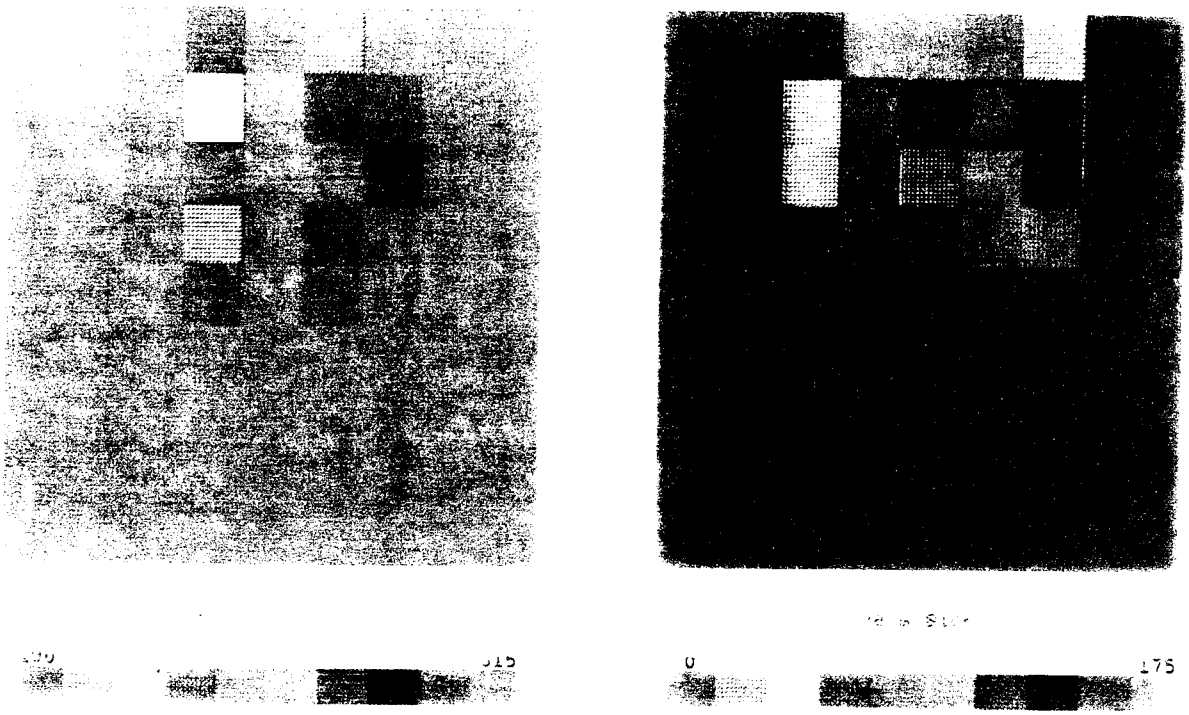

Figure A.3.9 Baseline S Velocity, Vertical Slice

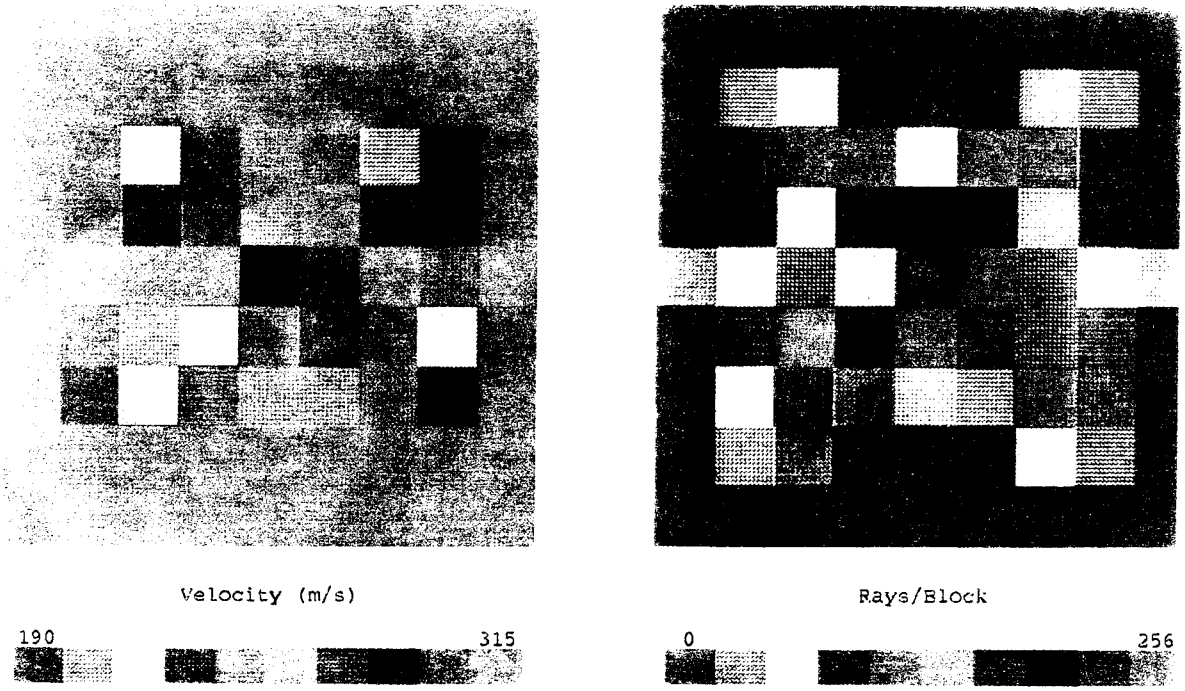

Figure A.3.10 Baseline S Velocity, Horizontal Slice

Discussion. The ray coverage strongly controlled the resulting inversion results. Raypaths were strongly concentrated in regions between sources and receivers. The geometry of the source/receiver layout controlled the ability of the inversion routine to update the *a priori* model. This caused the inversion solution to be strongly controlled by the starting model. In the face of uncertain and possibly inconsistent data, the resulting velocity model was not allowed to change enough so as to provide a very low RMS misfit.

3.3 Freezing Soil.

Temperature and Resistivity. After 20 days of freezing, the temperature and resistance profiles were as shown in Figs. A.3.11 and A.3.12. The asphalt surface was held at a temperature of about -50°C (-58°F). The base of the tank was in contact with the concrete floor, which was considered to be held at a constant 25.5°C (78°F). The temperature profile shown in Figure A.3.11 shows a linear temperature transition consistent with boundary conditions.

In comparing the temperature and resistance curves of Figs. A.3.11, it becomes clear that, although the soil apparently consisted of three distinct regions, it experienced below-freezing temperatures in all areas. The soil resistance was seen to increase by several orders of magnitude in the upper region of the tank. This was assumed to coincide with the hard-frozen soil layer, extending down to at least 200 mm (7.9 in). Below this hard-frozen region was a transition region whose resistance was 10 times that of the baseline but much less than that of the hard-frozen region.

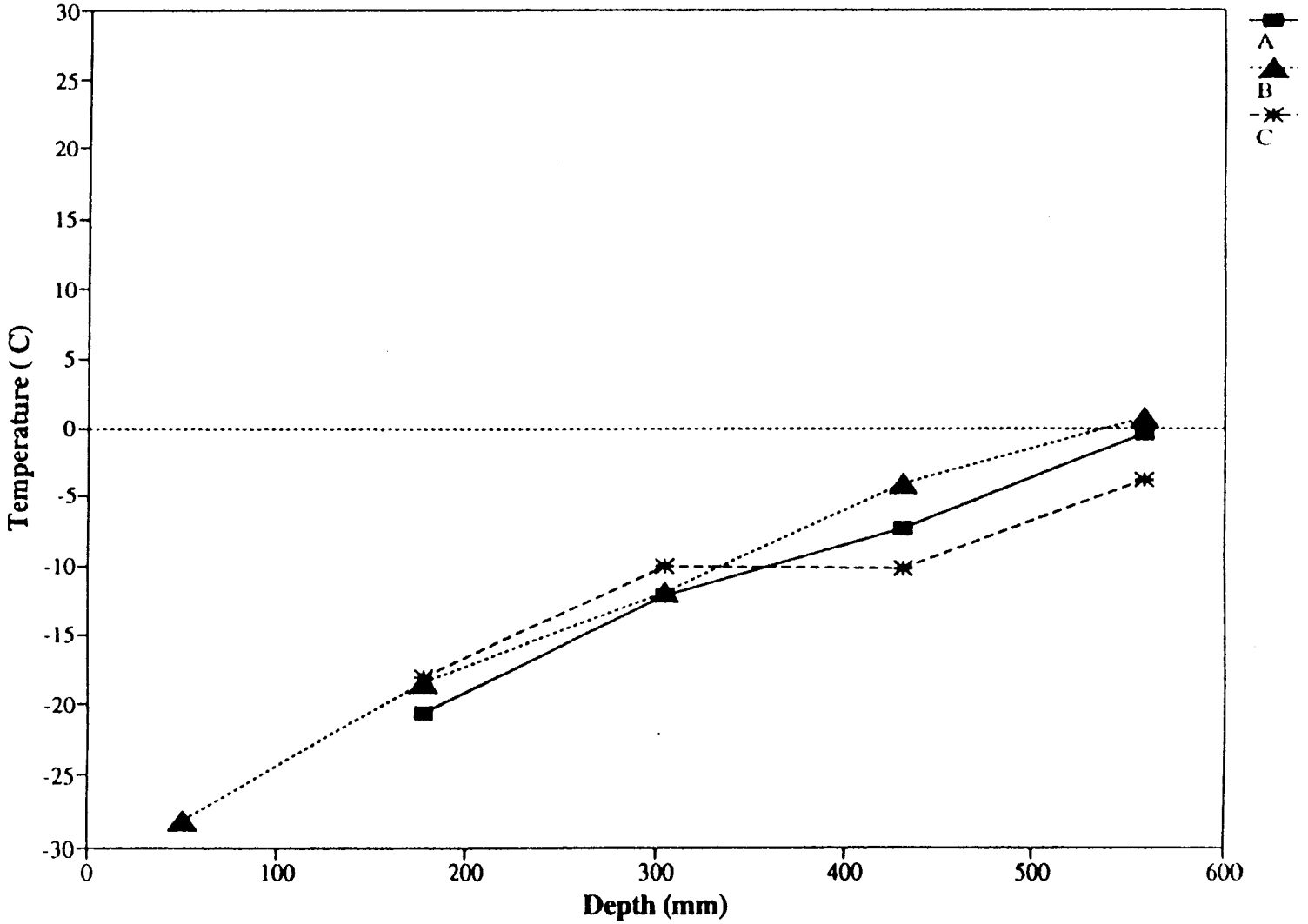

Figure A.3.11 Freezing Soil Temperature

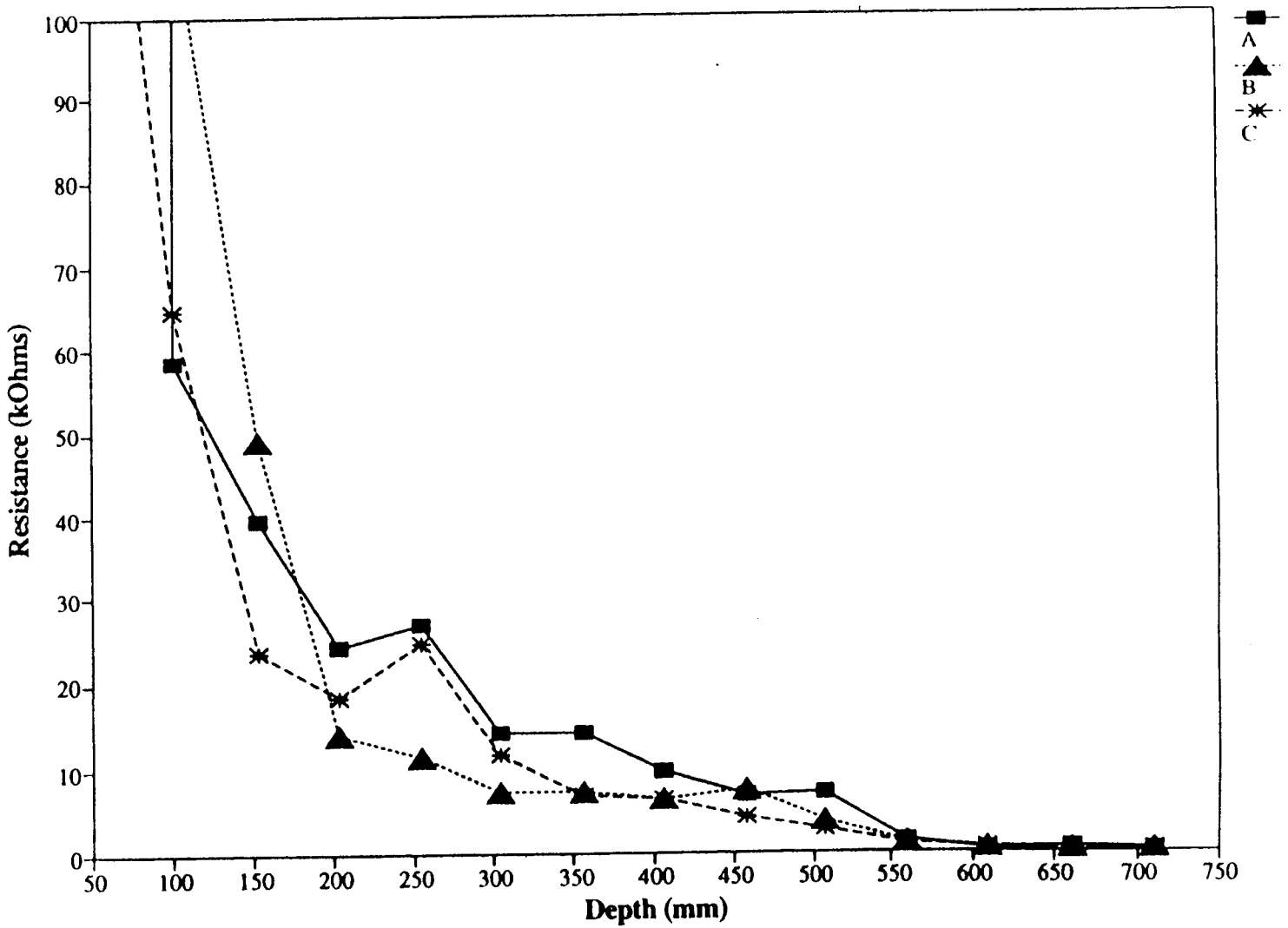

Figure A.3.12 Freezing Soil Resistance

Tomographic Results. The P- and S-inversions concluded with RMS misfits of 3.8 and 4.4, respectively. These misfits were slightly better than those obtained for the baseline results.

The velocities within the frozen tank clearly indicated an upper high-velocity region within the soil (Figs. A.3.13 and A.3.15). This region was at a depth of 16.9 to 33.9 cm (6.7 to 13.3 in) and had similar P and S results. The P-velocity was about six times greater than that of the unfrozen soil. The S-velocity was about three times greater. The ray coverage was comparable to that of the baseline tomography. It appears that the inversion was attempting to increase the *a priori* velocities down to a depth of 67.7 cm (26.7 in). The velocity region extended laterally across the entire tank (Figs. A.3.14 and A.3.16).

Discussion. As with the baseline data, the tomographic results were constrained by ray coverage. From the temperature and resistance plots, it appears that the frozen region extended down to about 50 cm (19.7 in). However, the region of greatest ray coverage extended down to only 33.8 cm (13.3 in), below which ray coverage rapidly diminished. This, coupled with the artificially low *a priori* uncertanties, did not allow the inversion to accurately determine the velocity in the lower portion of the tank. However, evidence from resistance and P- inversion results indicates that higher velocities did exist in the region.

3.4 Thawing Soil.

During thawing, the soil temperature was approximately isothermal, nearing 0°C (32°F) (Fig. A.3.17) . The resistance profile showed values intermediate of

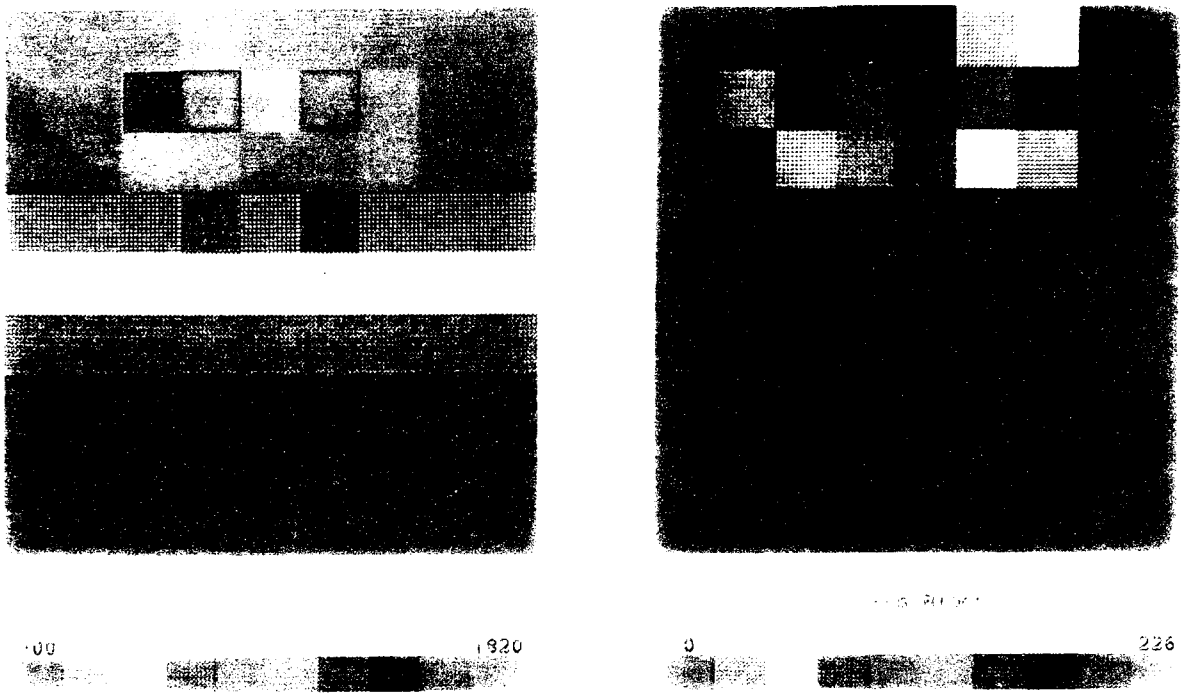

Figure A.3.13 Freezing Soil P Velocity, Vertical Slice

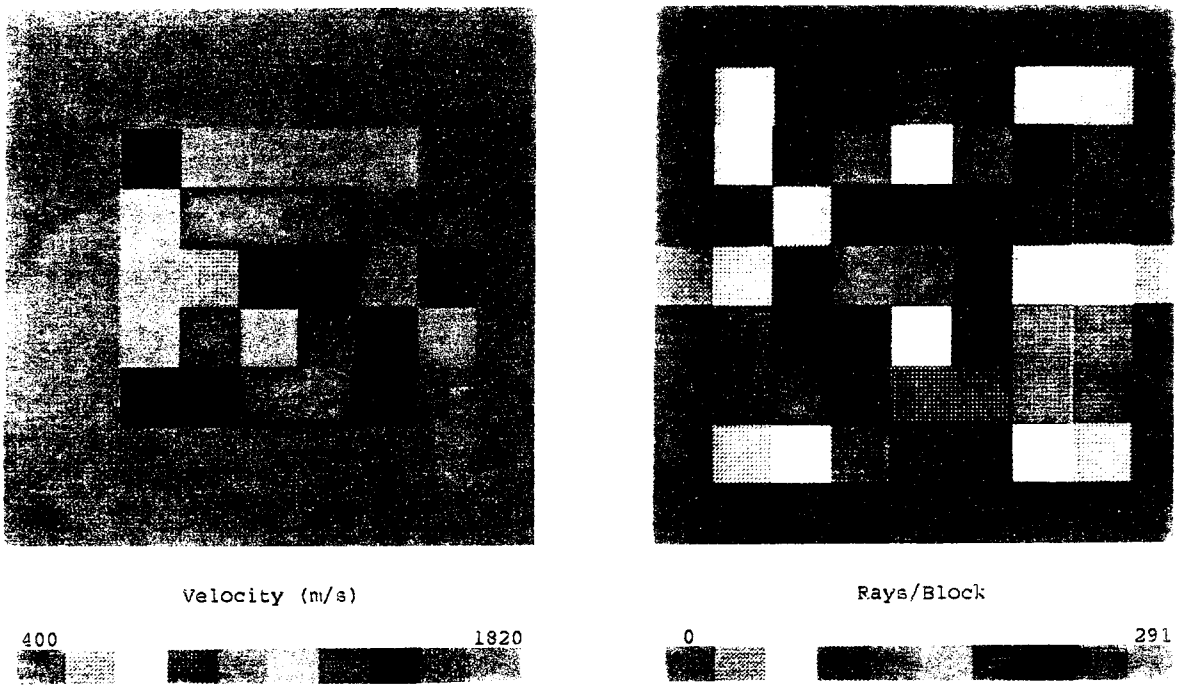

Figure A.3.14 Freezing Soil P Velocity, Horizontal Slice

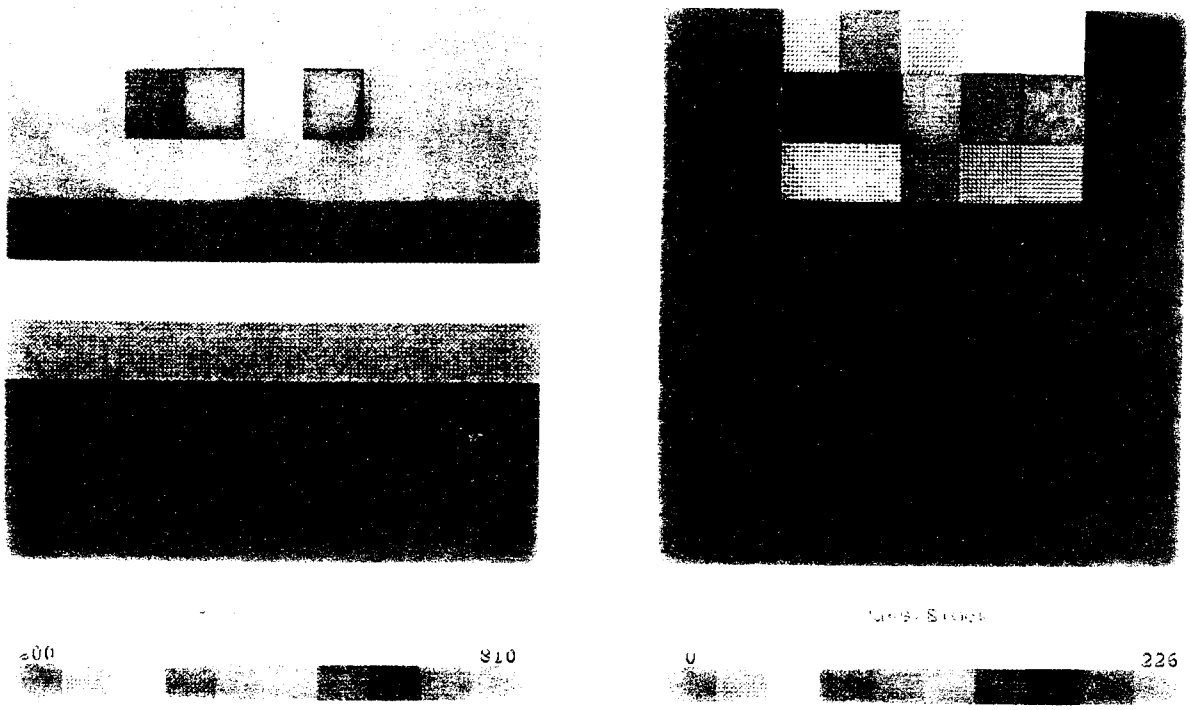

Figure A.3.15 Freezing Soil S Velocity, Vertical Slice

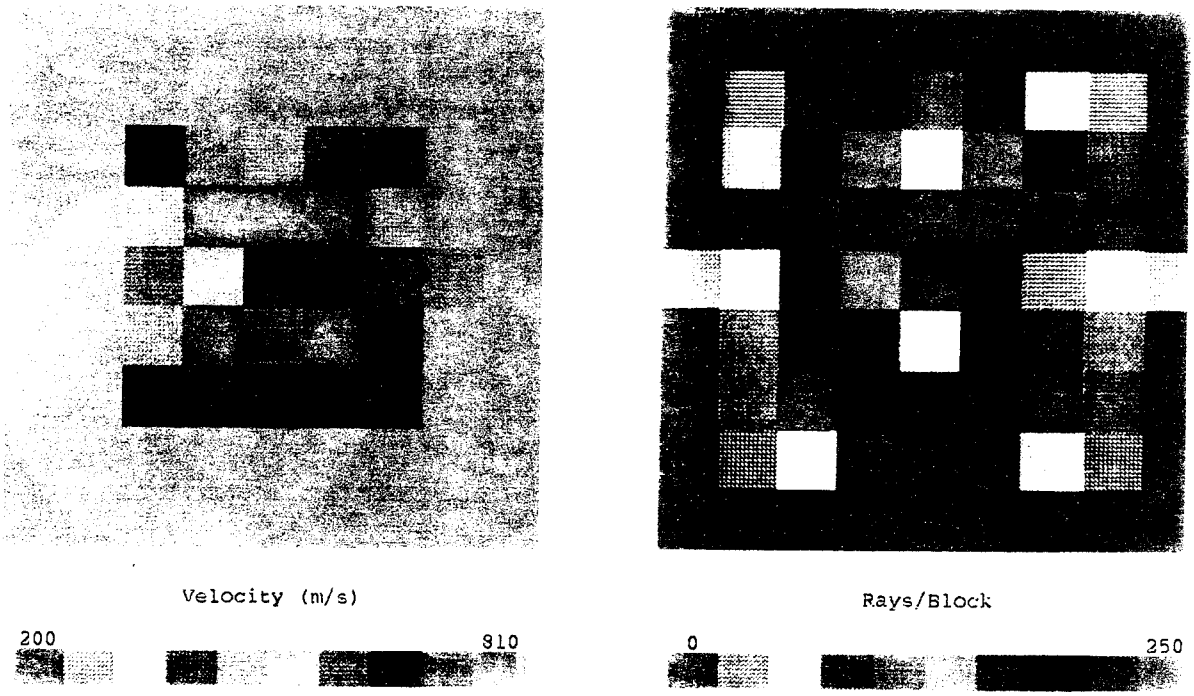

Figure A.3.16 Freezing Soil S Velocity, Horizontal Slice

those for baseline and frozen conditions. There still appeared to be a region of higher resistance above 25 cm (9.8 in)(Fig. A.3.18), but its partitioning into three resistance regions was not as distinct.

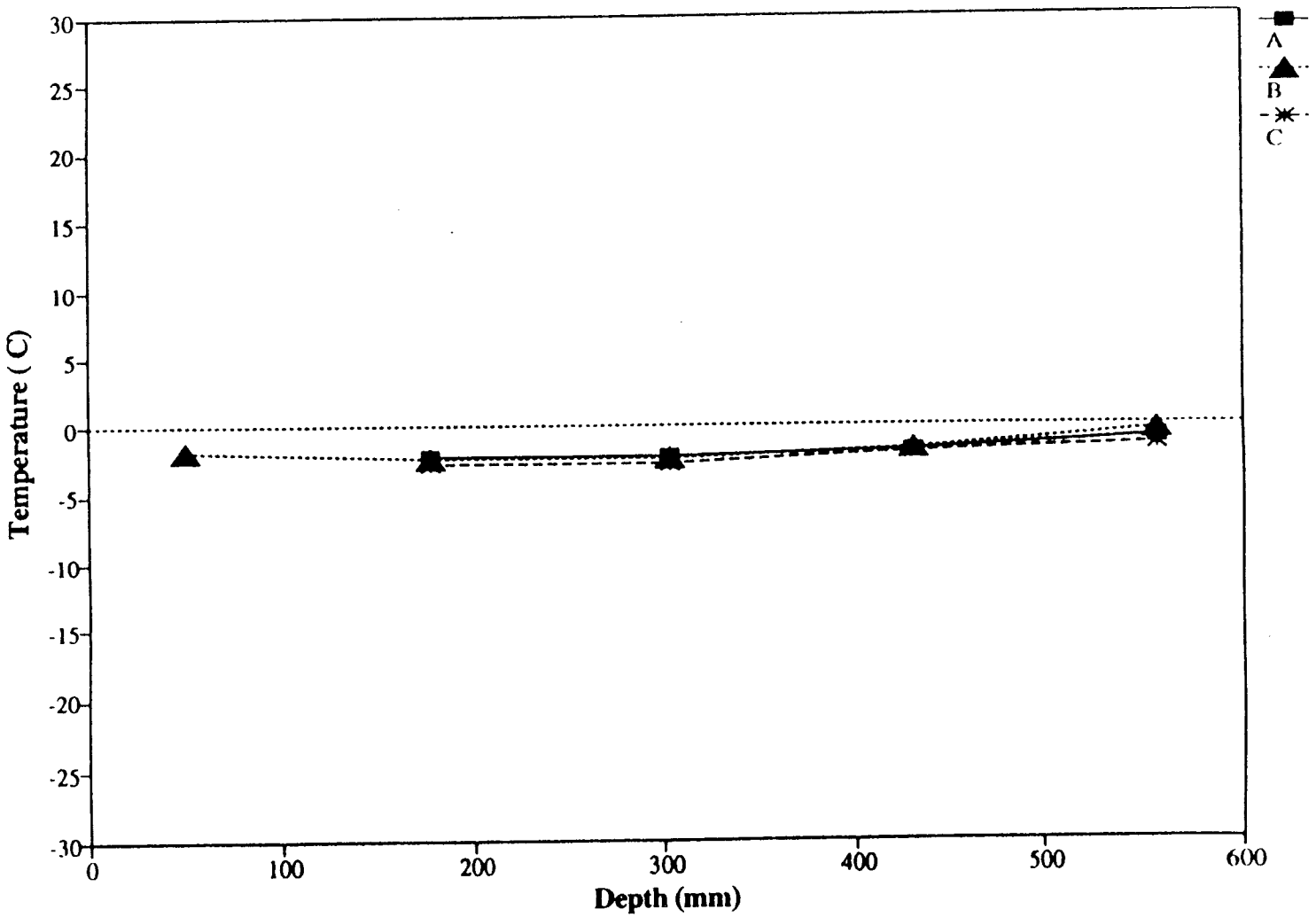

Figure A.3.17 Thawing Soil Temperature

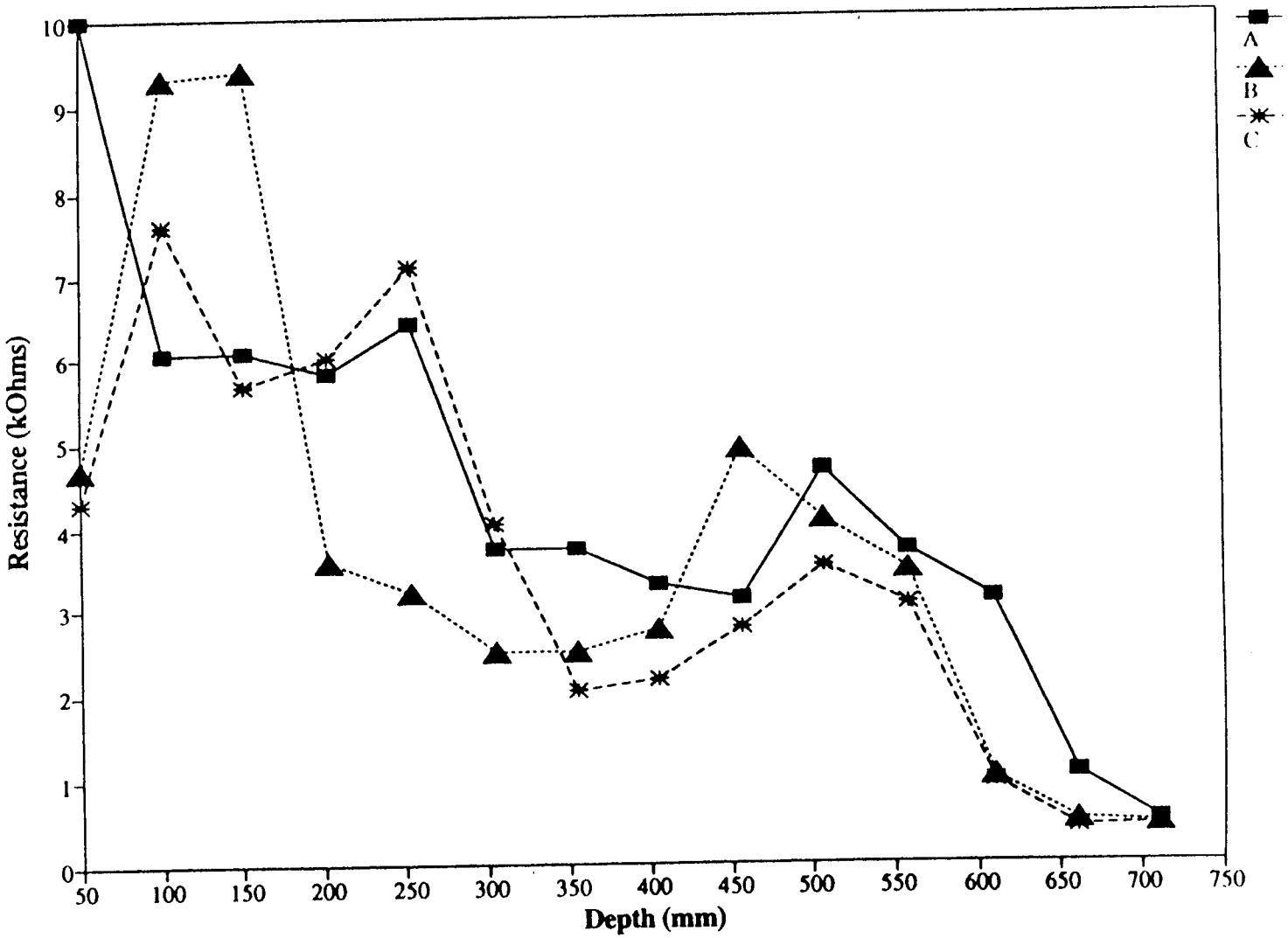

Figure A.3.18 Thawing Soil Resistance

References

Atkins, R.T., 1979, Determination of Frost Penetration by Soil Resistivity Measurements, U.S. Army Cold Regions Research and Engineering Laboratory Special Report 79-22, Hanover, New Hampshire.

Baker, M., 1993, Personal Communication.

Janoo, V.C., and Berg, R.L., 1993, Layer Moduli Determination During Freeze-Thaw Periods, Transportation Research Record, v. 1377, p.26-35.

Johnston, G.H. (ed), 1981, Permafrost: Engineering Design and Construction, John Wiley & Sons, New York, 540 pp.

Roblee, C.J., 1990, Development and Evaluation of Tomographic Seismic Imaging Techniques for Characterization of Geotechnical Sites, Ph.D. Dissertation, The University of Texas at Austin.

Scales, J.A., 1987, "Tomographic Inversion via the Conjugate Gradient Method," Amoco Production Company, Research Center, Tulsa, Oklahoma.

Scales, J.A., Gersztenkorn, A., and Treitel, S., 1988, Fast lp Solution of Large, Sparse, Linear Systems: Application to Seismic Travel Time Tomography, Journal of Computational Physics, v. 75, p. 413-433.

Seguin, M.K. and Frydecki, J., 1990, "Approach to Gravity Estimation of the Volume Ice Fraction in Discontinuous Permafrost," International Journal of Mining, V26, No.4.

Vidale, J., 1988, "Finite Difference Calculation of Travel Times," Bulletin of the Seismological Society of America, Vol. 78, No. 6, pp. 2062-2076, December.

Appendix

Solving a Linear System of Equations using *A Priori* Information

We can write a set of linear equations in the form

$$\mathbf{A}\,\hat{p} = \vec{d}\ , \qquad \text{(eq. A.1)}$$

where **A** is a matrix containing, for the travel time tomography problem, raypath lengths through a model block. $\hat{\mathbf{p}}$ is a vector containing block slowness values, and **d** is a vector containing the observed travel times. We can incorporate data uncertainties in this equation by weighting our data:

$$w_d\,\mathbf{A}\,\hat{p} = w_d\,\vec{d}\ , \qquad \text{(eq. A.2)}$$

where w_d is a diagonal matrix containing data weights.

We may have some idea of the value of $\hat{\mathbf{p}}$ beforehand, with associated weights on this *a priori* knowledge. We can express this information as

$$w_p\,\hat{p} = w_p\,\langle p\rangle\ , \qquad \text{(eq. A.3)}$$

where w_p is a diagonal matrix containing *a priori* parameter weights, and $<\mathrm{p}>$ is a vector containing the *a priori* parameter values.

Equations A.2 and A.3 can be written as an augmented matrix:

$$\begin{pmatrix} w_d & 0 \\ 0 & w_p \end{pmatrix} \begin{pmatrix} \mathbf{A} \\ I \end{pmatrix} \hat{p} = \begin{pmatrix} w_d & 0 \\ 0 & w_p \end{pmatrix} \begin{pmatrix} d \\ \langle p\rangle \end{pmatrix} \qquad \text{(eq. A.4)}$$

Multiplying,

$$\begin{pmatrix} w_d\mathbf{A} \\ w_p \end{pmatrix} \hat{p} = \begin{pmatrix} w_d & d \\ w_p & \langle p\rangle \end{pmatrix} \qquad \text{(eq. A.5)}$$

Squaring this equation gives

$$\begin{pmatrix} w_d^T \mathbf{A}^T & w_p^T \end{pmatrix} \begin{pmatrix} w_d \mathbf{A} \\ w_p \end{pmatrix} \hat{p} = \begin{pmatrix} w_d^T \mathbf{A}^T & w_p^T \end{pmatrix} \begin{pmatrix} w_d & d \\ w_p & \langle p \rangle \end{pmatrix} \qquad \text{(eq.A.6)}$$

And finally, after multiplication, we arrive at

$$\left(\mathbf{A}^T w_d^2 \mathbf{A} + w_p^2\right)\hat{p} = \mathbf{A}^T w_d^2 d + w_p^2 \langle p \rangle \qquad \text{(eq. A.7)}$$

To solve for $\hat{p}$, we multiply both sides of equation A.7 by the inverse of $(A^T w_d^2 A + w_p^2)$. Thus,

$$\hat{p} = \left(\mathbf{A}^T w_d^2 \mathbf{A} + w_p^2\right)^{-1} \mathbf{A}^T w_d^2 \quad d + \left(\mathbf{A}^T w_d^2 \mathbf{A} + w_p^2\right)^{-1} w_p^2 \quad \langle p \rangle \qquad \text{(eq. A.8)}$$

Equation A.8 can be seen to be a combination of terms involving the observed data, **d**, the *a priori* information, <p>, and the data and *a priori* uncertainties. The calculated value of $\hat{p}$ will range from the data-controlled value to the *a priori* value, depending upon the relative sizes of the uncertainties. If the data uncertainty is much smaller than the *a priori* uncertainty, the solution will tend toward the data-controlled value. If the data are known with much less uncertainty than the *a priori* value of <p>, the solution will tend toward <p>. In essence, this method of solution will tend toward the *a priori* value unless the data give compelling evidence to the contrary.

Applied to this study, Equation A.8 becomes the following:

$$\Delta \hat{s} = \left(\mathbf{A}^T w_d^2 \mathbf{A} + w_p^2\right)^{-1} \mathbf{A}^T w_d^2 \quad \Delta t + \left(\mathbf{A}^T w_d^2 \mathbf{A} + w_p^2\right)^{-1} w_p^2 \quad \langle \Delta s \rangle \ , \qquad \text{(eq. A.9)}$$

where Δs is the calculated change in block slowness, Δt is the travel time residual, and $\langle \Delta s \rangle$ is the change in block slowness of the *a priori* model.

Appendix B

SOIL RESISTIVITY PROFILES ON THE TEST DATES
WITHIN THE SUBGRADE SOILS

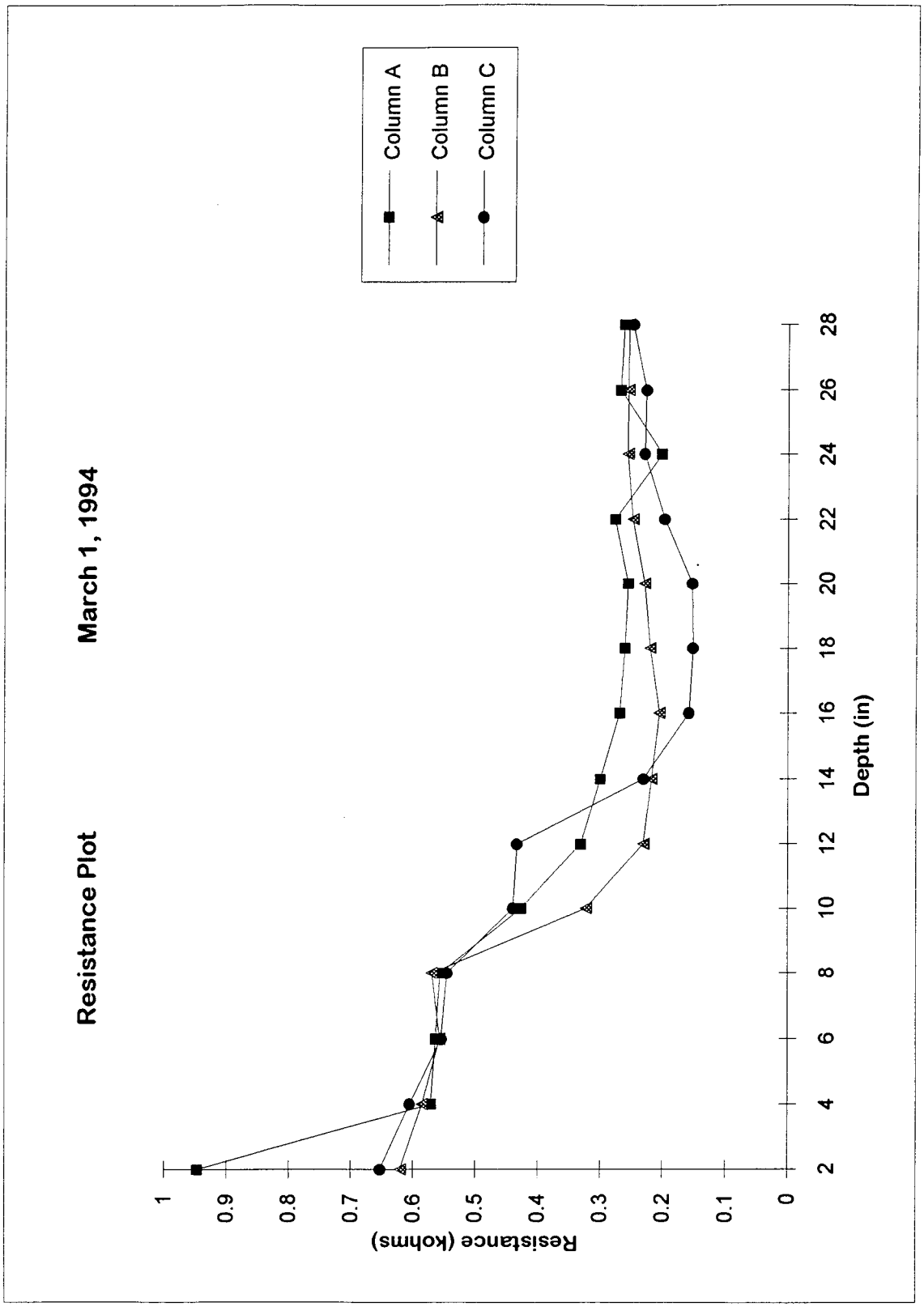
Resistance Plot
March 1, 1994
Column A
Column B
Column C
Resistance (kohms)
1
0.9
0.8
0.7
0.6
0.5
0.4
0.3
0.2
0.1
0
Depth (in)
2
4
6
8
10
12
14
16
18
20
22
24
26
28

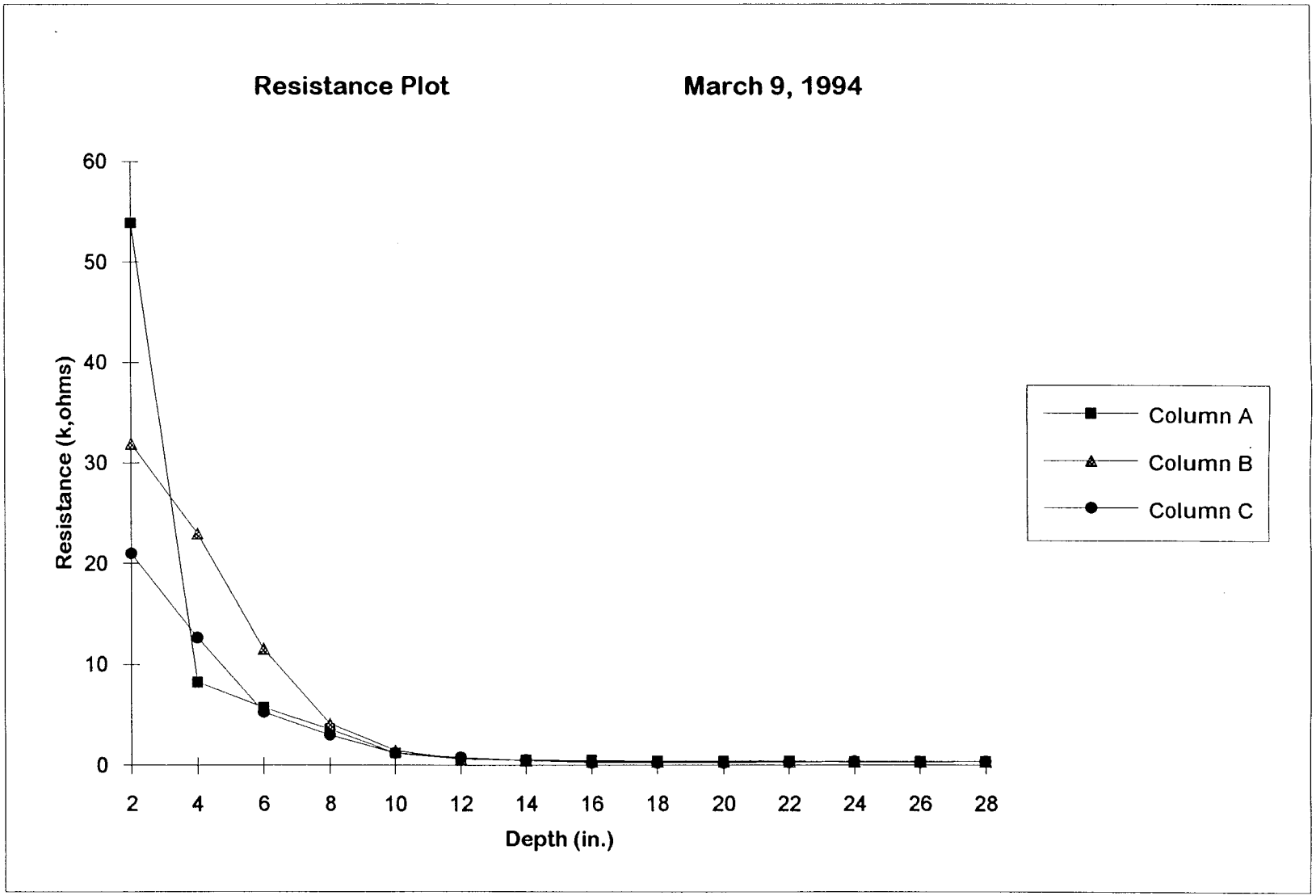
Resistance Plot
March 9, 1994
Resistance (k,ohms)
60
50
40
30
20
10
0
2
4
6
8
10
12
14
16
18
20
22
24
26
28
Depth (in.)
Column A
Column B
Column C

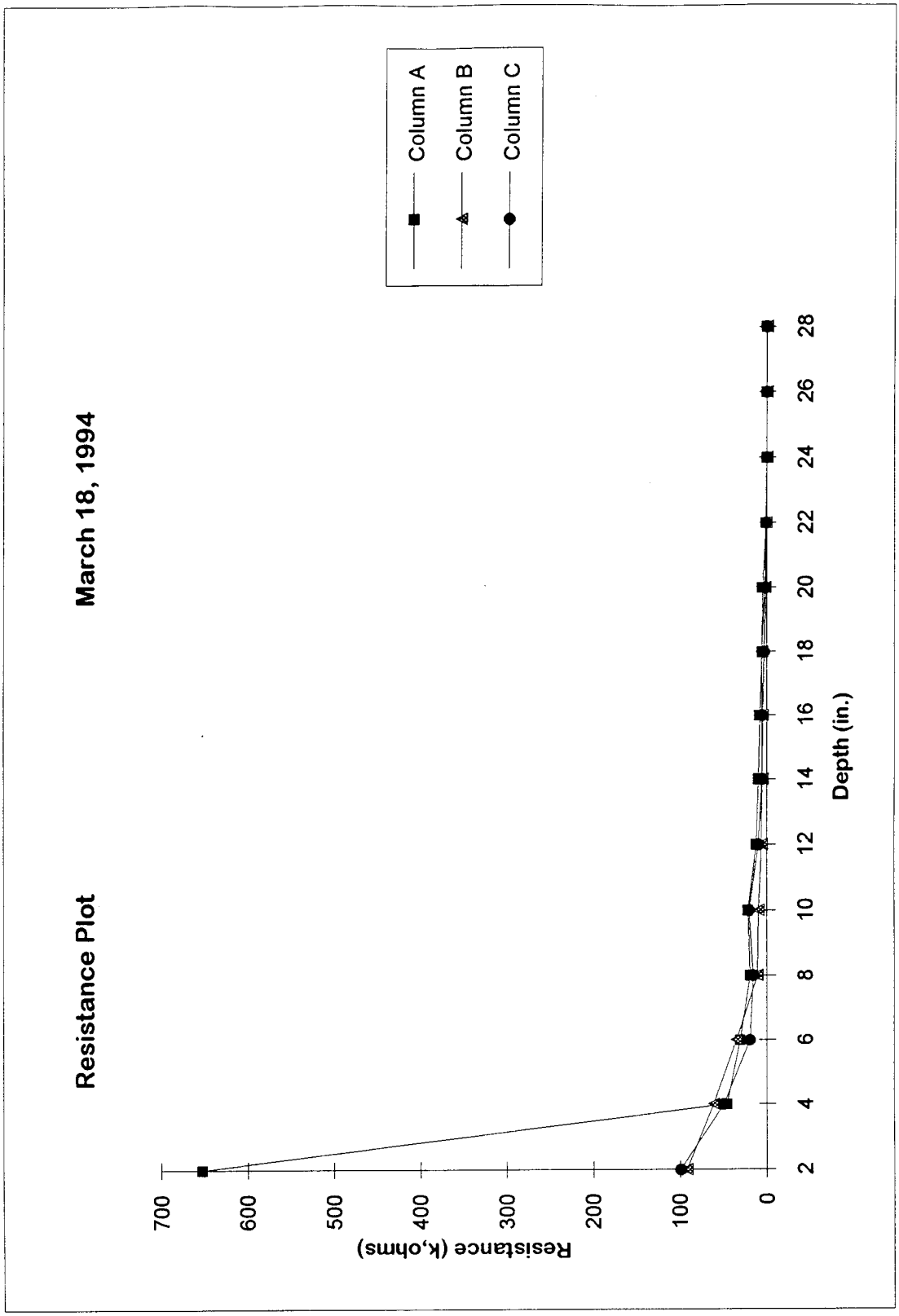
Resistance Plot
March 18, 1994
Column A
Column B
Column C
Resistance (k,ohms)
700
600
500
400
300
200
100
0
2
4
6
8
10
12
14
16
18
20
22
24
26
28
Depth (in.)

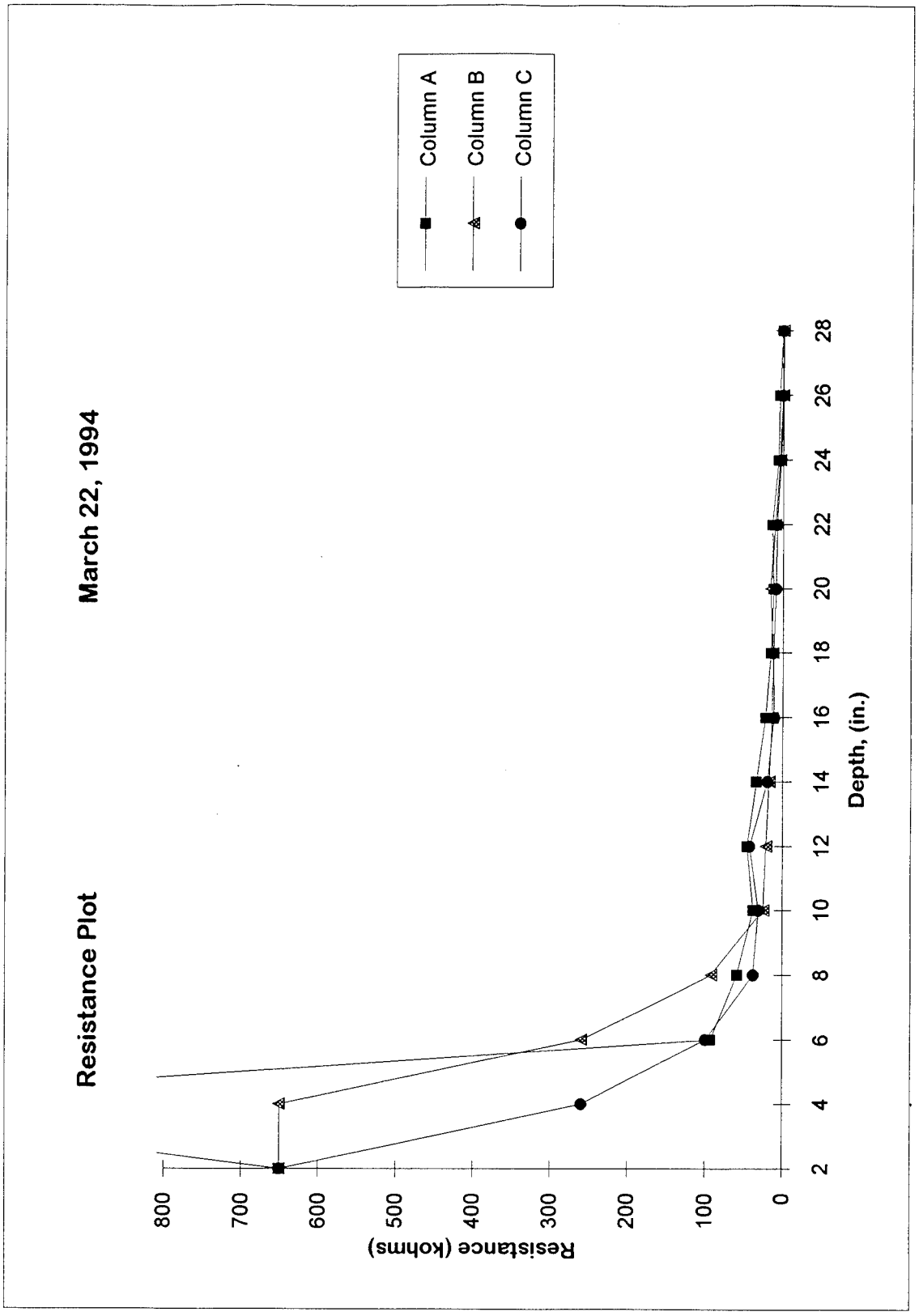
Resistance Plot
March 22, 1994
Column A
Column B
Column C
Resistance (kohms)
800
700
600
500
400
300
200
100
0
2
4
6
8
10
12
14
16
18
20
22
24
26
28
Depth, (in.)

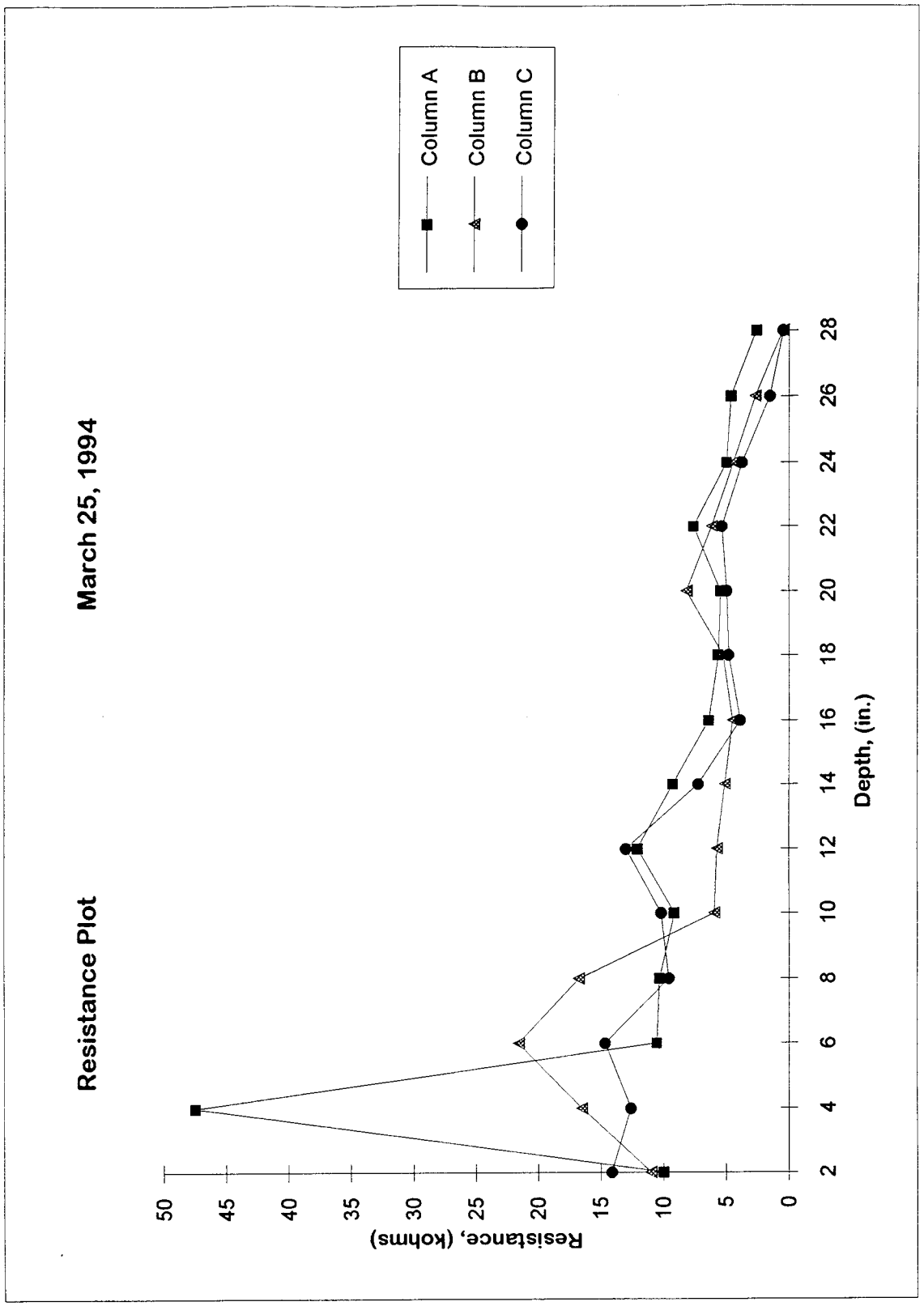
Resistance Plot
March 25, 1994
Column A
Column B
Column C
Resistance, (kohms)
0
5
10
15
20
25
30
35
40
45
50
Depth, (in.)
2
4
6
8
10
12
14
16
18
20
22
24
26
28

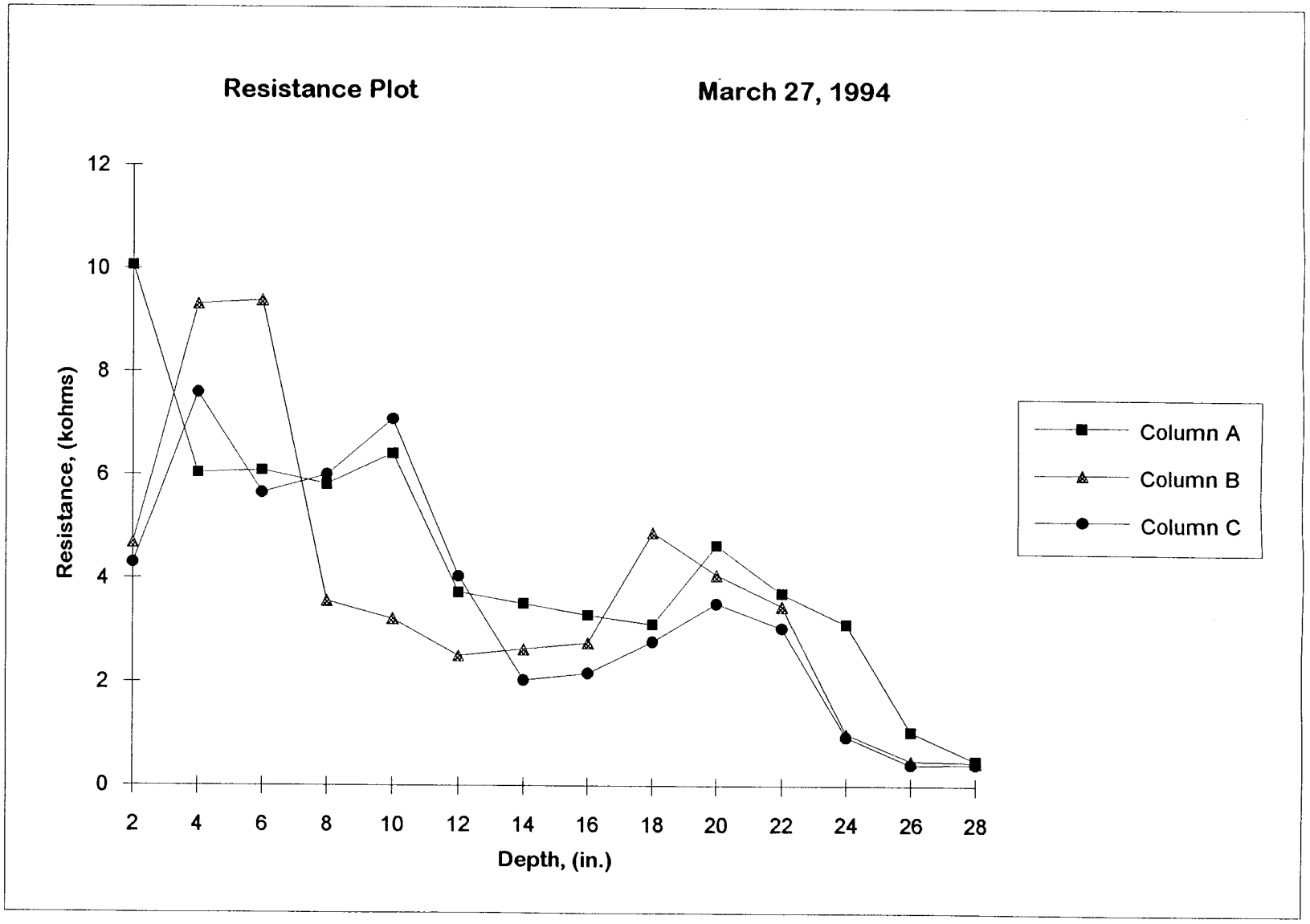
Resistance Plot
March 27, 1994
Resistance, (kohms)
12
10
8
6
4
2
0
2
4
6
8
10
12
14
16
18
20
22
24
26
28
Depth, (in.)
Column A
Column B
Column C

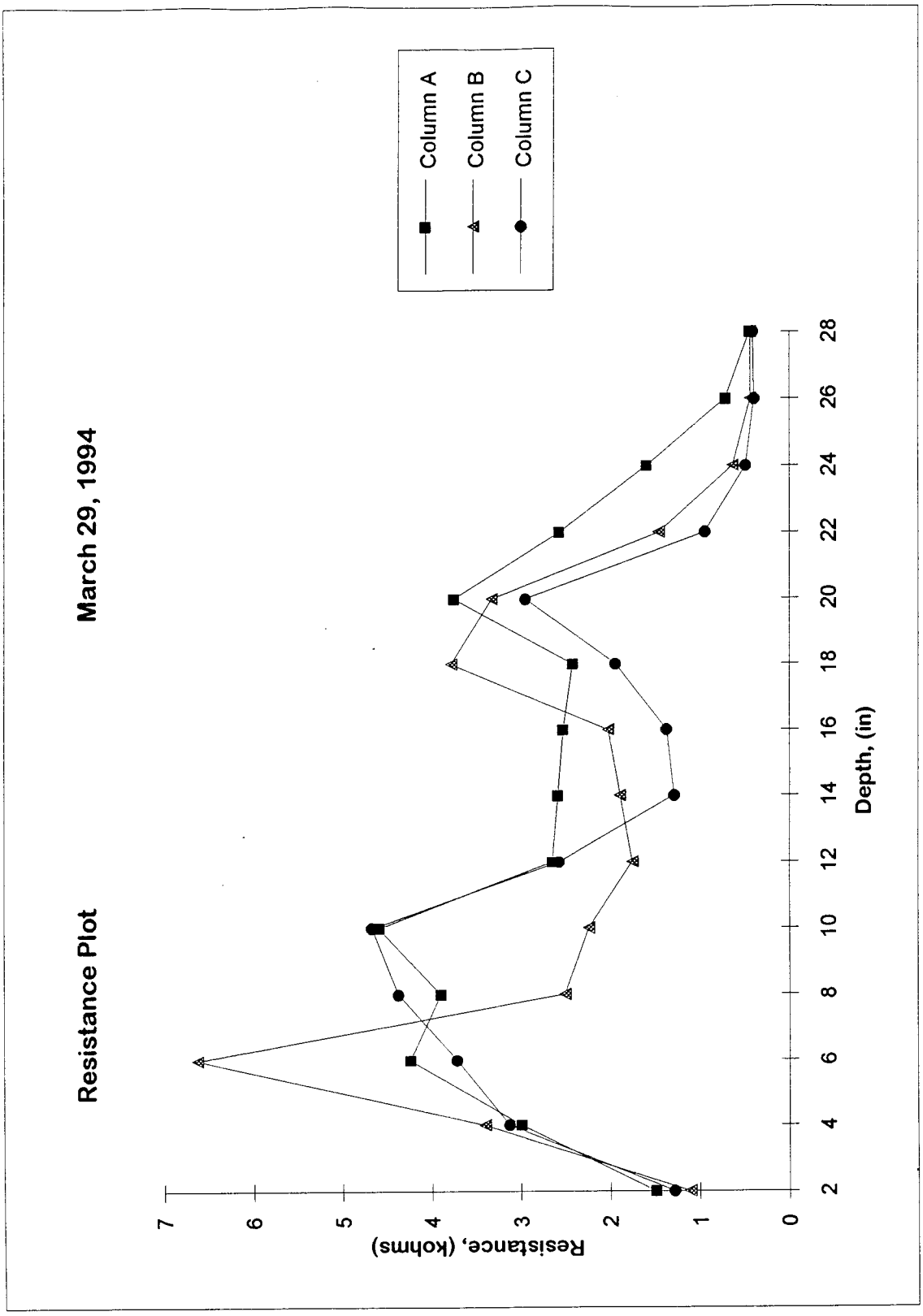
Resistance Plot
March 29, 1994
Column A
Column B
Column C
Resistance, (kohms)
Depth, (in)
0
1
2
3
4
5
6
7
2
4
6
8
10
12
14
16
18
20
22
24
26
28

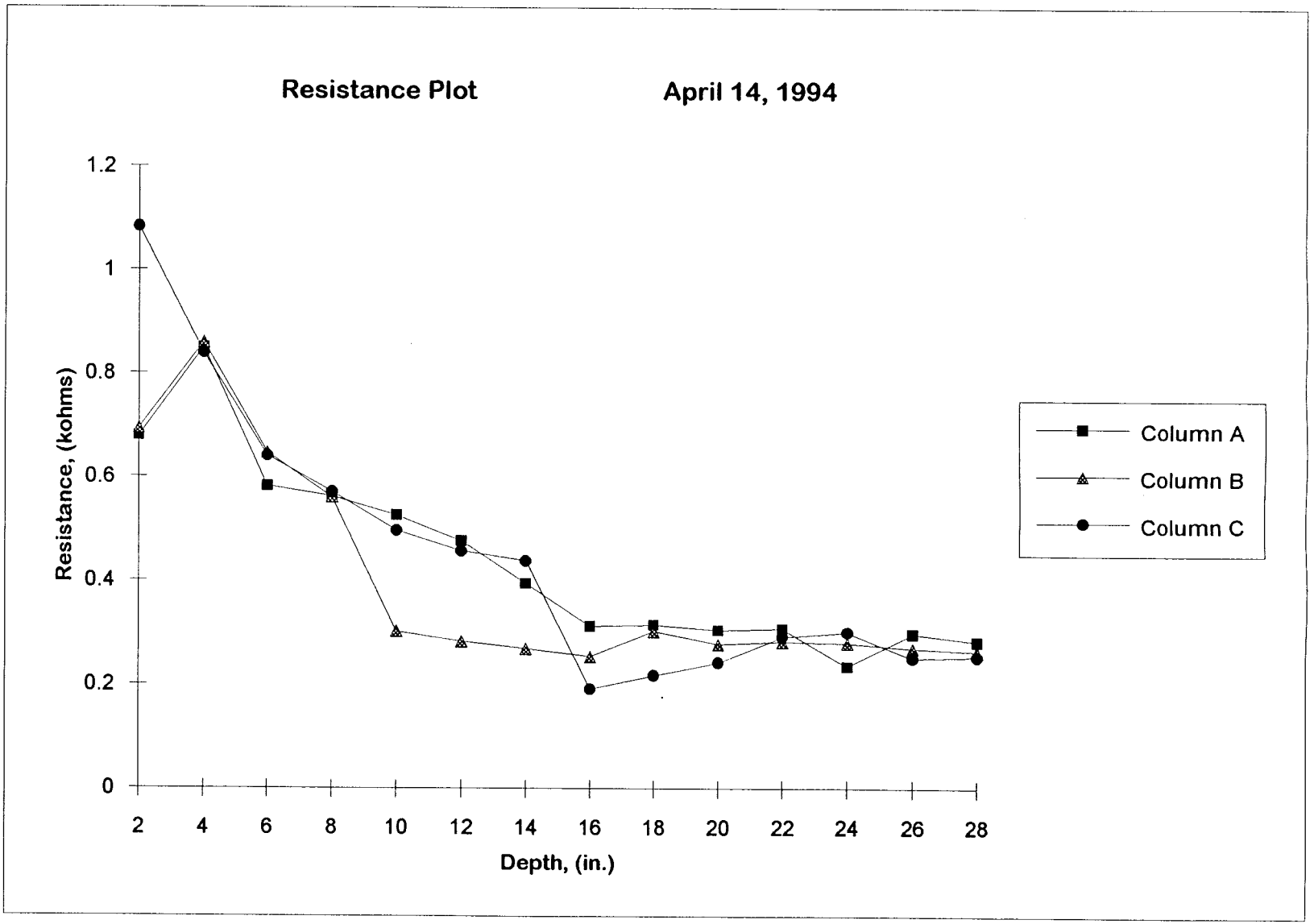
Resistance Plot
April 14, 1994
Resistance, (kohms)
1.2
1
0.8
0.6
0.4
0.2
0
2
4
6
8
10
12
14
16
18
20
22
24
26
28
Depth, (in.)
Column A
Column B
Column C

Appendix C

SOIL TEMPERATURE PROFILES ON THE TEST DATES
WITHIN THE SUBGRADE SOILS

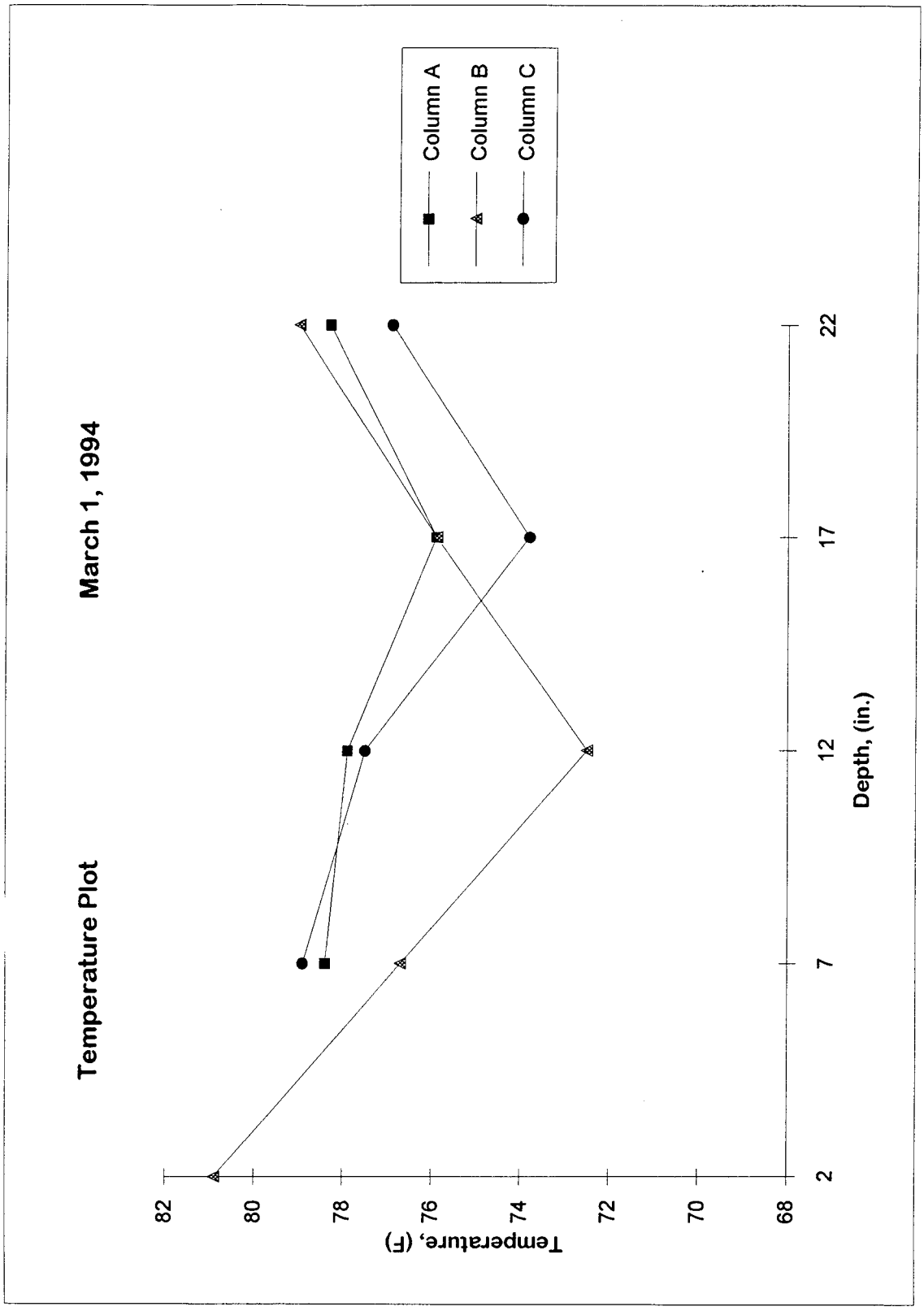
Temperature Plot
March 1, 1994
Column A
Column B
Column C
Temperature, (F)
82
80
78
76
74
72
70
68
2
7
12
17
22
Depth, (in.)

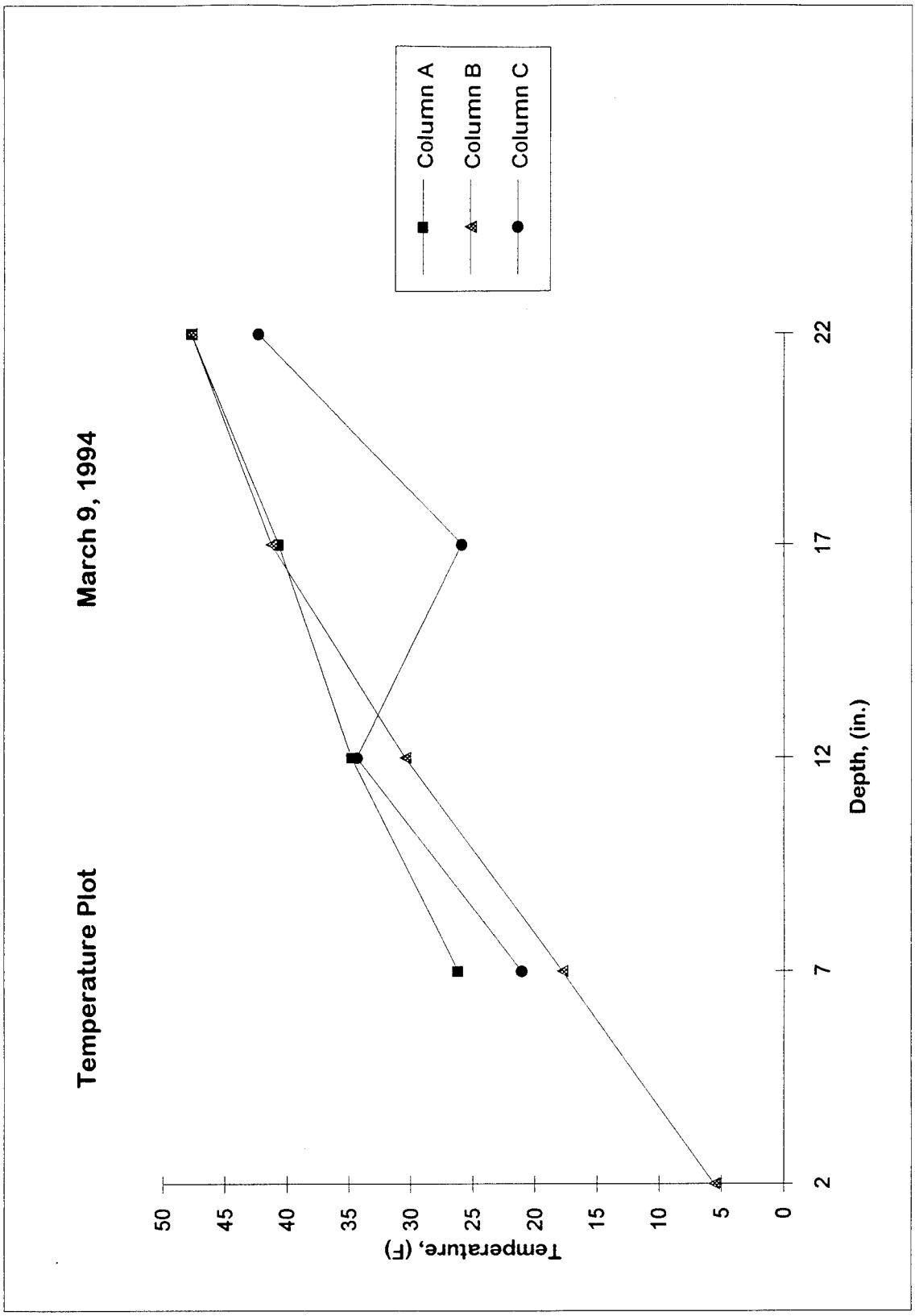
Temperature Plot
March 9, 1994
Column A
Column B
Column C
Temperature, (F)
50
45
40
35
30
25
20
15
10
5
0
2
7
12
17
22
Depth, (in.)

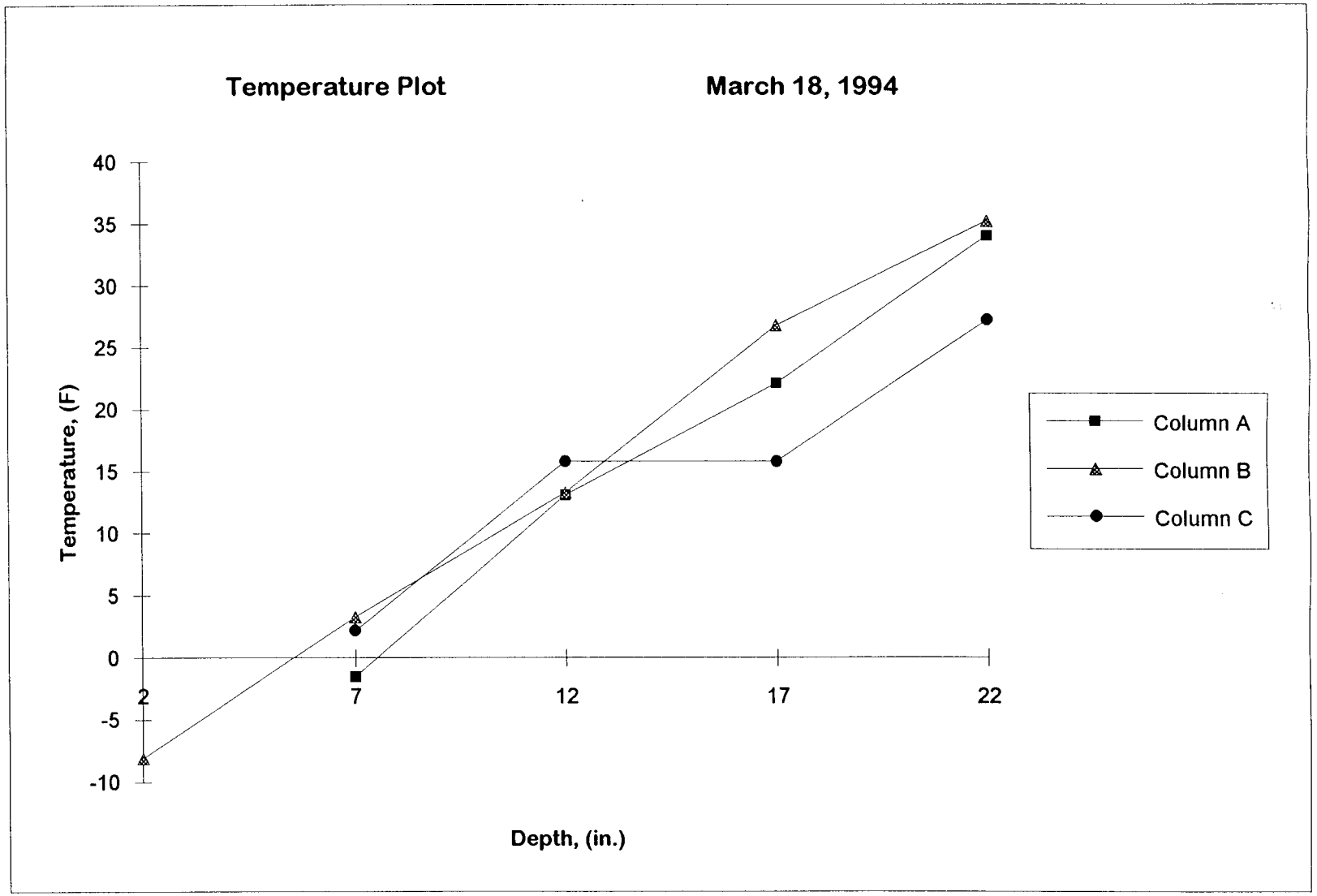
Temperature Plot
March 18, 1994
Temperature, (F)
40
35
30
25
20
15
10
5
0
-5
-10
2
7
12
17
22
Depth, (in.)
Column A
Column B
Column C

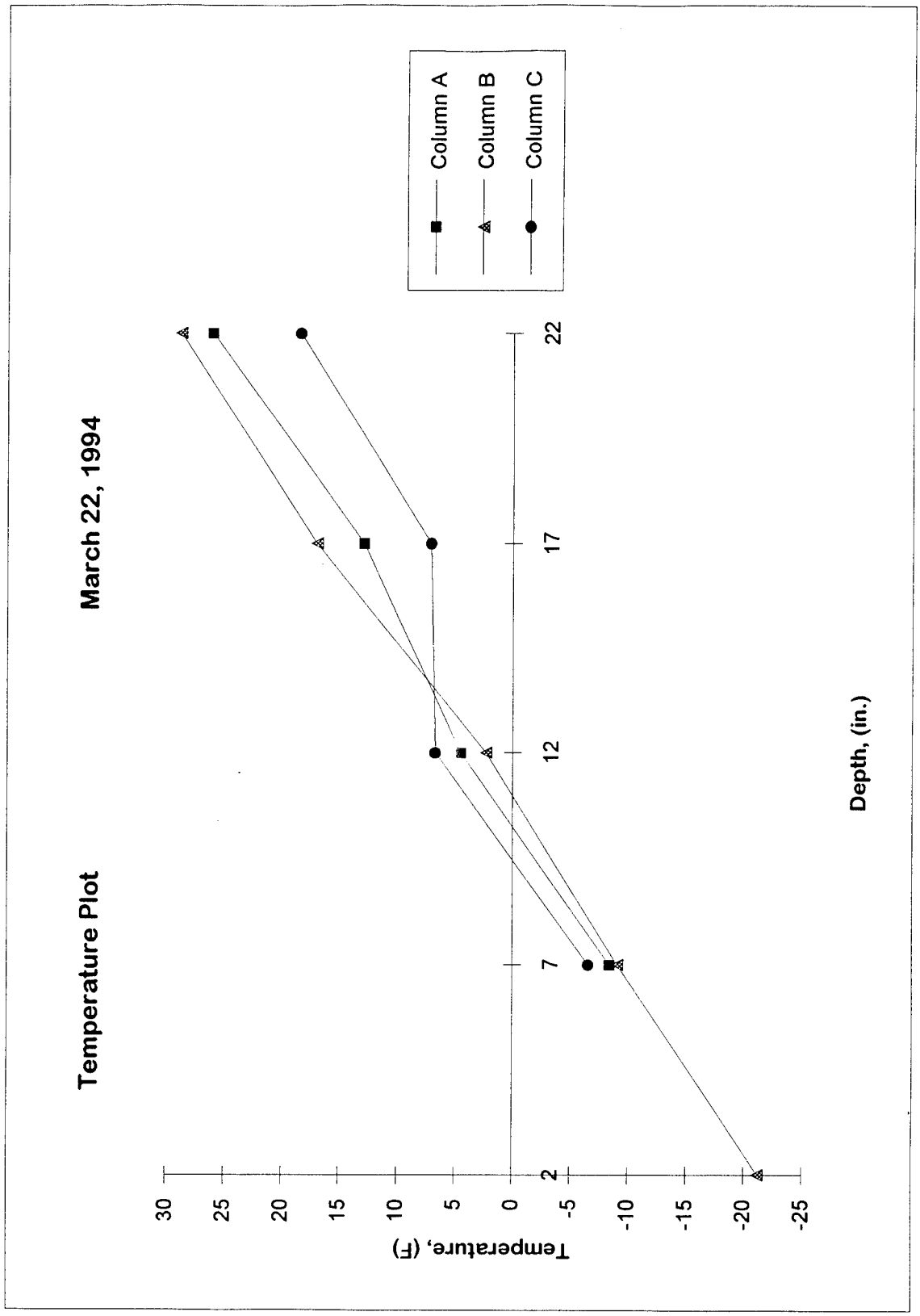
Temperature Plot
March 22, 1994
Column A
Column B
Column C
Temperature, (F)
30
25
20
15
10
5
0
-5
-10
-15
-20
-25
2
7
12
17
22
Depth, (in.)

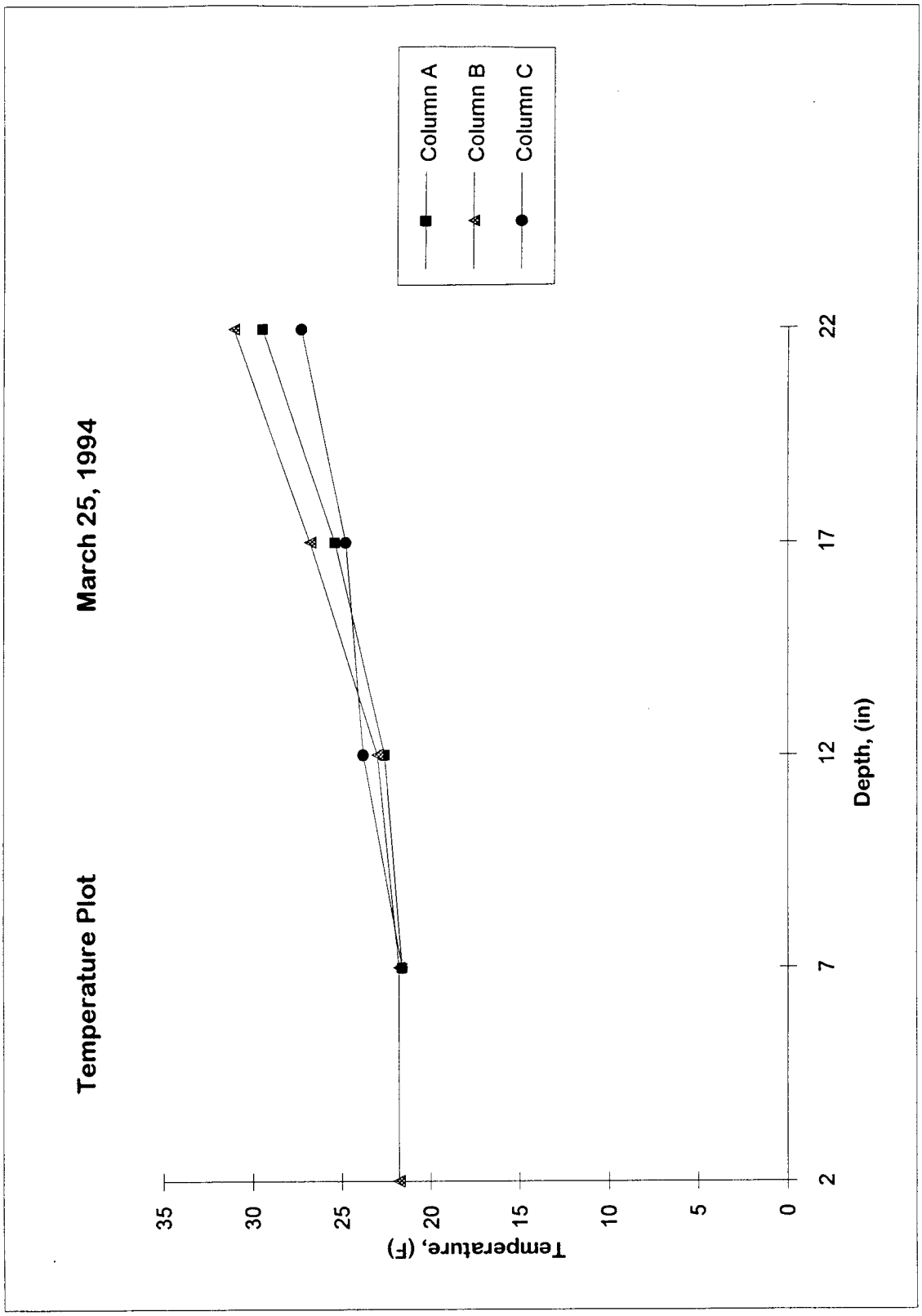
Temperature Plot
March 25, 1994
Column A
Column B
Column C
Temperature, (F)
35
30
25
20
15
10
5
0
2
7
12
17
22
Depth, (in)

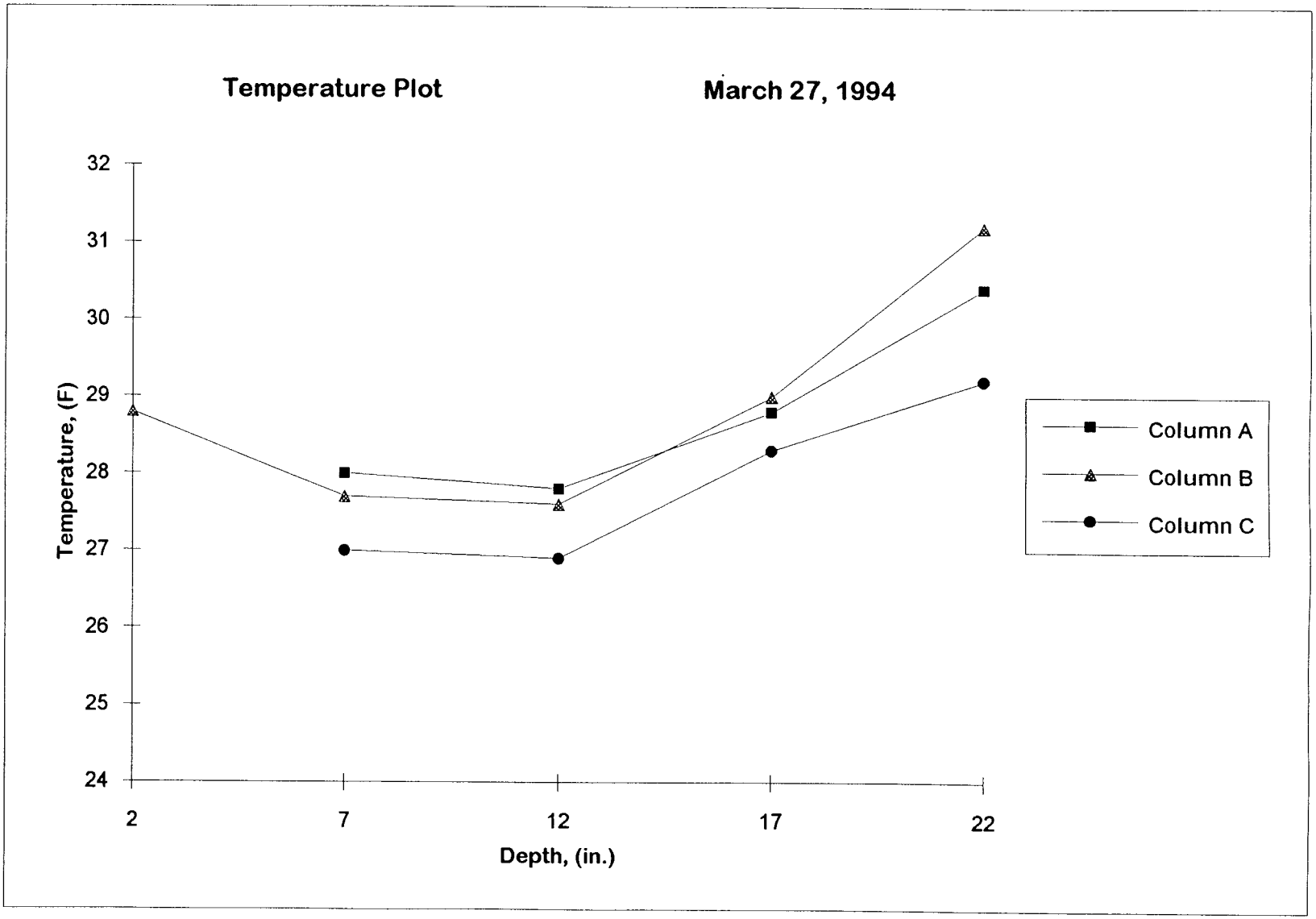
Temperature Plot
March 27, 1994
Temperature, (F)
32
31
30
29
28
27
26
25
24
2
7
12
17
22
Depth, (in.)
Column A
Column B
Column C

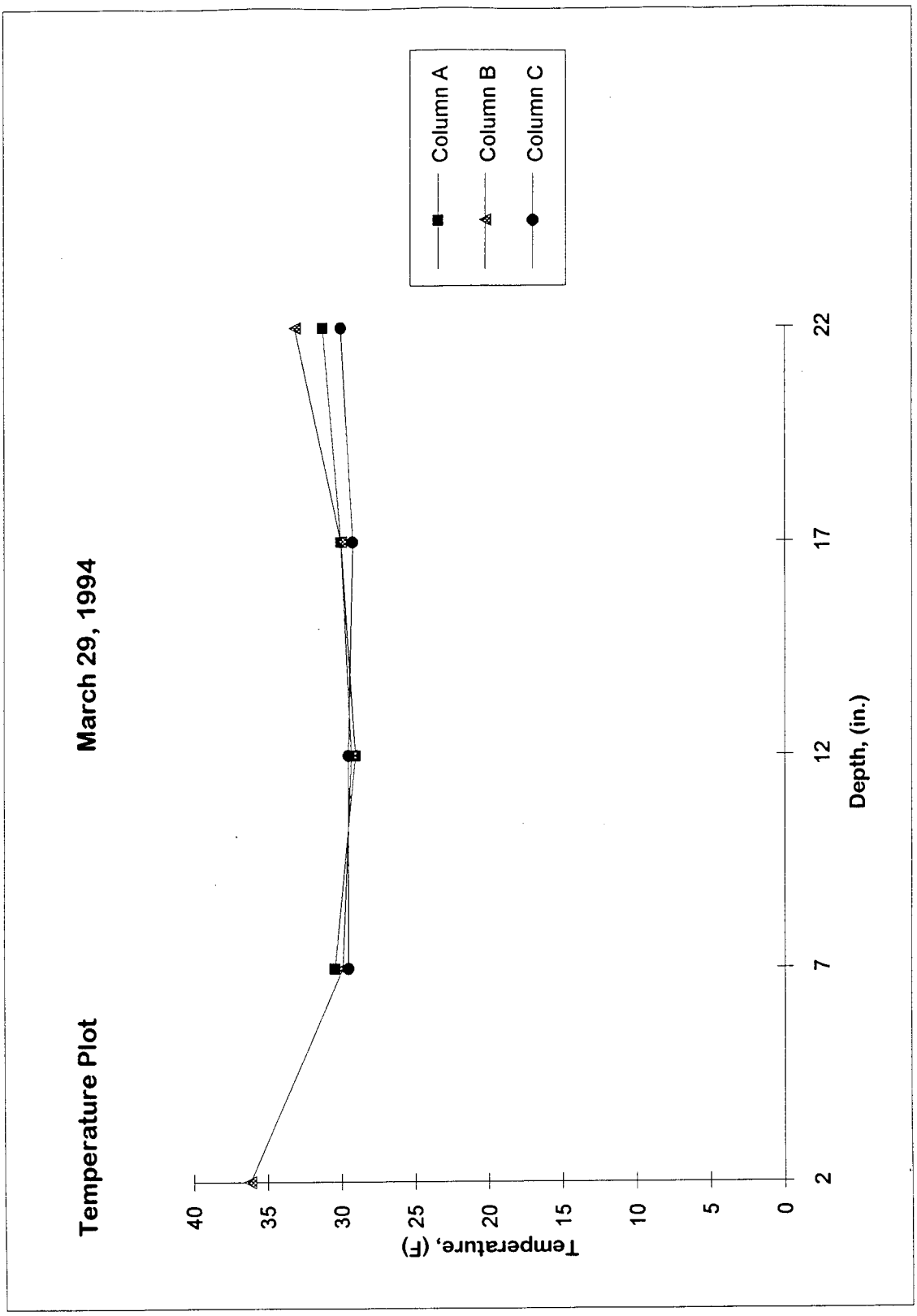
Temperature Plot
March 29, 1994
Column A
Column B
Column C
Temperature, (F)
40
35
30
25
20
15
10
5
0
2
7
12
17
22
Depth, (in.)

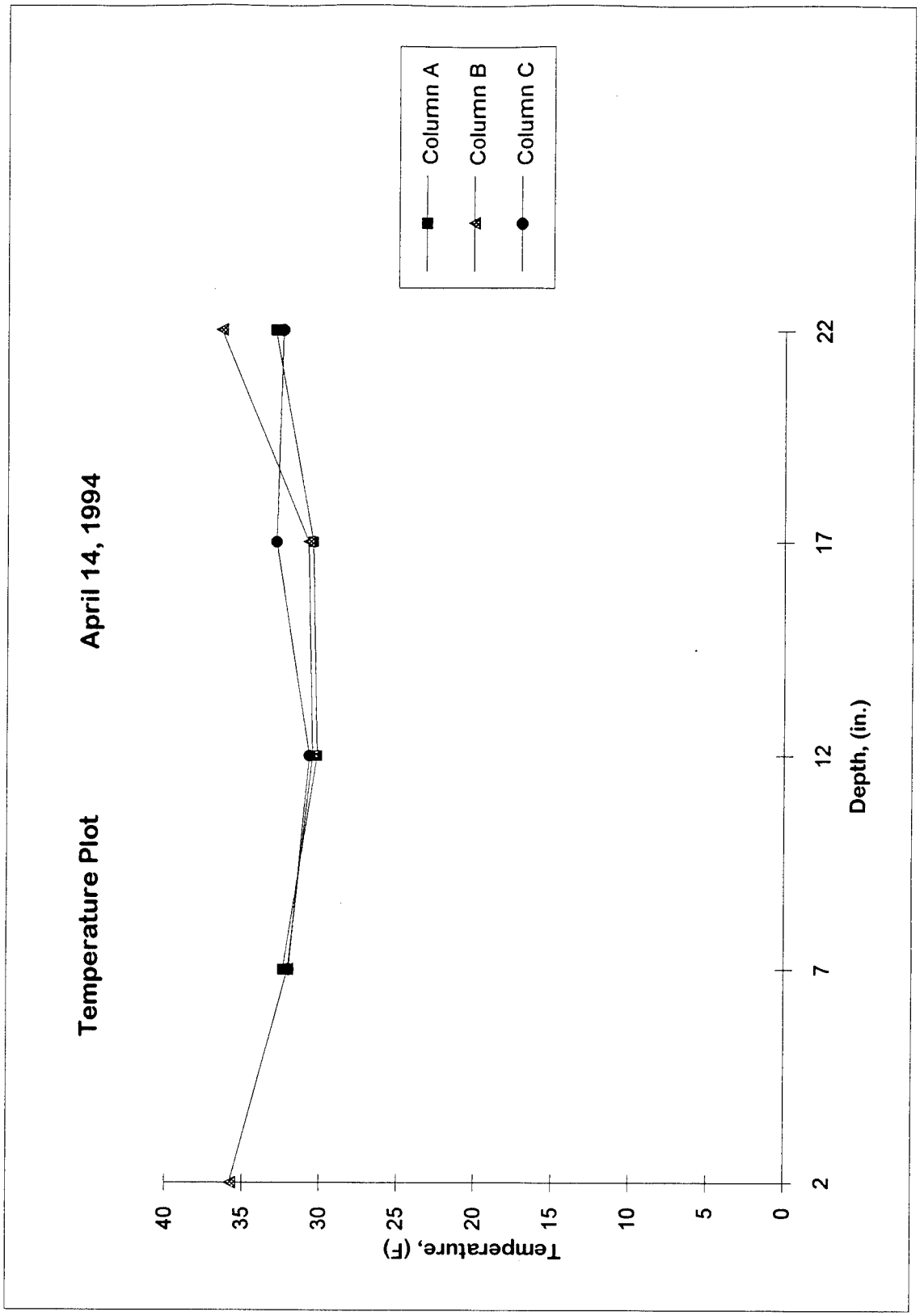
Temperature Plot
April 14, 1994
Column A
Column B
Column C
Temperature, (F)
40
35
30
25
20
15
10
5
0
2
7
12
17
22
Depth, (in.)

Appendix D

CONTOUR MAPS OF VERTICAL DEFLECTIONS MEASURED

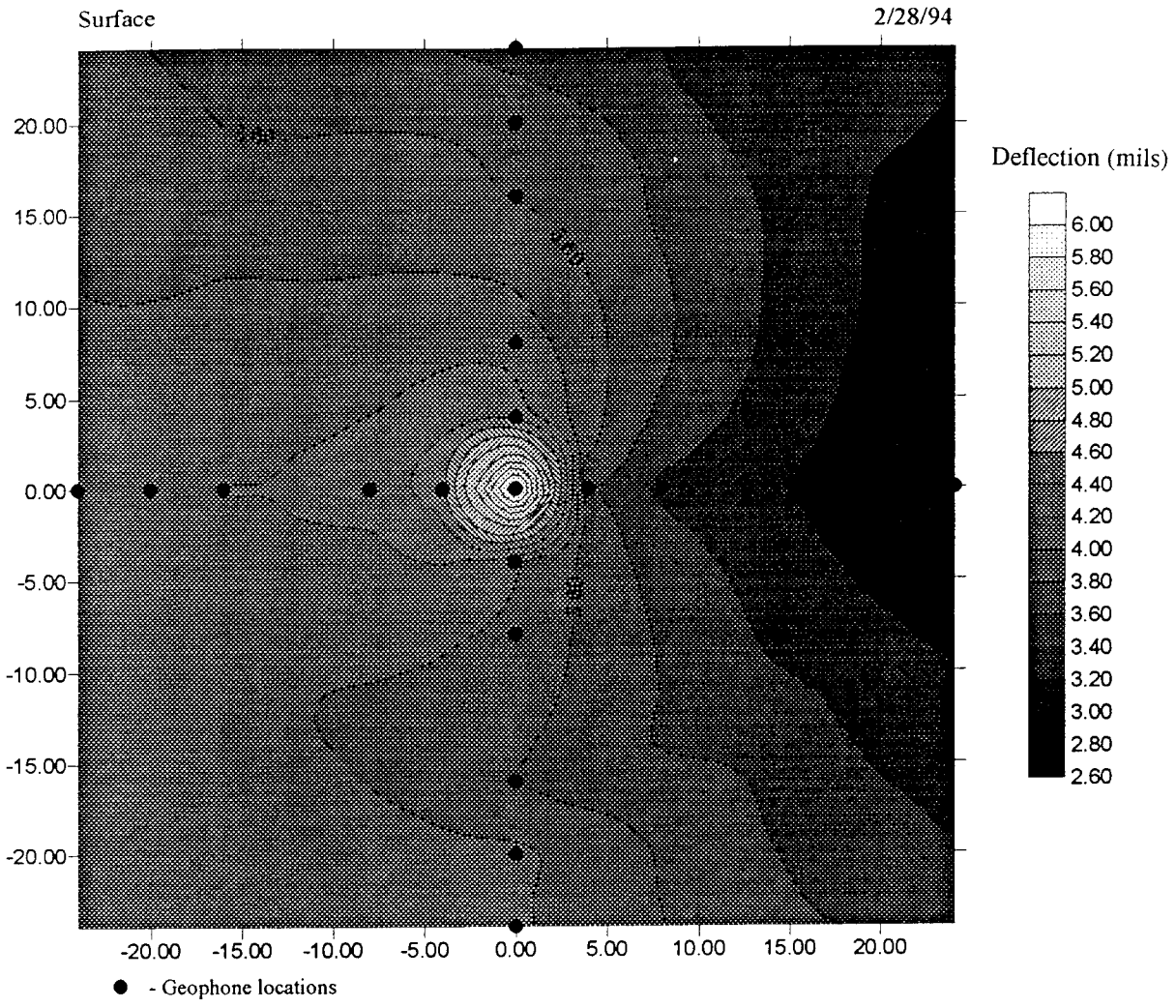
Surface
2/28/94
20.00
15.00
10.00
5.00
0.00
-5.00
-10.00
-15.00
-20.00
-20.00 -15.00 -10.00 -5.00 0.00 5.00 10.00 15.00 20.00
● - Geophone locations
Deflection (mils)
6.00
5.80
5.60
5.40
5.20
5.00
4.80
4.60
4.40
4.20
4.00
3.80
3.60
3.40
3.20
3.00
2.80
2.60

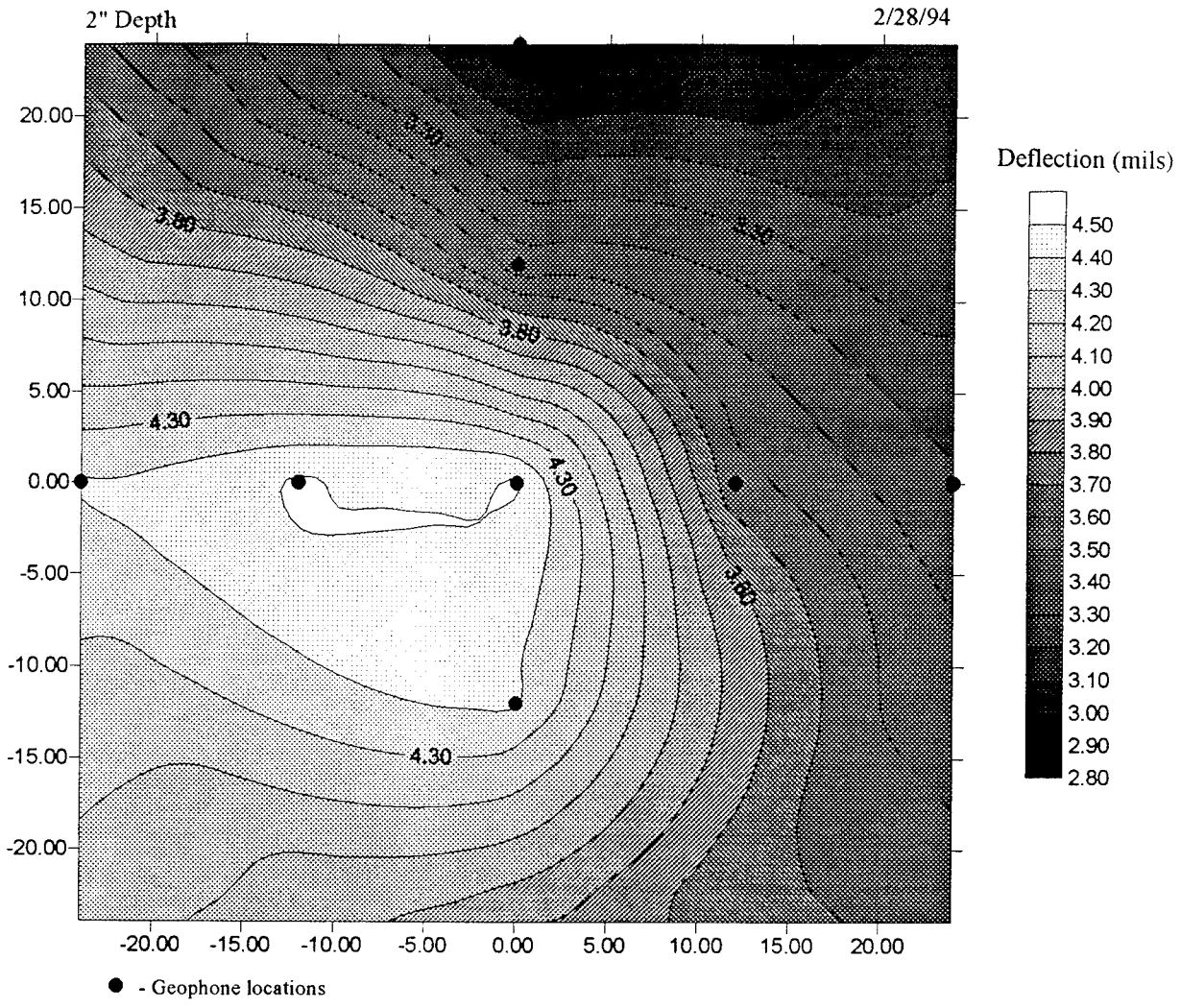
2" Depth
2/28/94
20.00
15.00
10.00
5.00
0.00
-5.00
-10.00
-15.00
-20.00
3.80
4.30
4.30
3.80
4.30
-20.00
-15.00
-10.00
-5.00
0.00
5.00
10.00
15.00
20.00
● - Geophone locations
Deflection (mils)
4.50
4.40
4.30
4.20
4.10
4.00
3.90
3.80
3.70
3.60
3.50
3.40
3.30
3.20
3.10
3.00
2.90
2.80

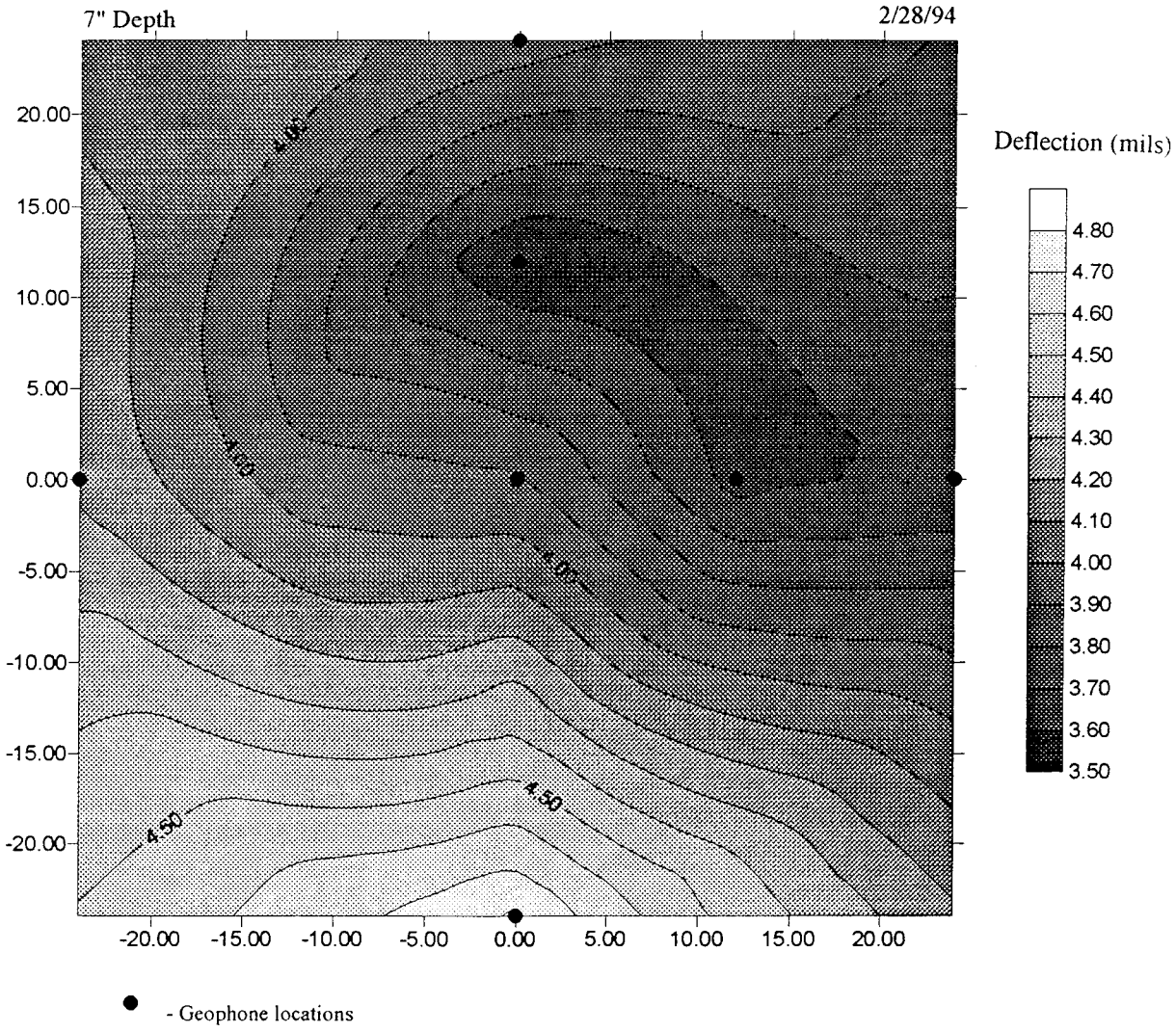
7" Depth
2/28/94
Deflection (mils)
4.80
4.70
4.60
4.50
4.40
4.30
4.20
4.10
4.00
3.90
3.80
3.70
3.60
3.50
20.00
15.00
10.00
5.00
0.00
-5.00
-10.00
-15.00
-20.00
-20.00
-15.00
-10.00
-5.00
0.00
5.00
10.00
15.00
20.00
4.50
4.50
4.50
4.50
- Geophone locations

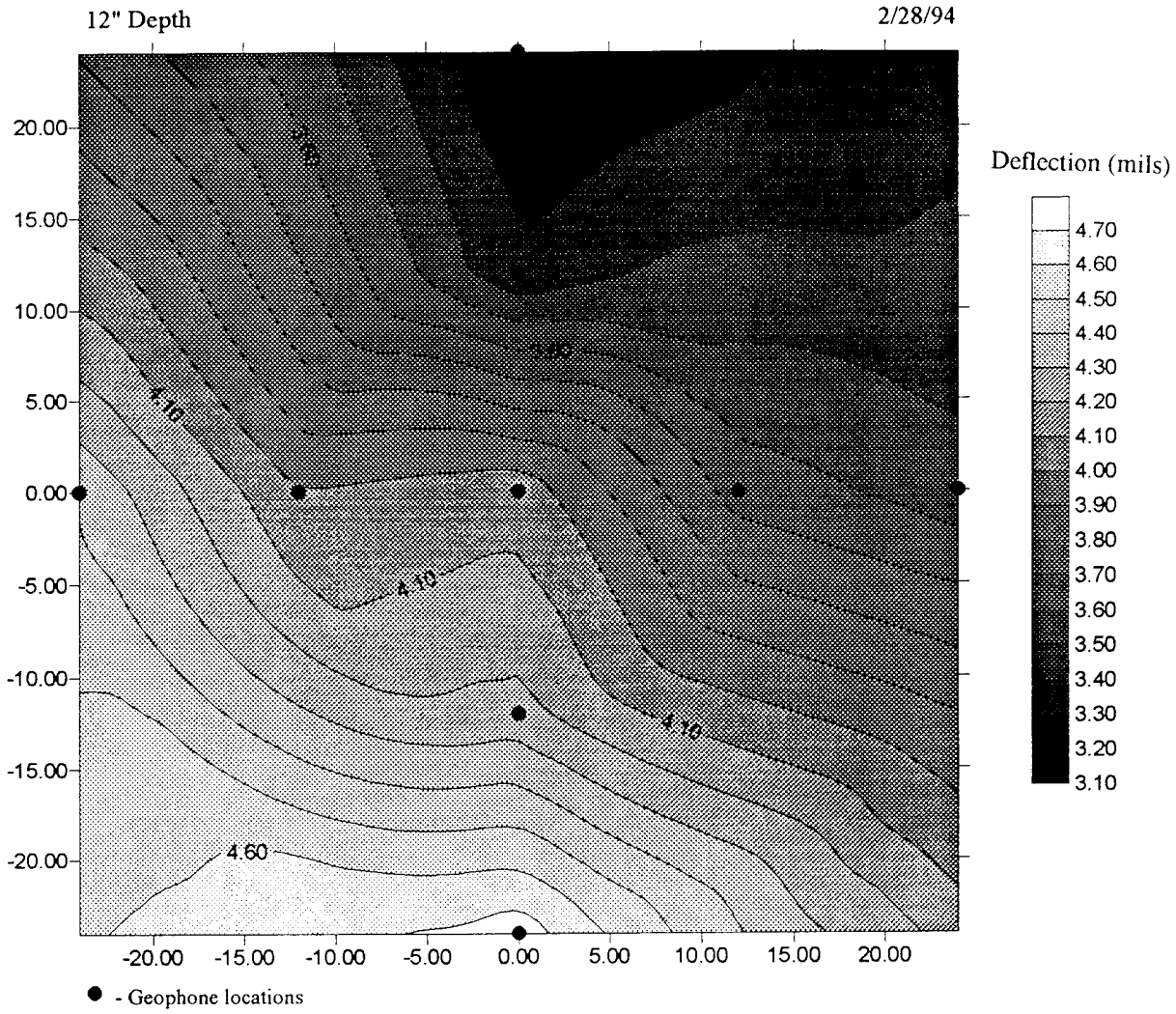
12" Depth
2/28/94
20.00
15.00
10.00
5.00
0.00
-5.00
-10.00
-15.00
-20.00
4.10
4.10
4.10
4.60
-20.00
-15.00
-10.00
-5.00
0.00
5.00
10.00
15.00
20.00
● - Geophone locations
Deflection (mils)
4.70
4.60
4.50
4.40
4.30
4.20
4.10
4.00
3.90
3.80
3.70
3.60
3.50
3.40
3.30
3.20
3.10

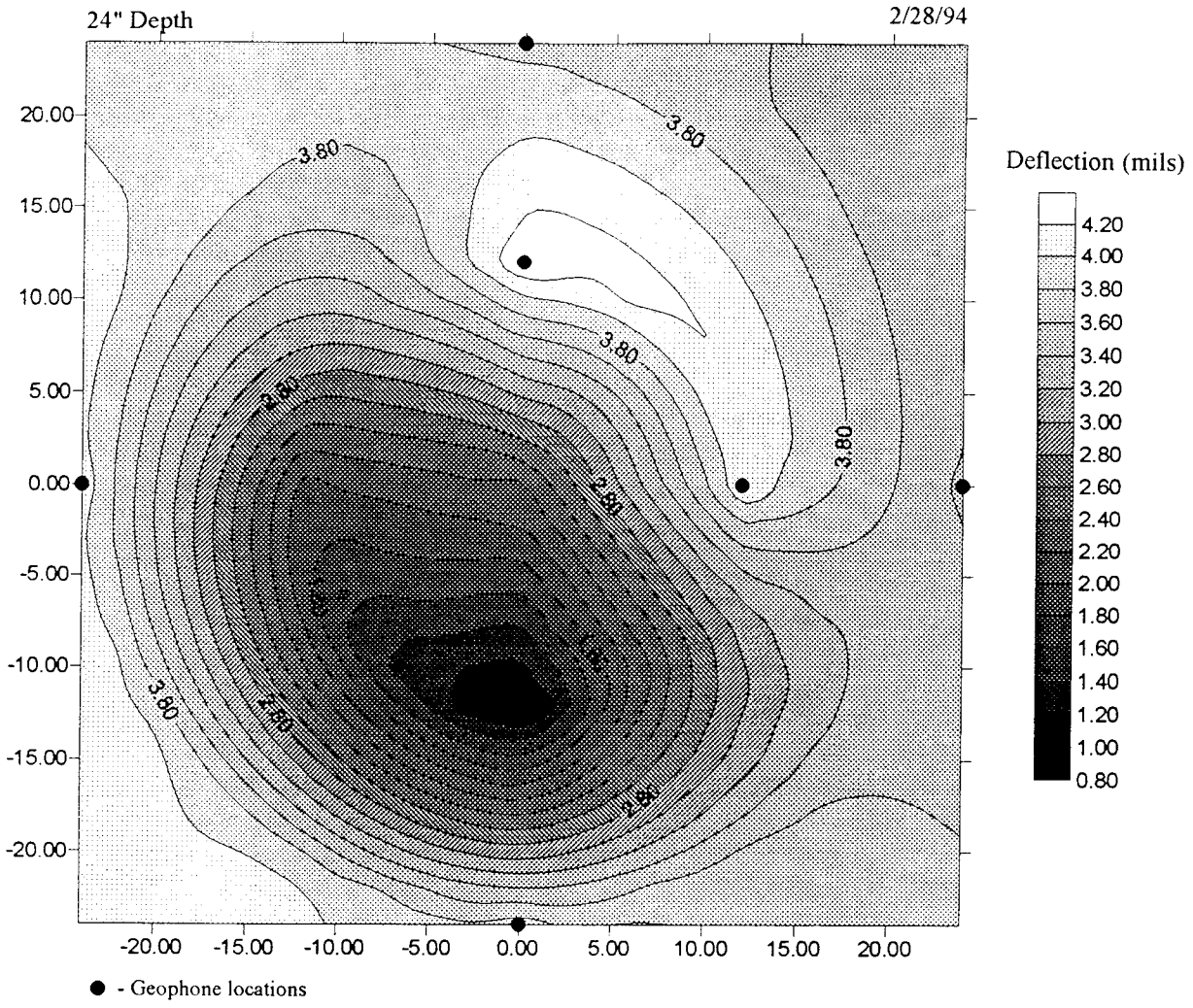
24" Depth
2/28/94
Deflection (mils)
4.20
4.00
3.80
3.60
3.40
3.20
3.00
2.80
2.60
2.40
2.20
2.00
1.80
1.60
1.40
1.20
1.00
0.80
20.00
15.00
10.00
5.00
0.00
-5.00
-10.00
-15.00
-20.00
-20.00 -15.00 -10.00 -5.00 0.00 5.00 10.00 15.00 20.00
● - Geophone locations

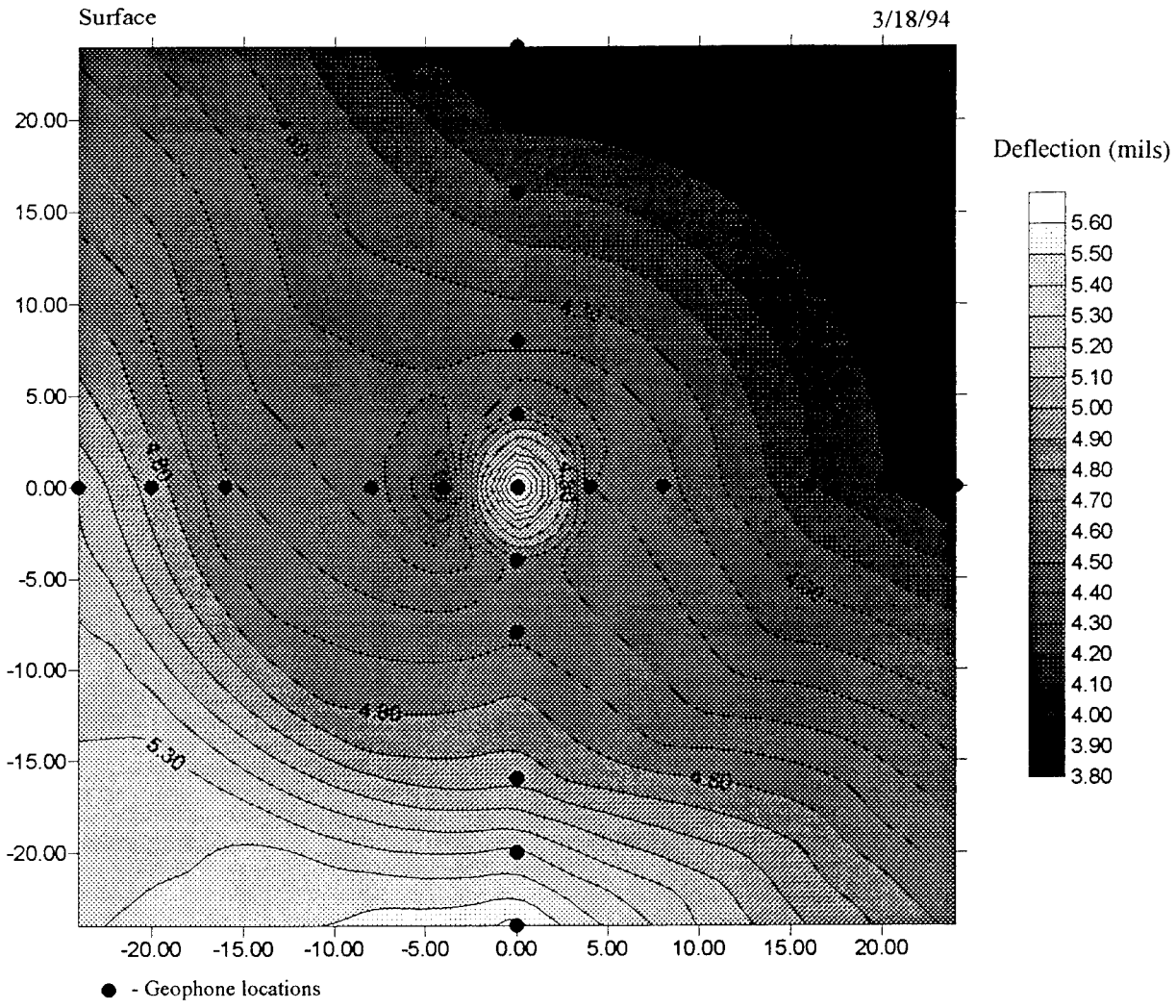
Surface
3/18/94
20.00
15.00
10.00
5.00
0.00
-5.00
-10.00
-15.00
-20.00
-20.00
-15.00
-10.00
-5.00
0.00
5.00
10.00
15.00
20.00
5.30
4.80
4.30
4.80
5.30
4.80
4.30
5.30
4.80
4.30
● - Geophone locations
Deflection (mils)
5.60
5.50
5.40
5.30
5.20
5.10
5.00
4.90
4.80
4.70
4.60
4.50
4.40
4.30
4.20
4.10
4.00
3.90
3.80

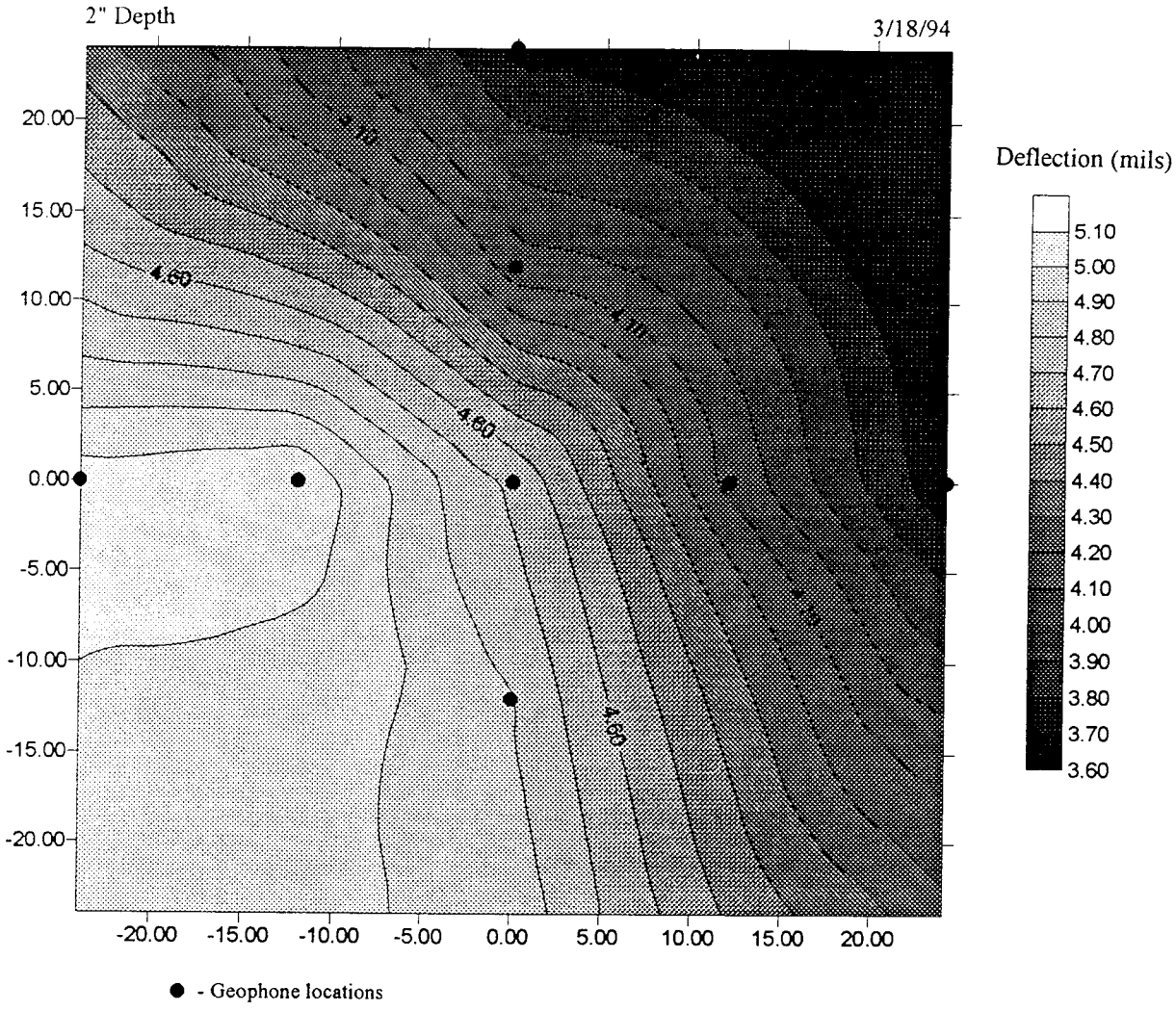
2" Depth
3/18/94
20.00
15.00
10.00
5.00
0.00
-5.00
-10.00
-15.00
-20.00
-20.00 -15.00 -10.00 -5.00 0.00 5.00 10.00 15.00 20.00
4.60
4.60
4.60
Deflection (mils)
5.10
5.00
4.90
4.80
4.70
4.60
4.50
4.40
4.30
4.20
4.10
4.00
3.90
3.80
3.70
3.60
● - Geophone locations

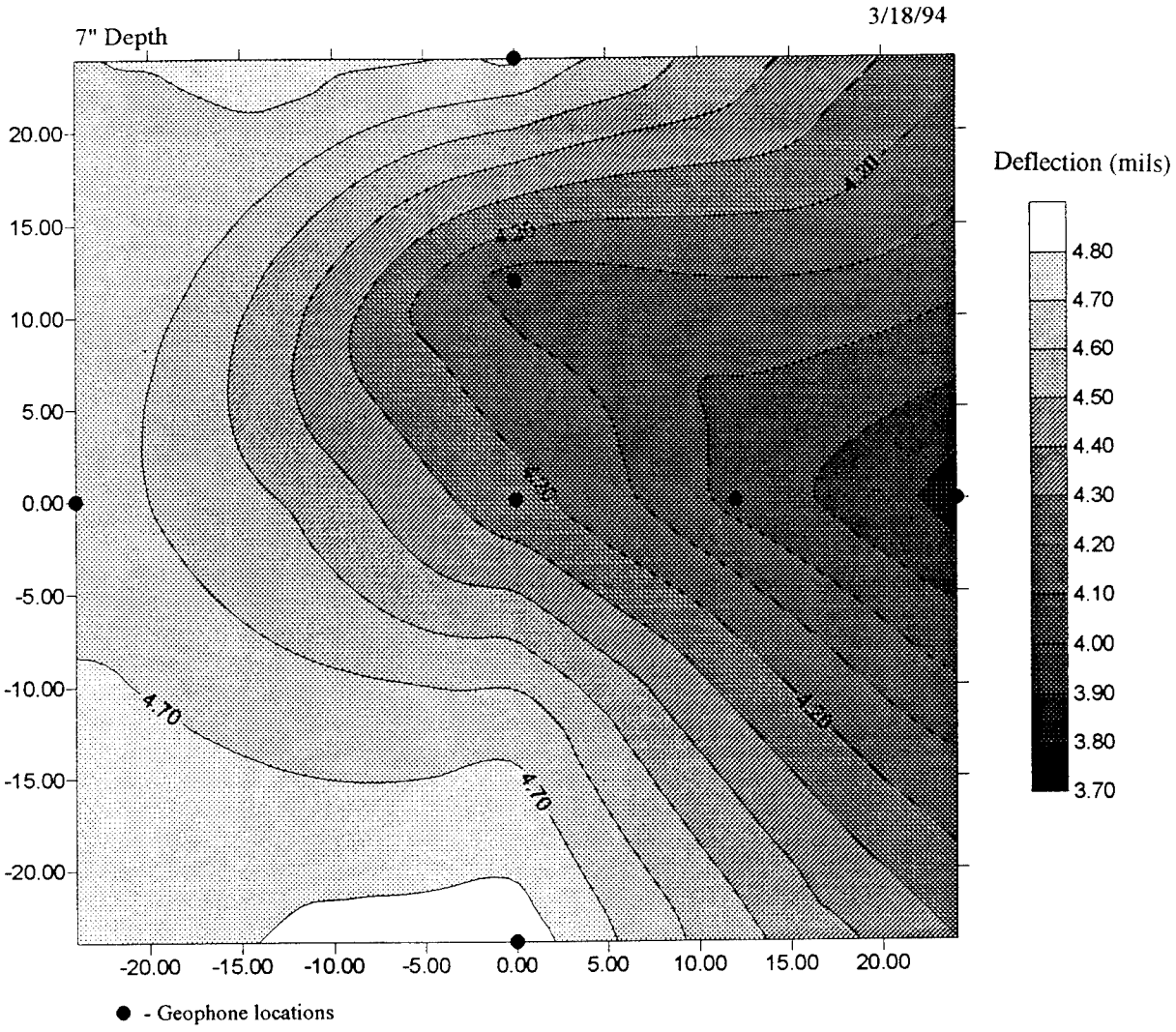
3/18/94
7" Depth
20.00
15.00
10.00
5.00
0.00
-5.00
-10.00
-15.00
-20.00
4.70
4.70
4.70
-20.00 -15.00 -10.00 -5.00 0.00 5.00 10.00 15.00 20.00
● - Geophone locations
Deflection (mils)
4.80
4.70
4.60
4.50
4.40
4.30
4.20
4.10
4.00
3.90
3.80
3.70

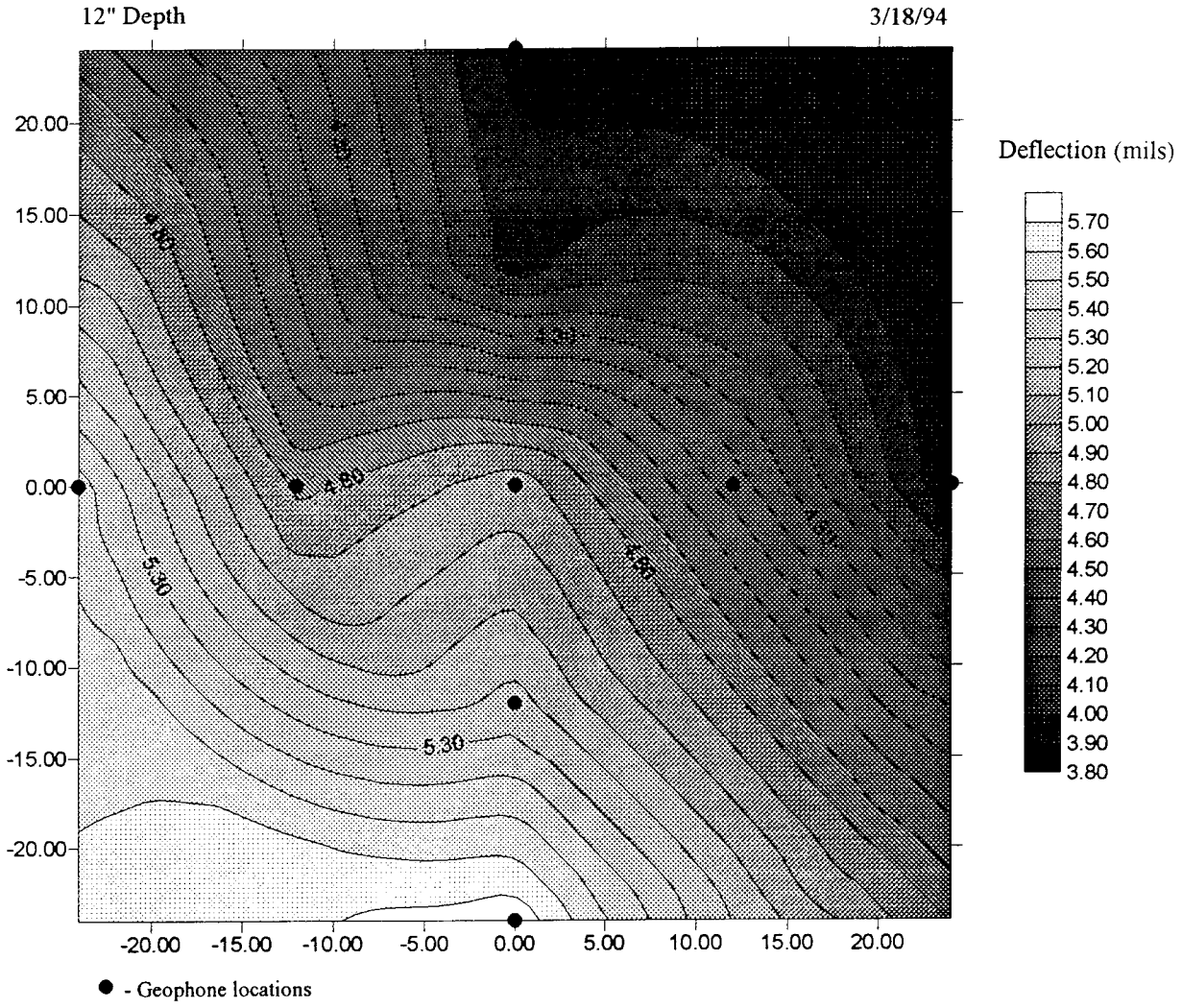
12" Depth
3/18/94
Deflection (mils)
5.70
5.60
5.50
5.40
5.30
5.20
5.10
5.00
4.90
4.80
4.70
4.60
4.50
4.40
4.30
4.20
4.10
4.00
3.90
3.80
20.00
15.00
10.00
5.00
0.00
-5.00
-10.00
-15.00
-20.00
-20.00
-15.00
-10.00
-5.00
0.00
5.00
10.00
15.00
20.00
5.30
● - Geophone locations

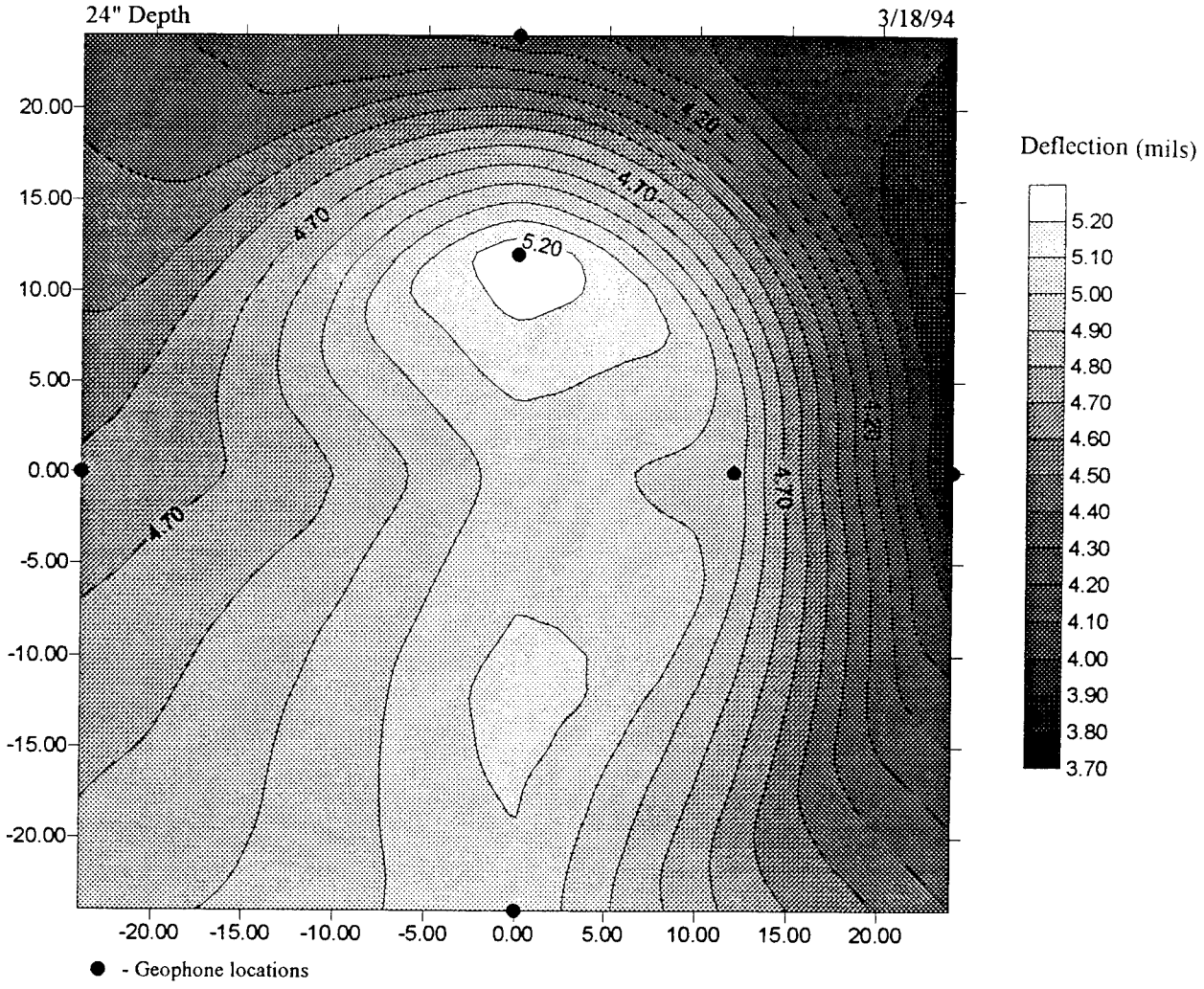
24" Depth
3/18/94
20.00
15.00
10.00
5.00
0.00
-5.00
-10.00
-15.00
-20.00
-20.00 -15.00 -10.00 -5.00 0.00 5.00 10.00 15.00 20.00
4.70
4.70
5.20
4.70
4.70
4.70
- Geophone locations
Deflection (mils)
5.20
5.10
5.00
4.90
4.80
4.70
4.60
4.50
4.40
4.30
4.20
4.10
4.00
3.90
3.80
3.70

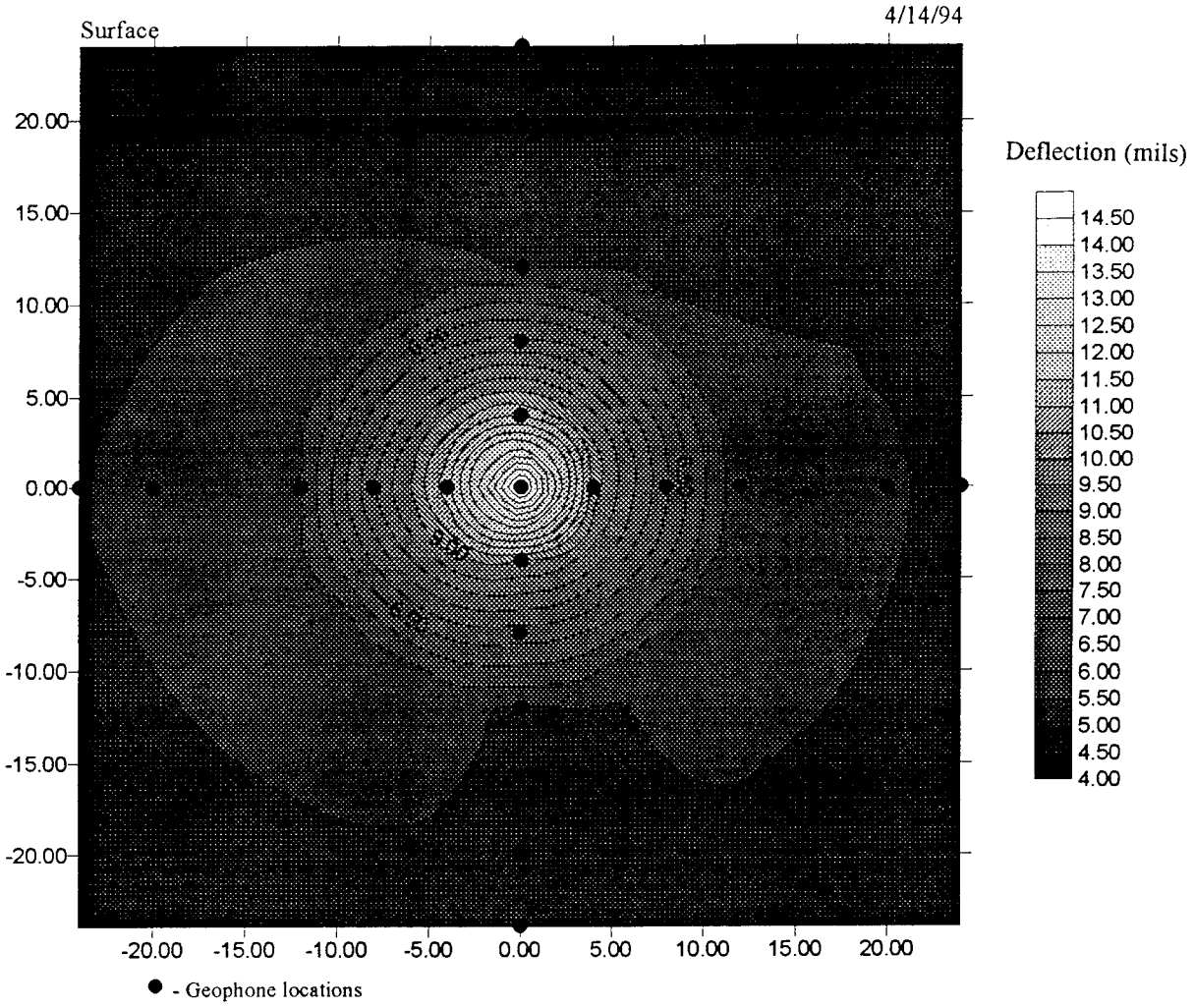
Surface
4/14/94
20.00
15.00
10.00
5.00
0.00
-5.00
-10.00
-15.00
-20.00
-20.00 -15.00 -10.00 -5.00 0.00 5.00 10.00 15.00 20.00
● - Geophone locations
Deflection (mils)
14.50
14.00
13.50
13.00
12.50
12.00
11.50
11.00
10.50
10.00
9.50
9.00
8.50
8.00
7.50
7.00
6.50
6.00
5.50
5.00
4.50
4.00

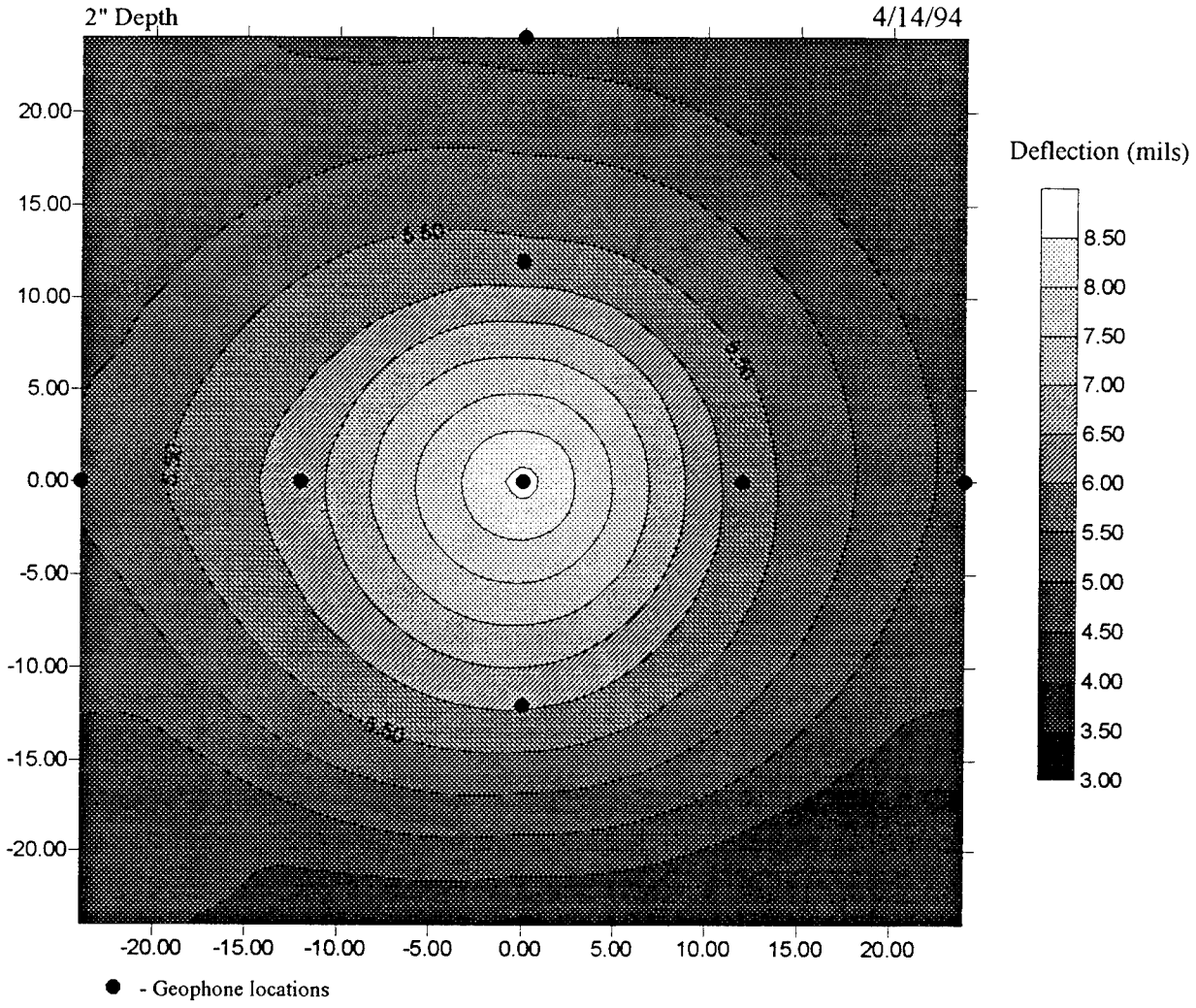
2" Depth
4/14/94
20.00
15.00
10.00
5.00
0.00
-5.00
-10.00
-15.00
-20.00
-20.00 -15.00 -10.00 -5.00 0.00 5.00 10.00 15.00 20.00
● - Geophone locations
Deflection (mils)
8.50
8.00
7.50
7.00
6.50
6.00
5.50
5.00
4.50
4.00
3.50
3.00

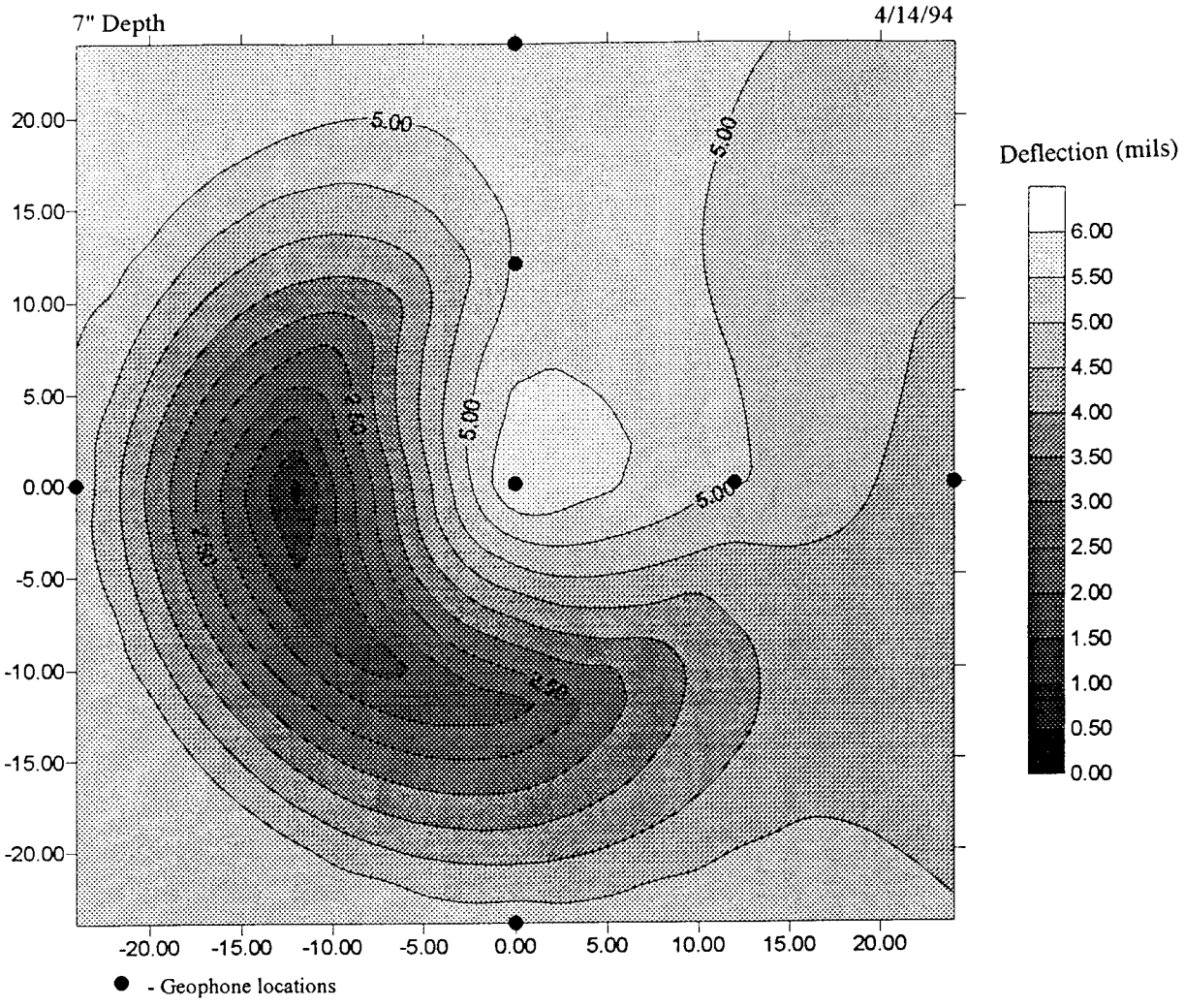
7" Depth
4/14/94
Deflection (mils)
6.00
5.50
5.00
4.50
4.00
3.50
3.00
2.50
2.00
1.50
1.00
0.50
0.00
20.00
15.00
10.00
5.00
0.00
-5.00
-10.00
-15.00
-20.00
-20.00 -15.00 -10.00 -5.00 0.00 5.00 10.00 15.00 20.00
- Geophone locations

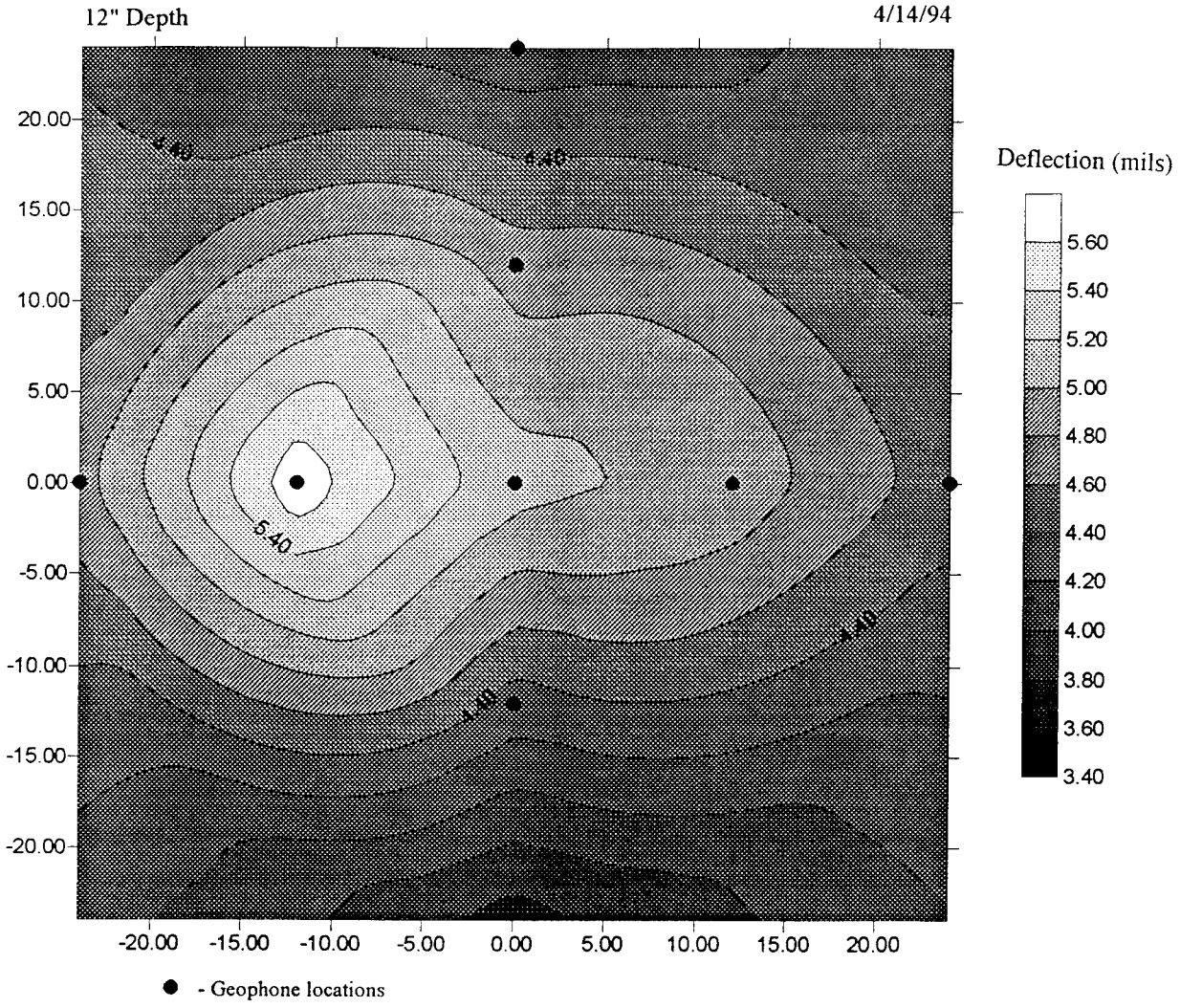
12" Depth
4/14/94
20.00
15.00
10.00
5.00
0.00
-5.00
-10.00
-15.00
-20.00
4.40
4.40
5.40
4.40
4.40
-20.00
-15.00
-10.00
-5.00
0.00
5.00
10.00
15.00
20.00
- Geophone locations
Deflection (mils)
5.60
5.40
5.20
5.00
4.80
4.60
4.40
4.20
4.00
3.80
3.60
3.40

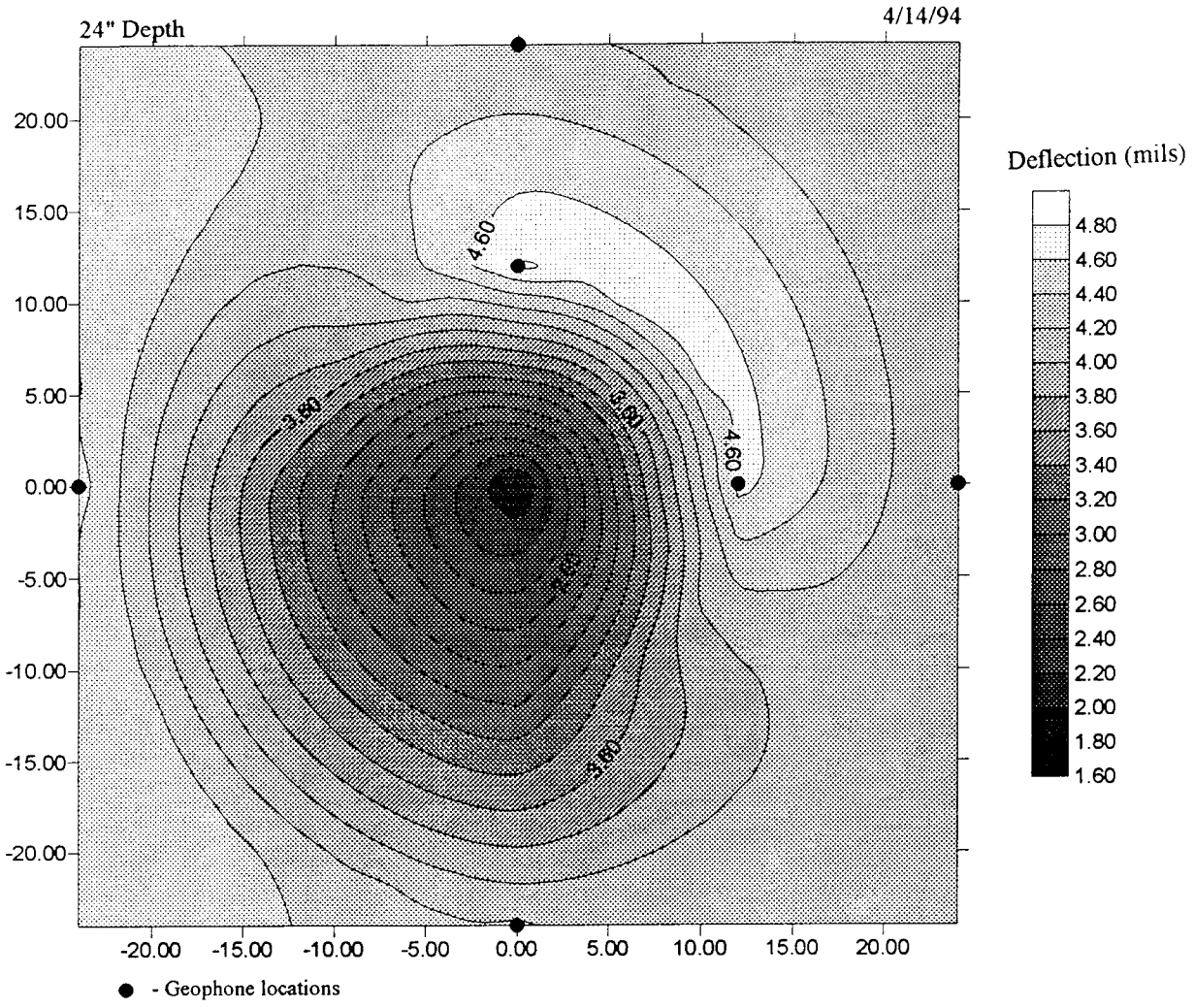
24" Depth
4/14/94
Deflection (mils)
4.80
4.60
4.40
4.20
4.00
3.80
3.60
3.40
3.20
3.00
2.80
2.60
2.40
2.20
2.00
1.80
1.60
20.00
15.00
10.00
5.00
0.00
-5.00
-10.00
-15.00
-20.00
-20.00
-15.00
-10.00
-5.00
0.00
5.00
10.00
15.00
20.00
4.60
3.80
3.80
4.60
2.60
3.80
● - Geophone locations

Appendix E

COMPARISON OF MEASURED AND PREDICTED DEFLECTIONS

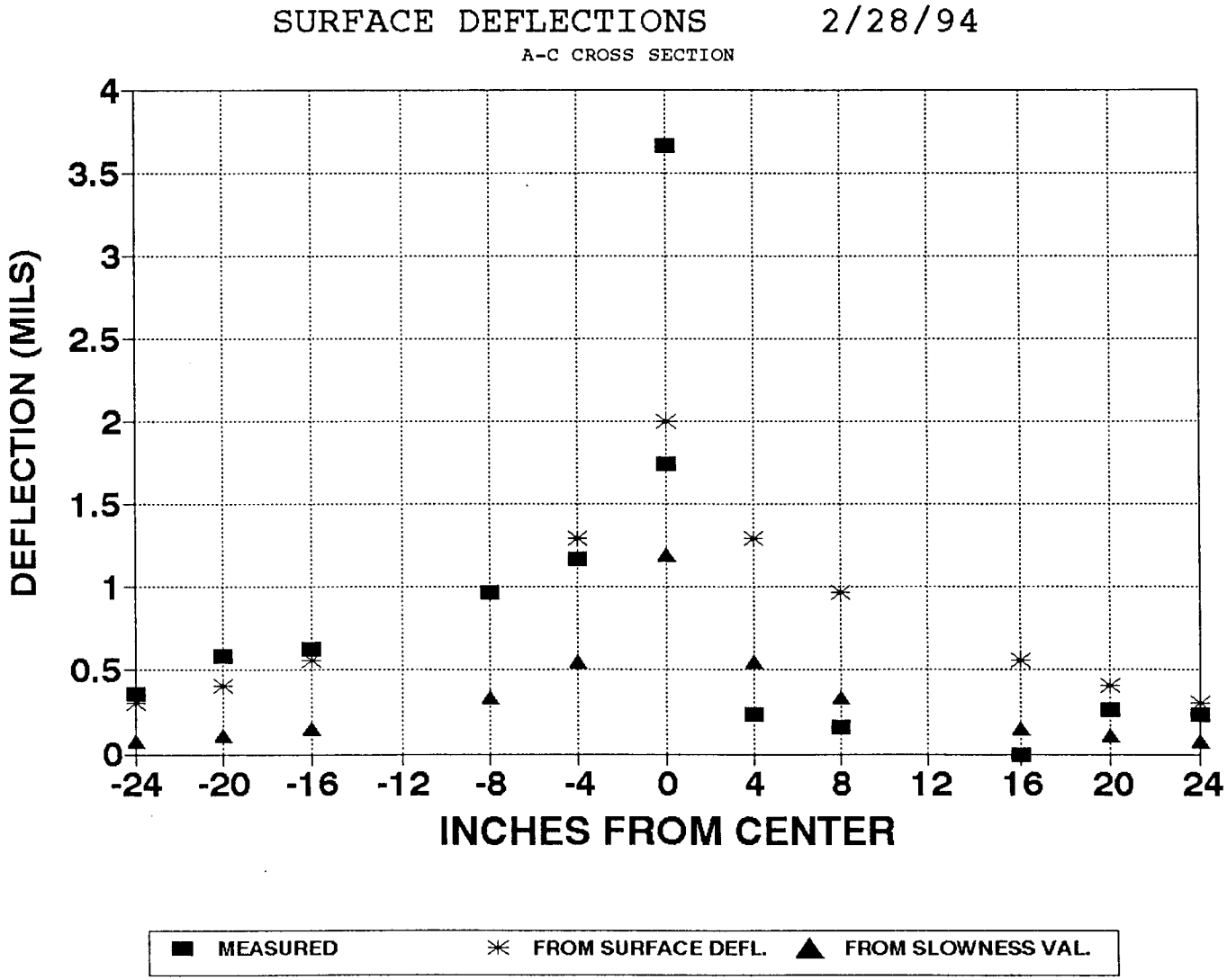
SURFACE DEFLECTIONS 2/28/94
A-C CROSS SECTION
DEFLECTION (MILS)
4
3.5
3
2.5
2
1.5
1
0.5
0
-24 -20 -16 -12 -8 -4 0 4 8 12 16 20 24
INCHES FROM CENTER
MEASURED
FROM SURFACE DEFL.
FROM SLOWNESS VAL.

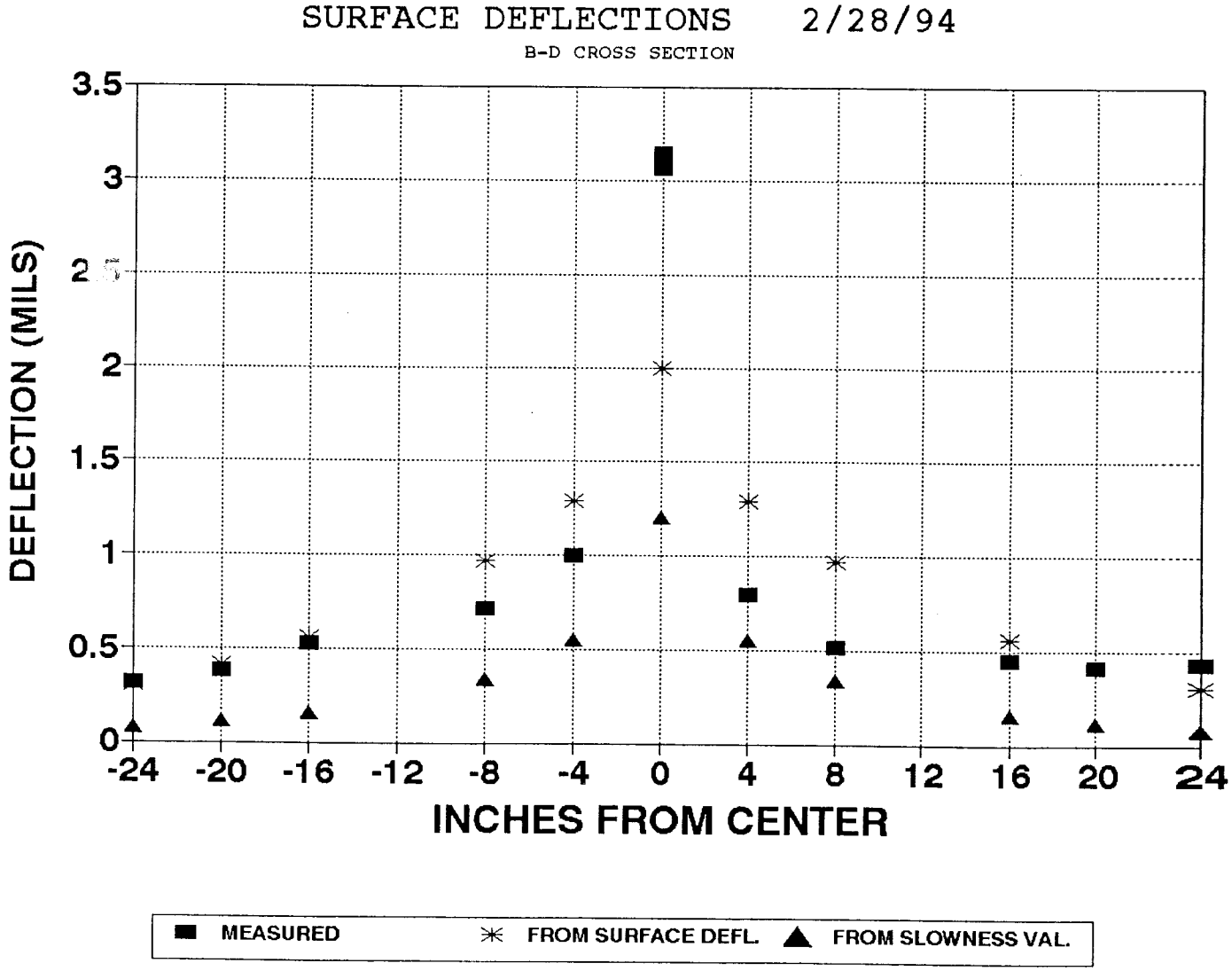
SURFACE DEFLECTIONS 2/28/94
B-D CROSS SECTION
DEFLECTION (MILS)
3.5
3
2
1.5
1
0.5
0
-24 -20 -16 -12 -8 -4 0 4 8 12 16 20 24
INCHES FROM CENTER
MEASURED
FROM SURFACE DEFL.
FROM SLOWNESS VAL.

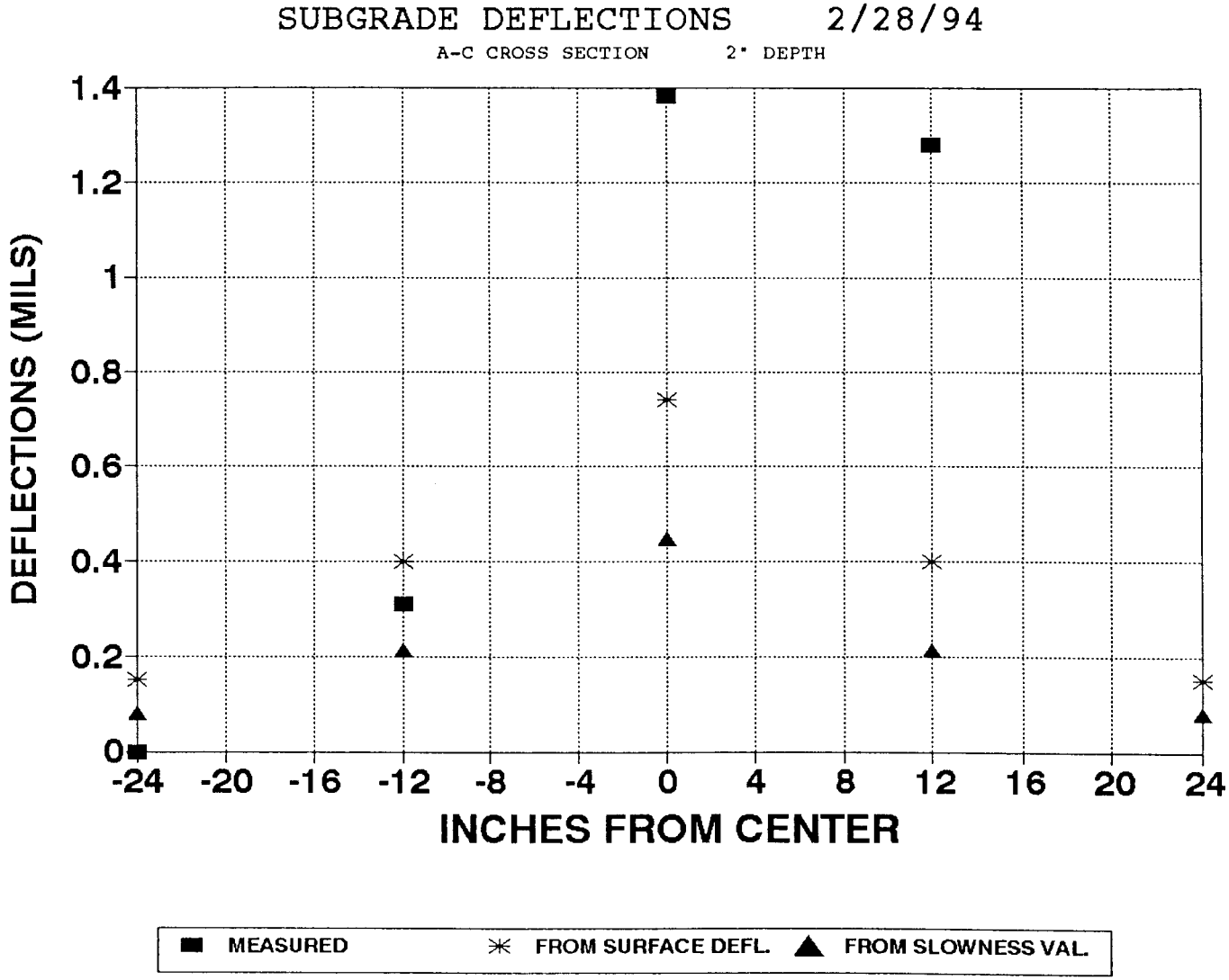
SUBGRADE DEFLECTIONS 2/28/94
A-C CROSS SECTION 2" DEPTH
DEFLECTIONS (MILS)
1.4
1.2
1
0.8
0.6
0.4
0.2
0
-24 -20 -16 -12 -8 -4 0 4 8 12 16 20 24
INCHES FROM CENTER
MEASURED
FROM SURFACE DEFL.
FROM SLOWNESS VAL.

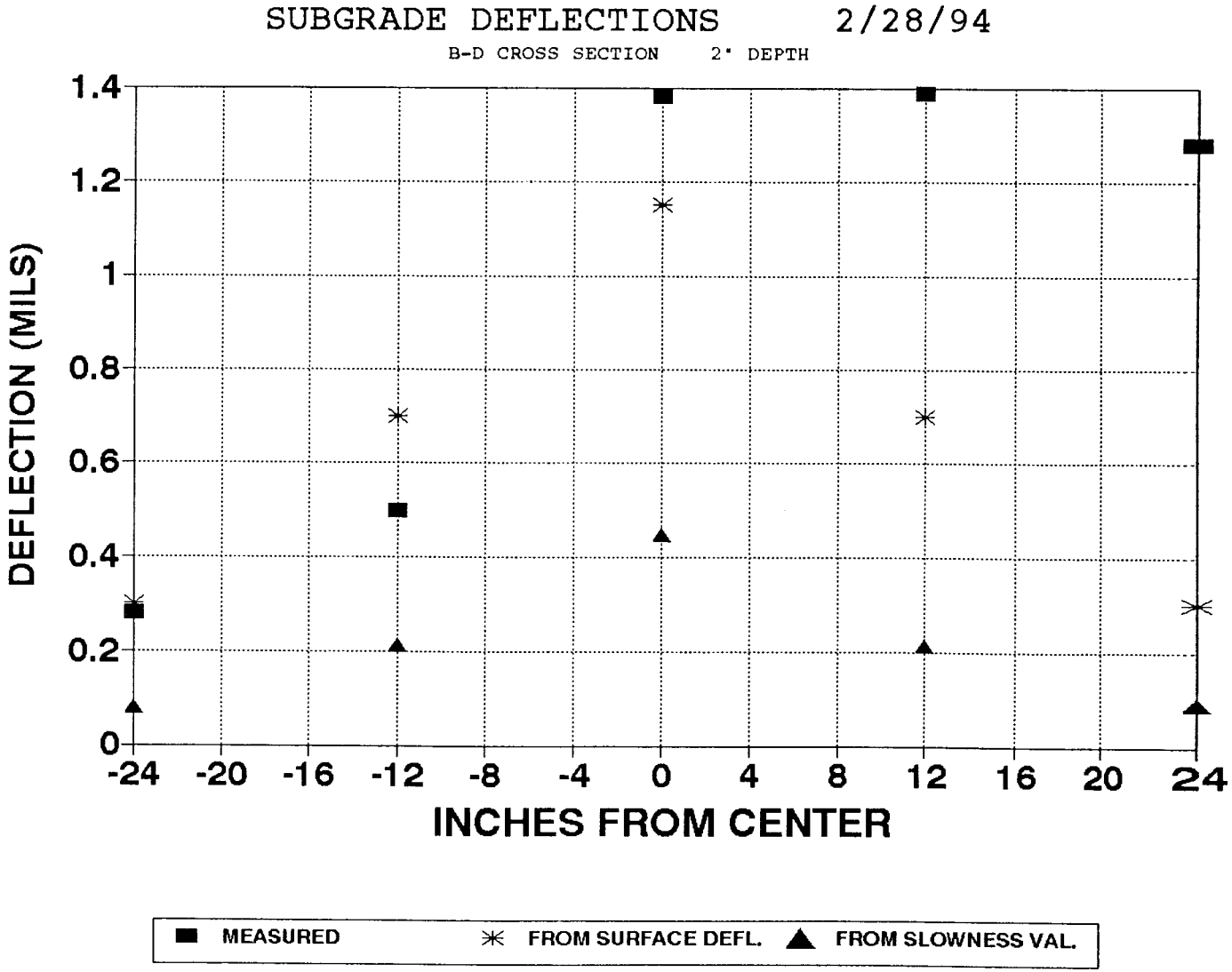
SUBGRADE DEFLECTIONS 2/28/94
B-D CROSS SECTION 2' DEPTH
DEFLECTION (MILS)
1.4
1.2
1
0.8
0.6
0.4
0.2
0
-24 -20 -16 -12 -8 -4 0 4 8 12 16 20 24
INCHES FROM CENTER
MEASURED
FROM SURFACE DEFL.
FROM SLOWNESS VAL.

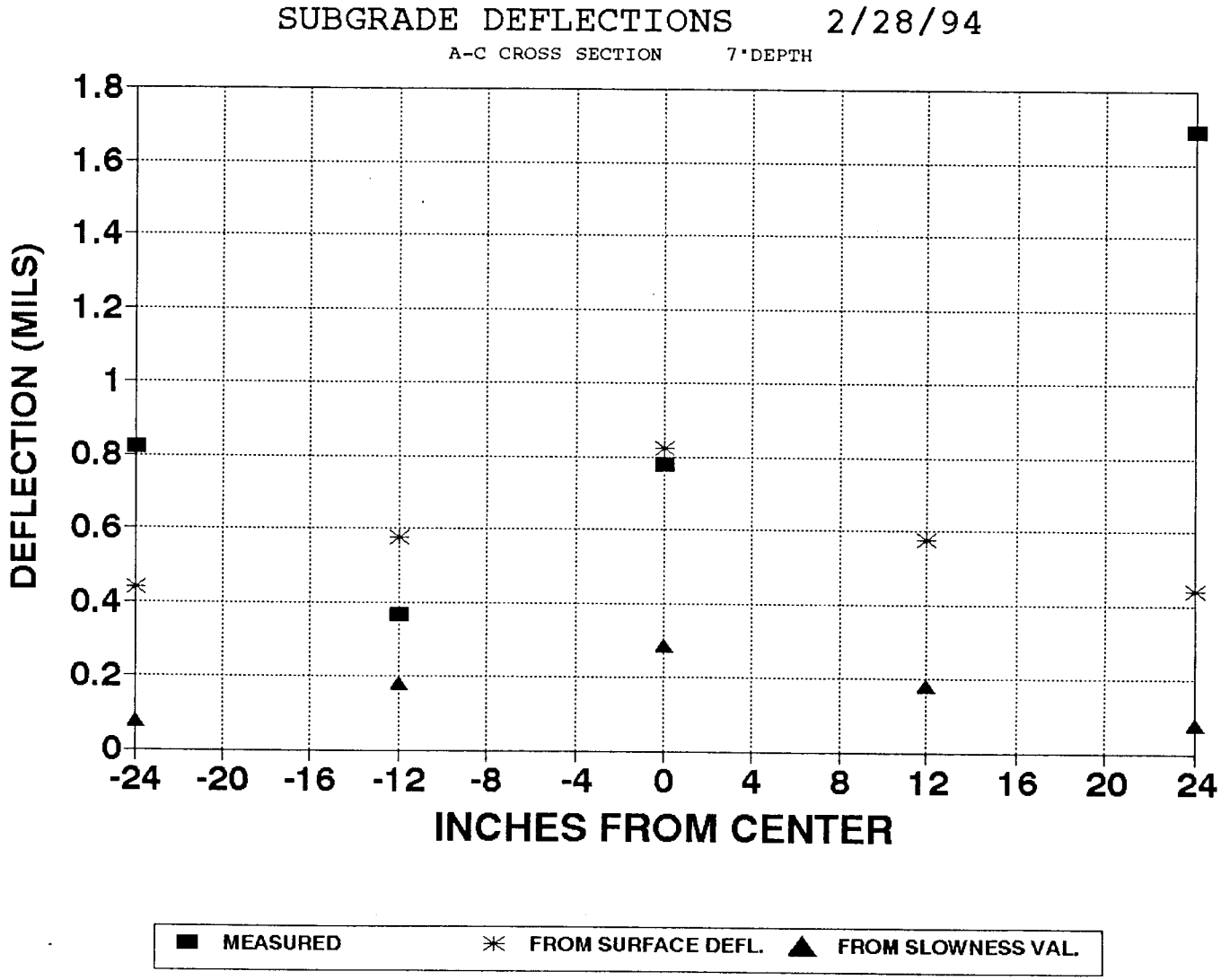
SUBGRADE DEFLECTIONS 2/28/94
A-C CROSS SECTION 7'DEPTH
DEFLECTION (MILS)
1.8
1.6
1.4
1.2
1
0.8
0.6
0.4
0.2
0
-24 -20 -16 -12 -8 -4 0 4 8 12 16 20 24
INCHES FROM CENTER
MEASURED
FROM SURFACE DEFL.
FROM SLOWNESS VAL.

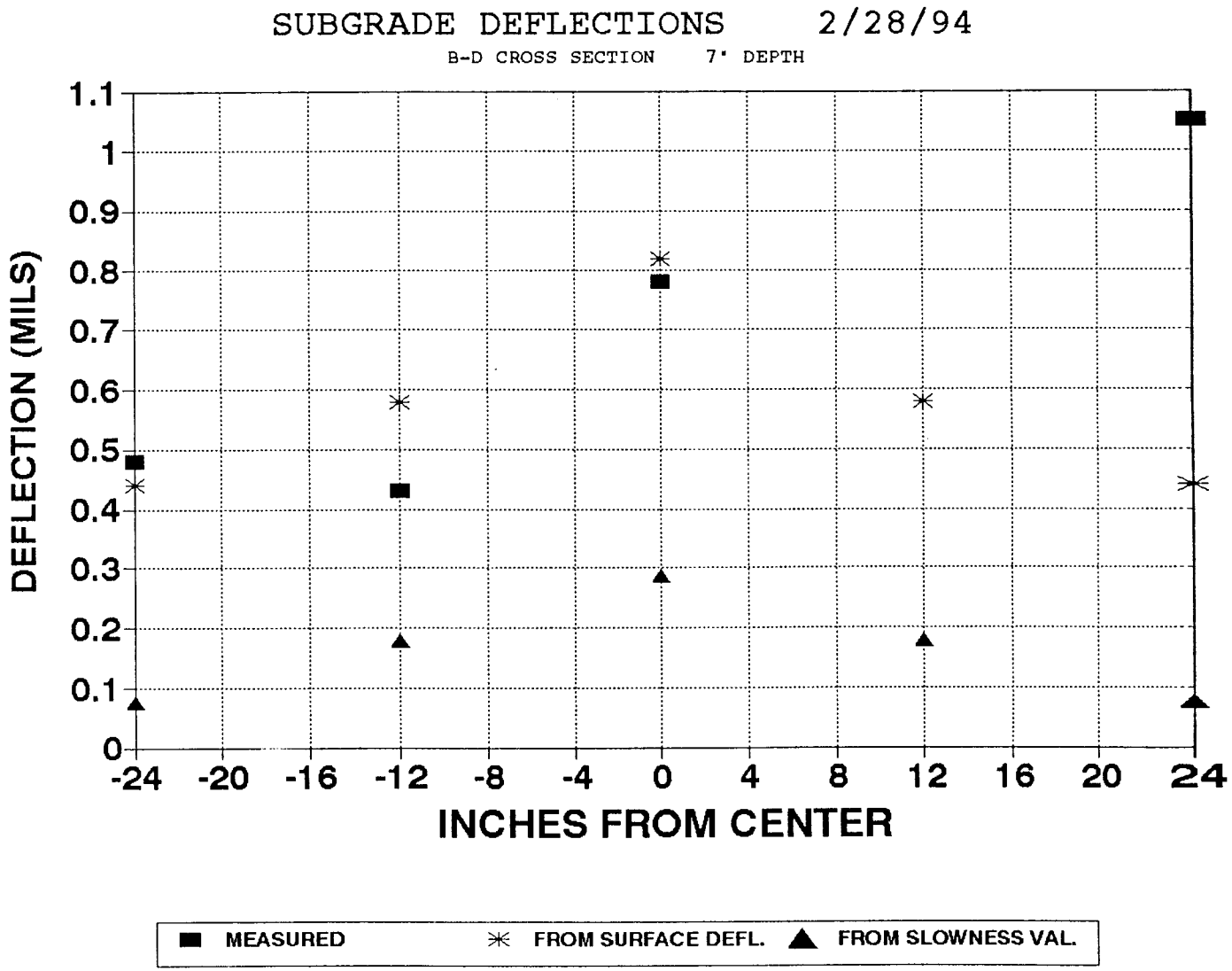
SUBGRADE DEFLECTIONS 2/28/94
B-D CROSS SECTION 7" DEPTH
DEFLECTION (MILS)
1.1
1
0.9
0.8
0.7
0.6
0.5
0.4
0.3
0.2
0.1
0
-24 -20 -16 -12 -8 -4 0 4 8 12 16 20 24
INCHES FROM CENTER
MEASURED
FROM SURFACE DEFL.
FROM SLOWNESS VAL.

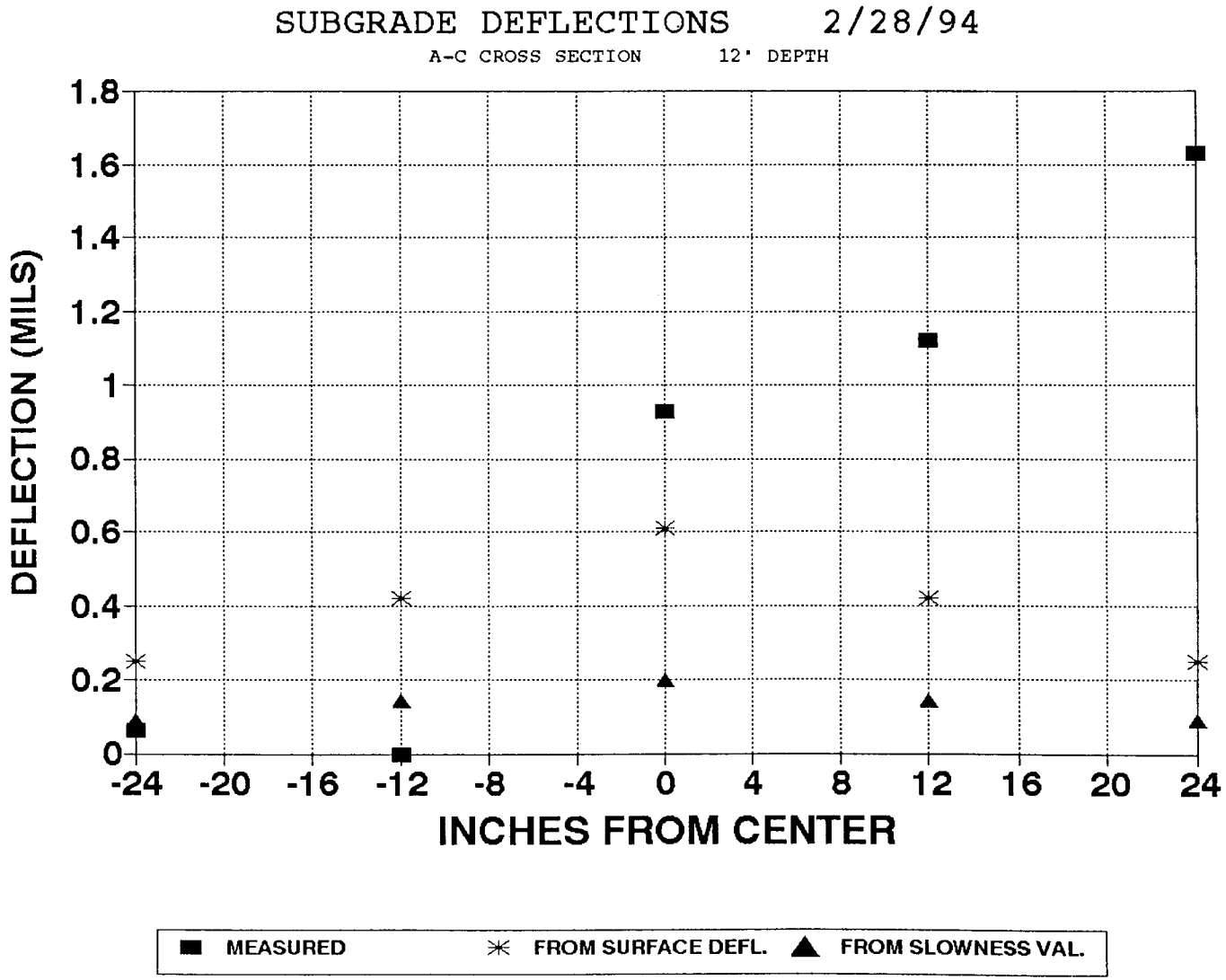
SUBGRADE DEFLECTIONS 2/28/94
A-C CROSS SECTION 12' DEPTH
DEFLECTION (MILS)
1.8
1.6
1.4
1.2
1
0.8
0.6
0.4
0.2
0
-24 -20 -16 -12 -8 -4 0 4 8 12 16 20 24
INCHES FROM CENTER
MEASURED
FROM SURFACE DEFL.
FROM SLOWNESS VAL.

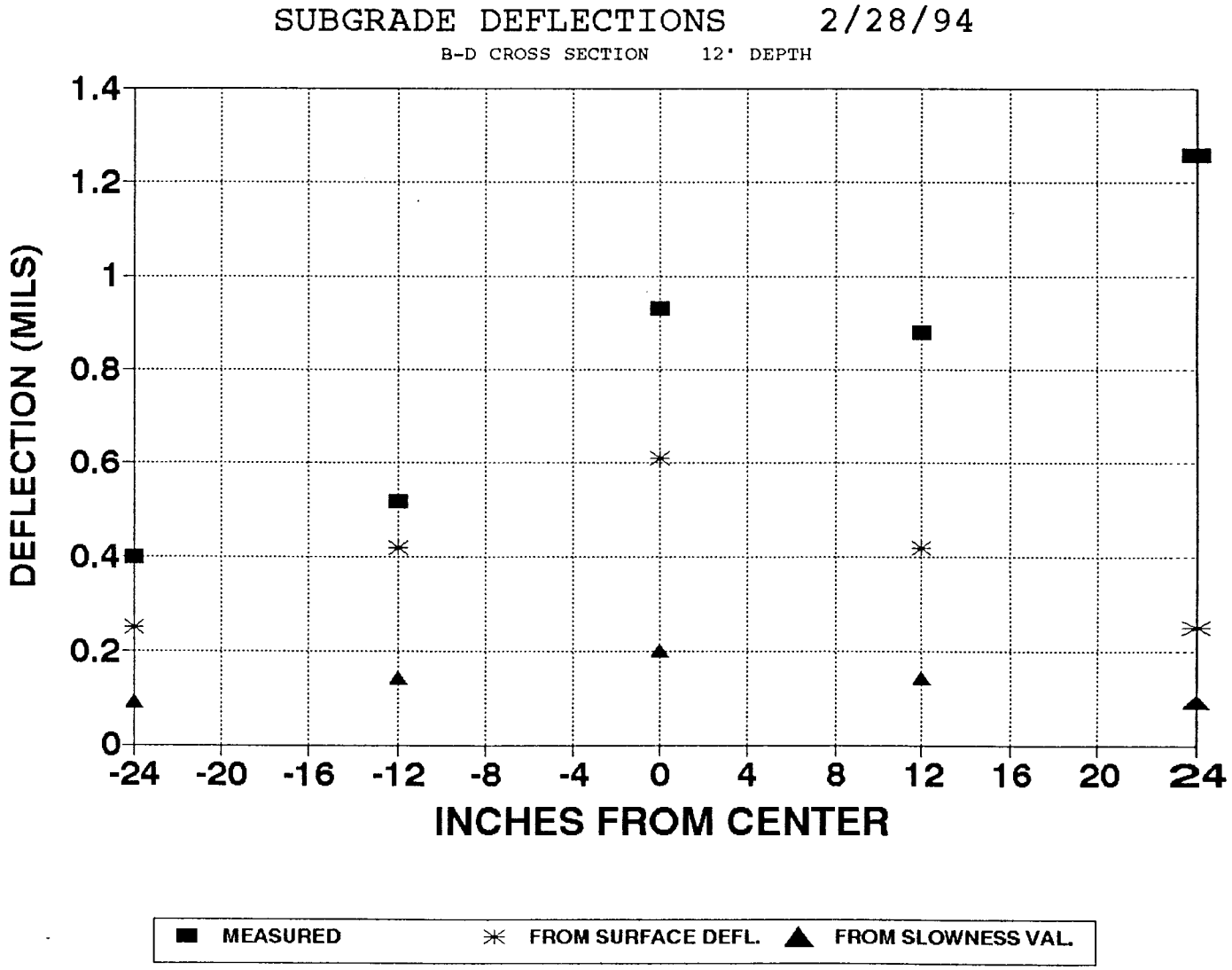
SUBGRADE DEFLECTIONS 2/28/94
B-D CROSS SECTION 12' DEPTH
DEFLECTION (MILS)
1.4
1.2
1
0.8
0.6
0.4
0.2
0
-24 -20 -16 -12 -8 -4 0 4 8 12 16 20 24
INCHES FROM CENTER
MEASURED
FROM SURFACE DEFL.
FROM SLOWNESS VAL.

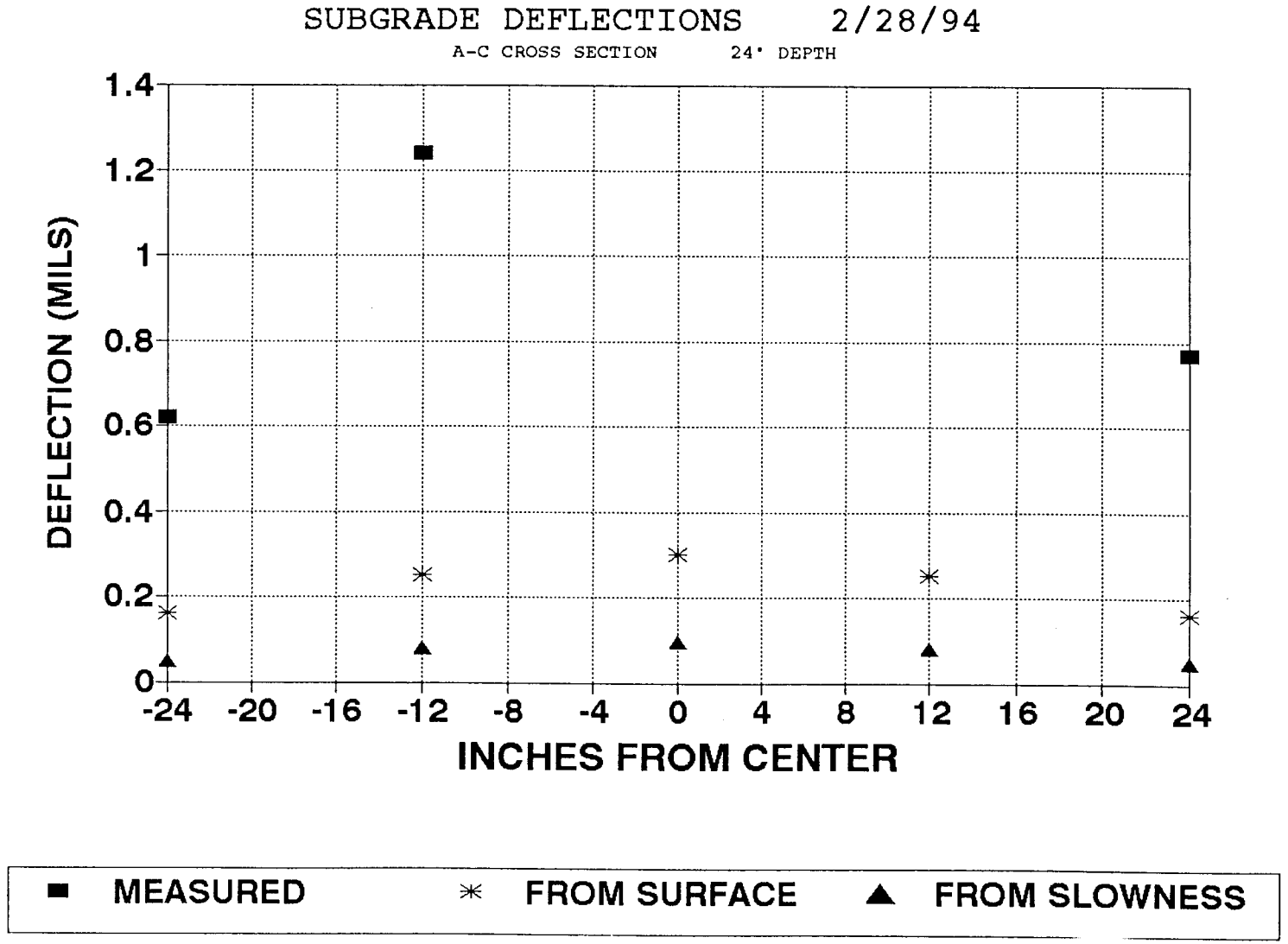
SUBGRADE DEFLECTIONS 2/28/94
A-C CROSS SECTION 24" DEPTH
DEFLECTION (MILS)
1.4
1.2
1
0.8
0.6
0.4
0.2
0
-24 -20 -16 -12 -8 -4 0 4 8 12 16 20 24
INCHES FROM CENTER
MEASURED
FROM SURFACE
FROM SLOWNESS

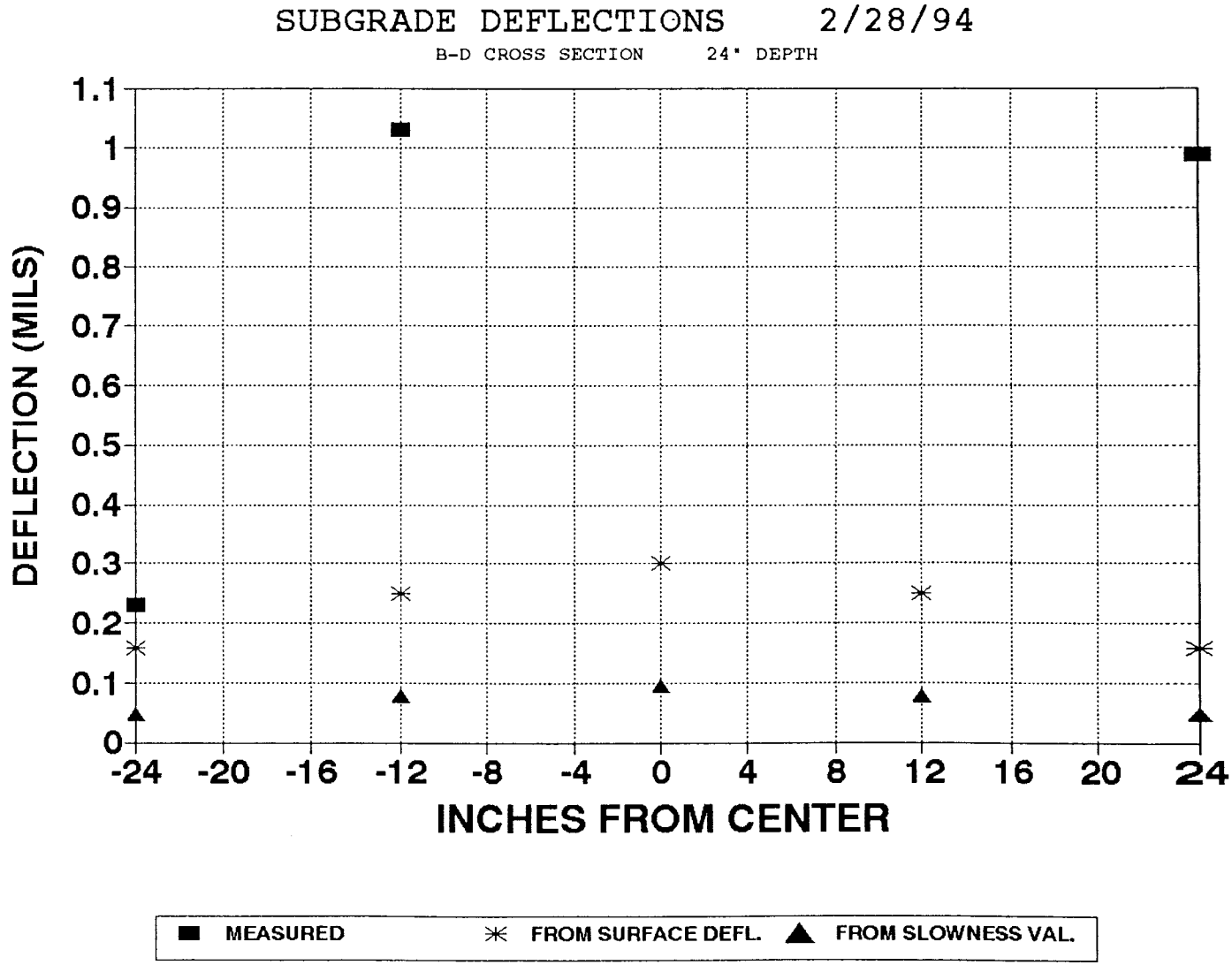
SUBGRADE DEFLECTIONS 2/28/94
B-D CROSS SECTION 24" DEPTH
DEFLECTION (MILS)
1.1
1
0.9
0.8
0.7
0.6
0.5
0.4
0.3
0.2
0.1
0
-24 -20 -16 -12 -8 -4 0 4 8 12 16 20 24
INCHES FROM CENTER
MEASURED
FROM SURFACE DEFL.
FROM SLOWNESS VAL.

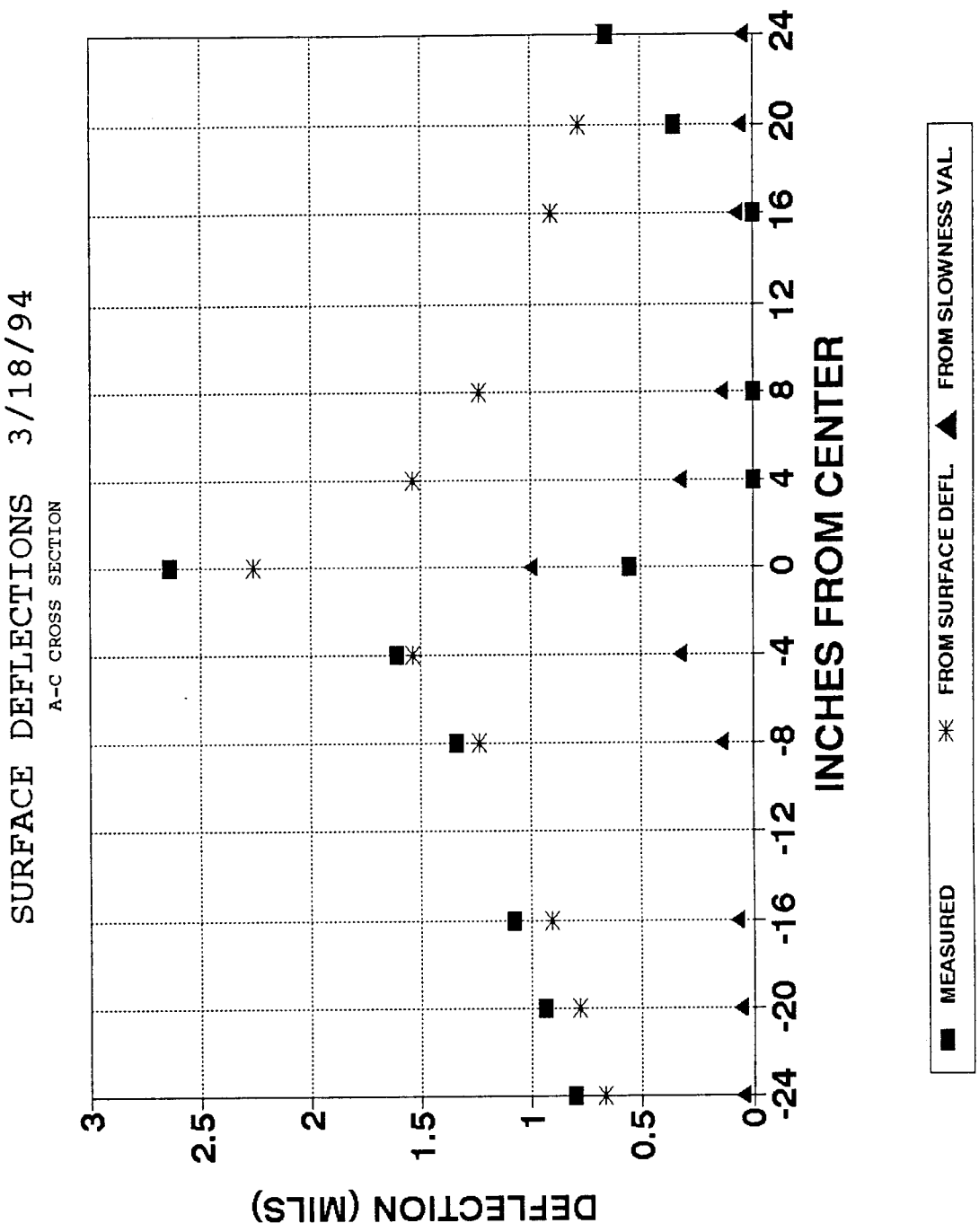
SURFACE DEFLECTIONS 3/18/94
A-C CROSS SECTION
DEFLECTION (MILS)
3
2.5
2
1.5
1
0.5
0
-24
-20
-16
-12
-8
-4
0
4
8
12
16
20
24
INCHES FROM CENTER
MEASURED
FROM SURFACE DEFL.
FROM SLOWNESS VAL.

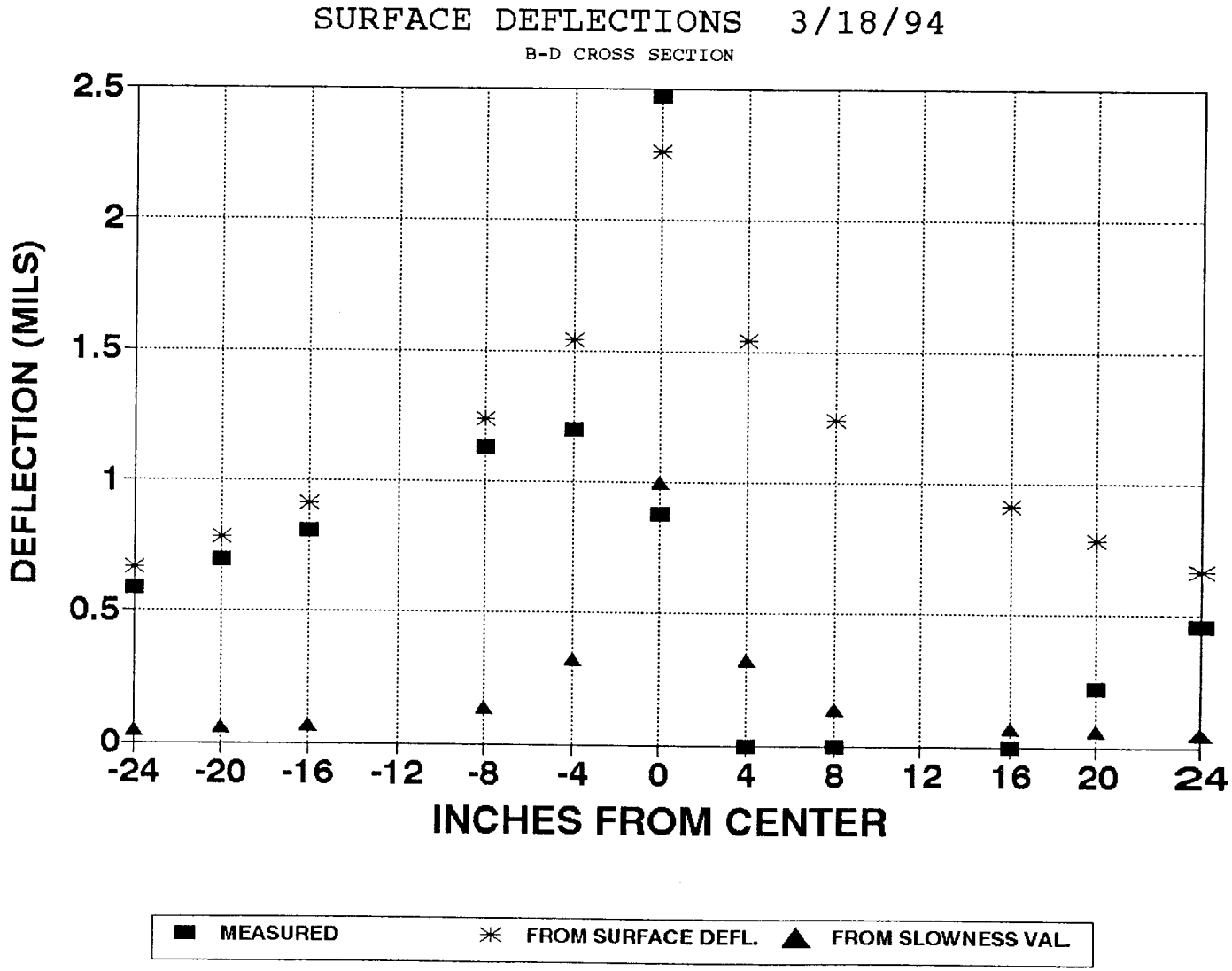
SURFACE DEFLECTIONS 3/18/94
B-D CROSS SECTION
DEFLECTION (MILS)
2.5
2
1.5
1
0.5
0
-24
-20
-16
-12
-8
-4
0
4
8
12
16
20
24
INCHES FROM CENTER
MEASURED
FROM SURFACE DEFL.
FROM SLOWNESS VAL.

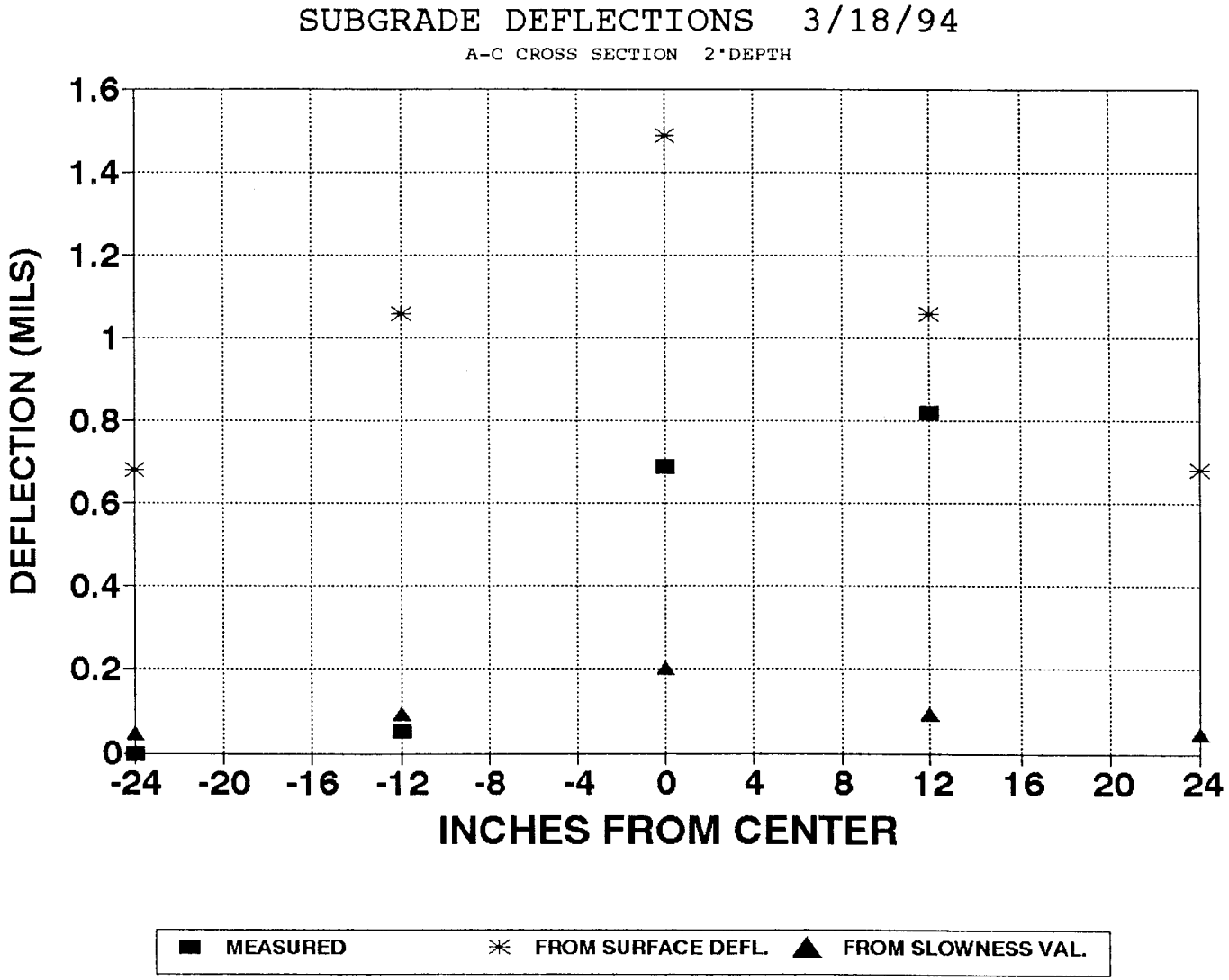
SUBGRADE DEFLECTIONS 3/18/94
A-C CROSS SECTION 2"DEPTH
DEFLECTION (MILS)
1.6
1.4
1.2
1
0.8
0.6
0.4
0.2
0
-24 -20 -16 -12 -8 -4 0 4 8 12 16 20 24
INCHES FROM CENTER
MEASURED
FROM SURFACE DEFL.
FROM SLOWNESS VAL.

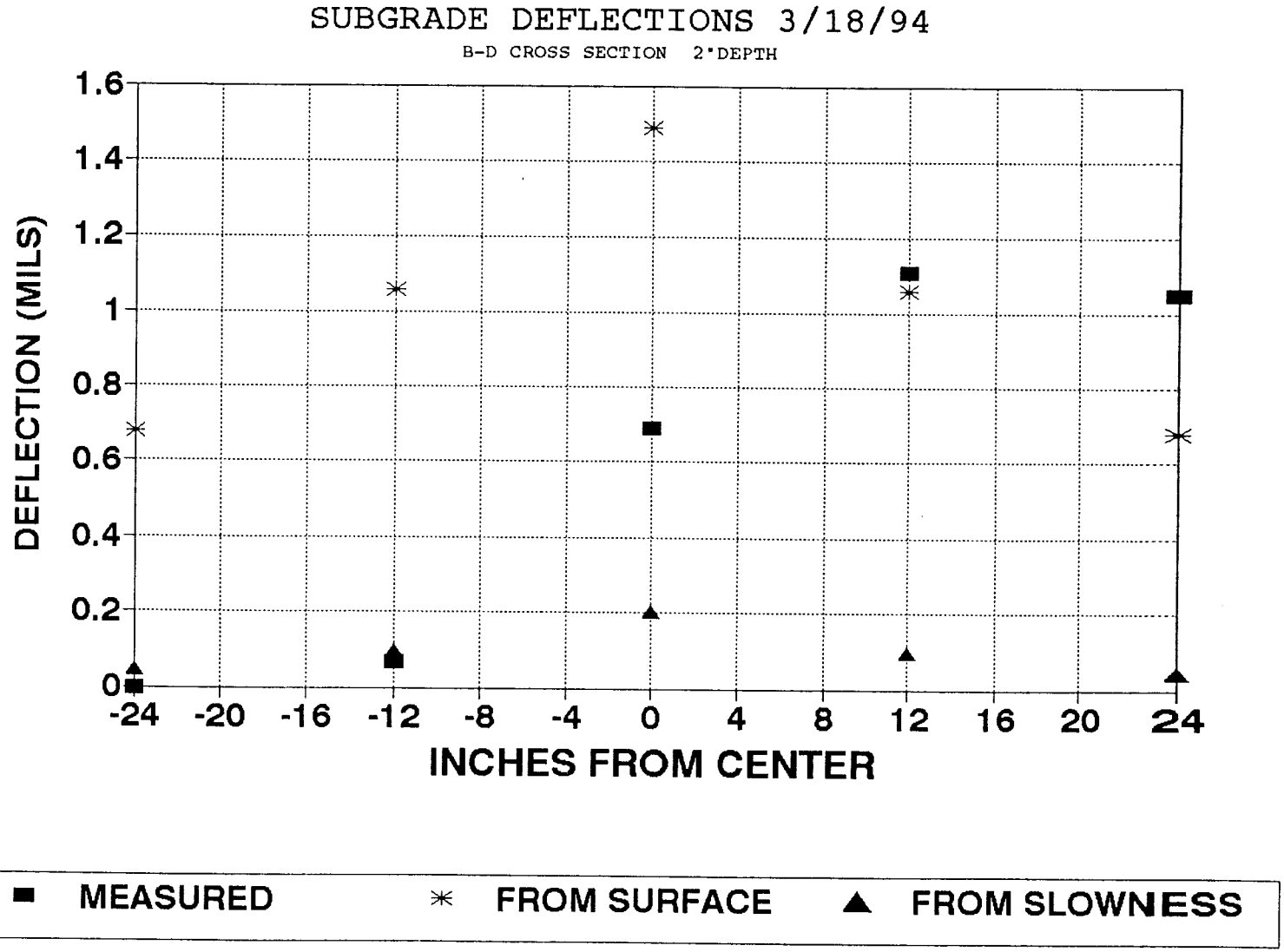
SUBGRADE DEFLECTIONS 3/18/94
B-D CROSS SECTION 2"DEPTH
DEFLECTION (MILS)
1.6
1.4
1.2
1
0.8
0.6
0.4
0.2
0
-24
-20
-16
-12
-8
-4
0
4
8
12
16
20
24
INCHES FROM CENTER
MEASURED
FROM SURFACE
FROM SLOWNESS

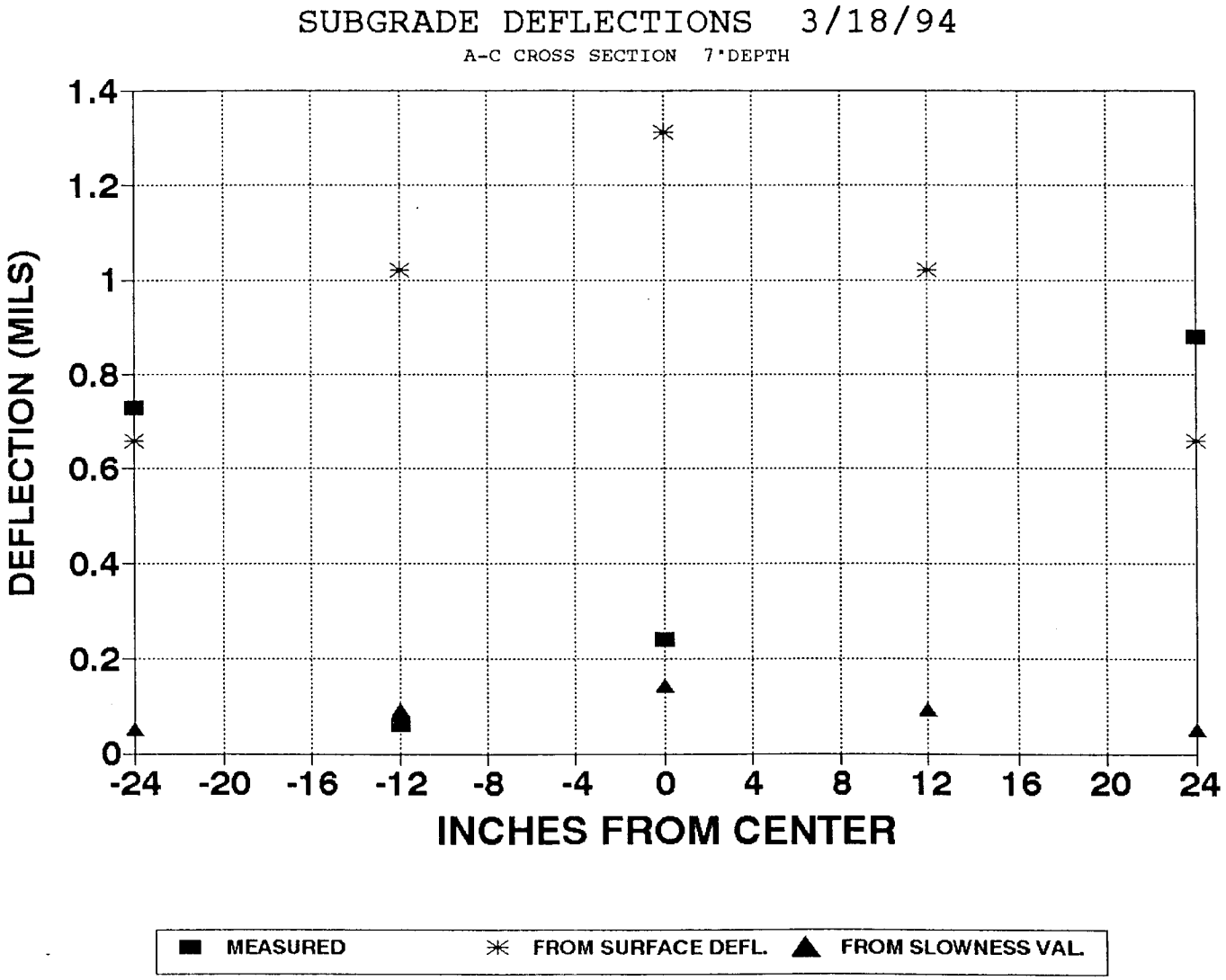
SUBGRADE DEFLECTIONS 3/18/94
A-C CROSS SECTION 7"DEPTH
DEFLECTION (MILS)
1.4
1.2
1
0.8
0.6
0.4
0.2
0
-24
-20
-16
-12
-8
-4
0
4
8
12
16
20
24
INCHES FROM CENTER
MEASURED
FROM SURFACE DEFL.
FROM SLOWNESS VAL.

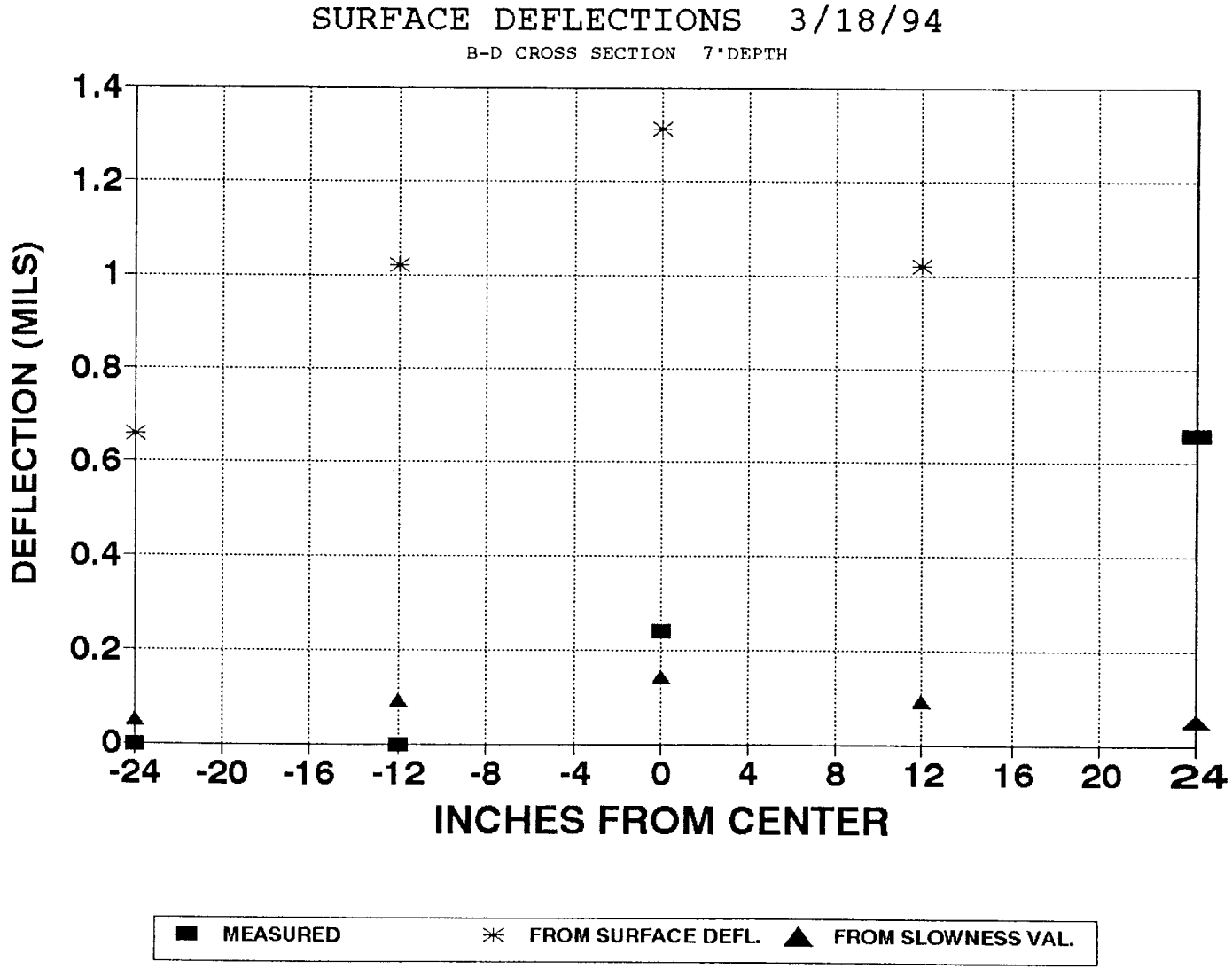
SURFACE DEFLECTIONS 3/18/94
B-D CROSS SECTION 7'DEPTH
DEFLECTION (MILS)
1.4
1.2
1
0.8
0.6
0.4
0.2
0
-24 -20 -16 -12 -8 -4 0 4 8 12 16 20 24
INCHES FROM CENTER
MEASURED
FROM SURFACE DEFL.
FROM SLOWNESS VAL.

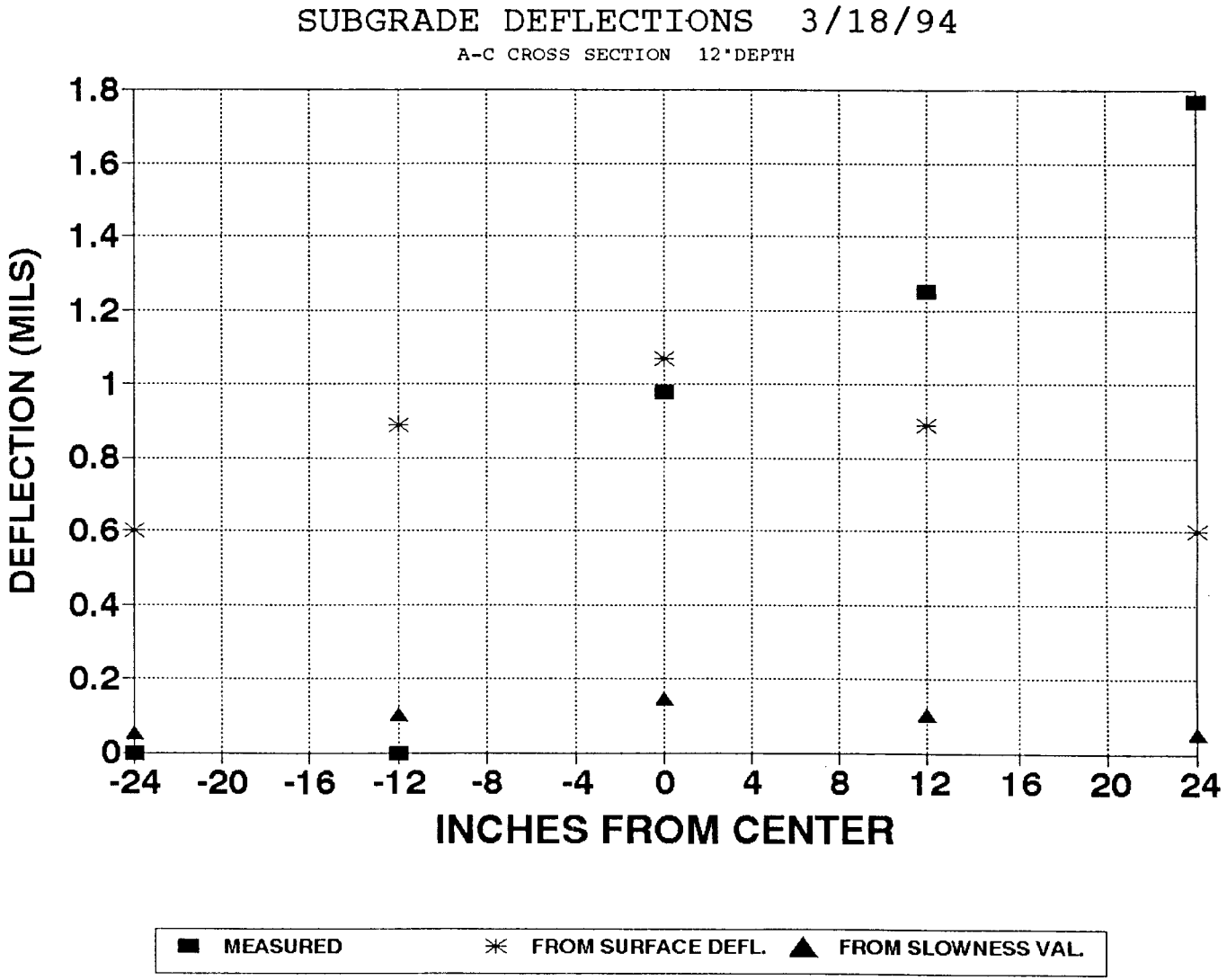
SUBGRADE DEFLECTIONS 3/18/94
A-C CROSS SECTION 12"DEPTH
DEFLECTION (MILS)
1.8
1.6
1.4
1.2
1
0.8
0.6
0.4
0.2
0
-24
-20
-16
-12
-8
-4
0
4
8
12
16
20
24
INCHES FROM CENTER
MEASURED
FROM SURFACE DEFL.
FROM SLOWNESS VAL.

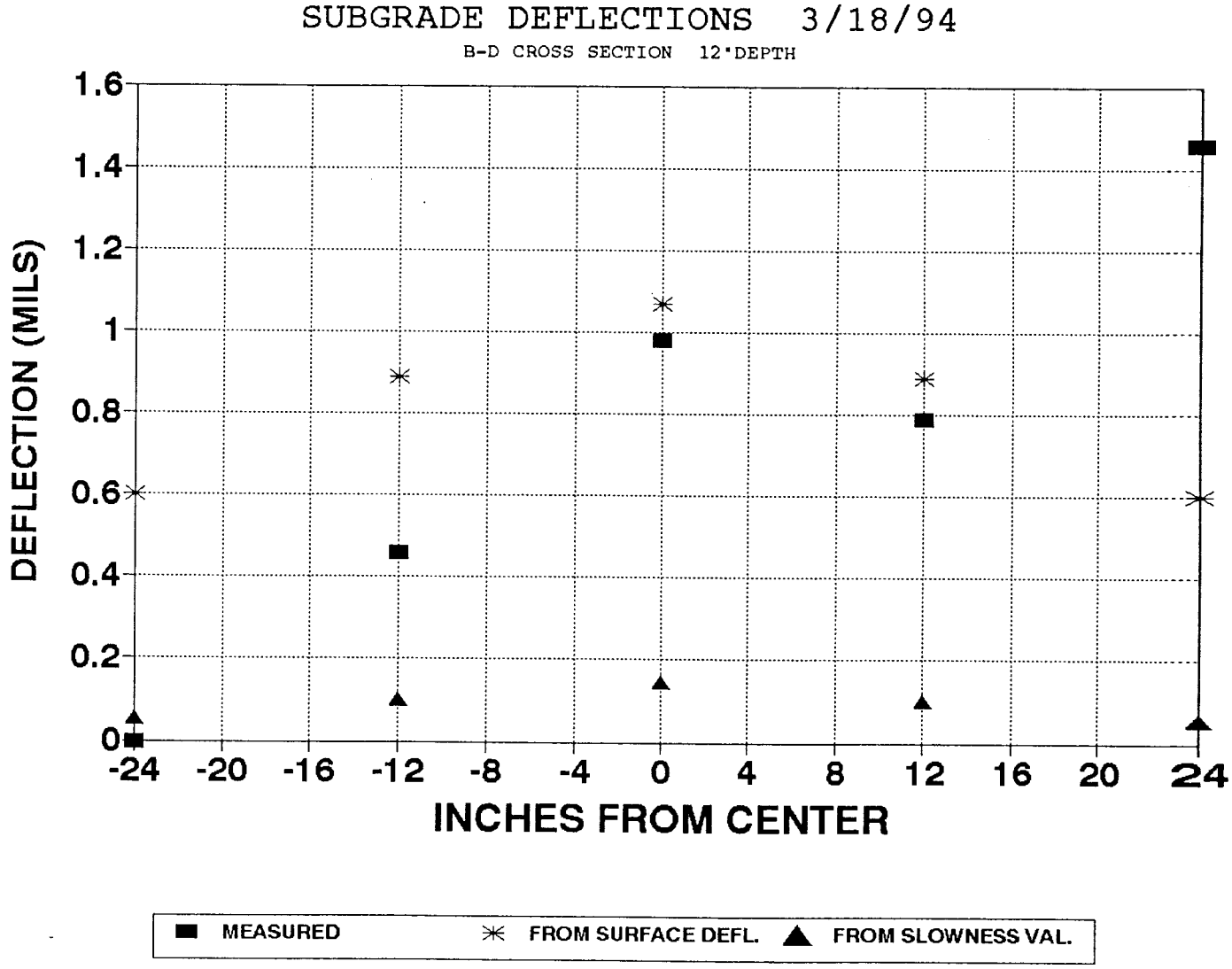
SUBGRADE DEFLECTIONS 3/18/94
B-D CROSS SECTION 12"DEPTH
DEFLECTION (MILS)
1.6
1.4
1.2
1
0.8
0.6
0.4
0.2
0
-24 -20 -16 -12 -8 -4 0 4 8 12 16 20 24
INCHES FROM CENTER
MEASURED
FROM SURFACE DEFL.
FROM SLOWNESS VAL.

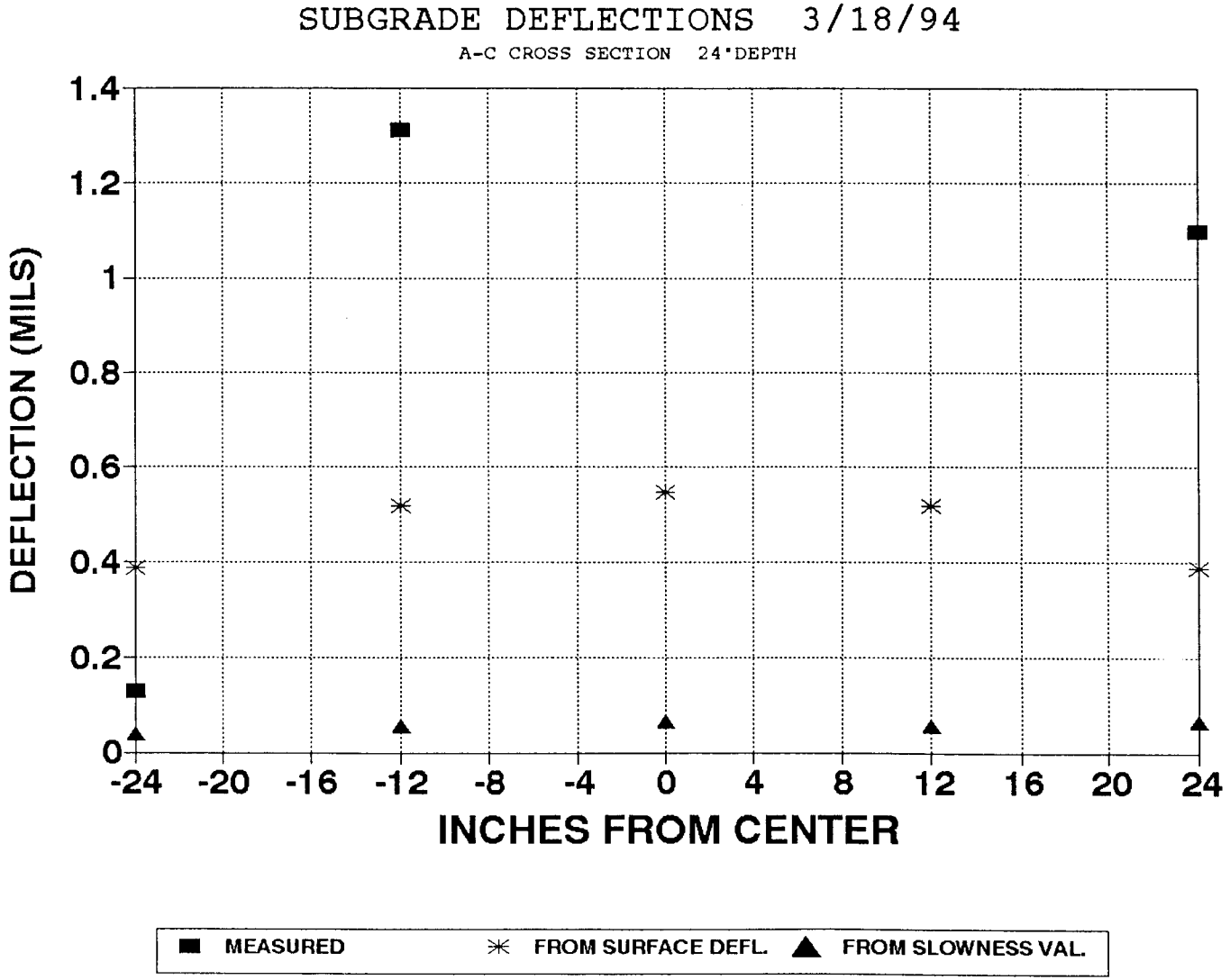
SUBGRADE DEFLECTIONS 3/18/94
A-C CROSS SECTION 24"DEPTH
DEFLECTION (MILS)
1.4
1.2
1
0.8
0.6
0.4
0.2
0
-24
-20
-16
-12
-8
-4
0
4
8
12
16
20
24
INCHES FROM CENTER
MEASURED
FROM SURFACE DEFL.
FROM SLOWNESS VAL.

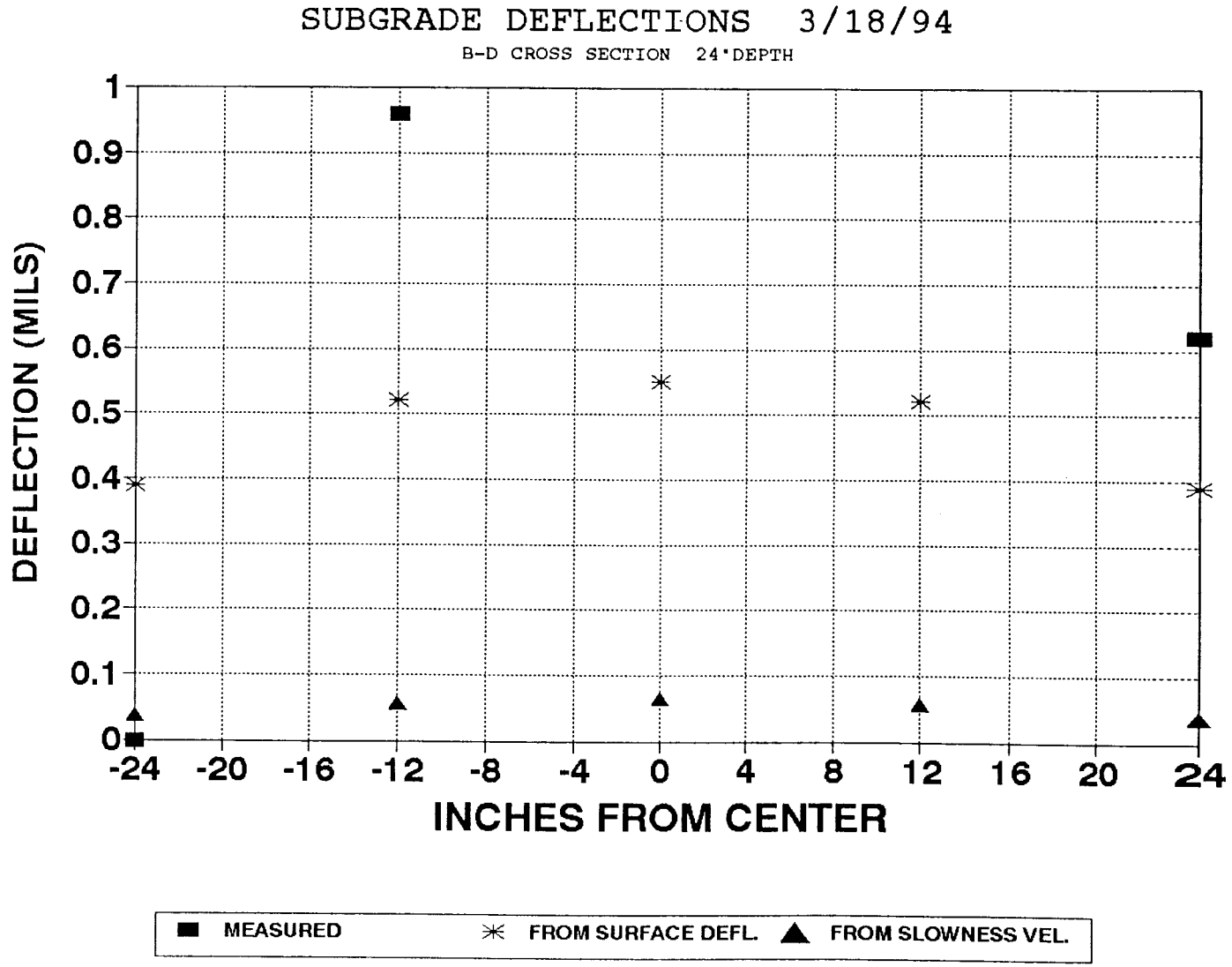
SUBGRADE DEFLECTIONS 3/18/94
B-D CROSS SECTION 24'DEPTH
DEFLECTION (MILS)
1
0.9
0.8
0.7
0.6
0.5
0.4
0.3
0.2
0.1
0
-24
-20
-16
-12
-8
-4
0
4
8
12
16
20
24
INCHES FROM CENTER
MEASURED
FROM SURFACE DEFL.
FROM SLOWNESS VEL.

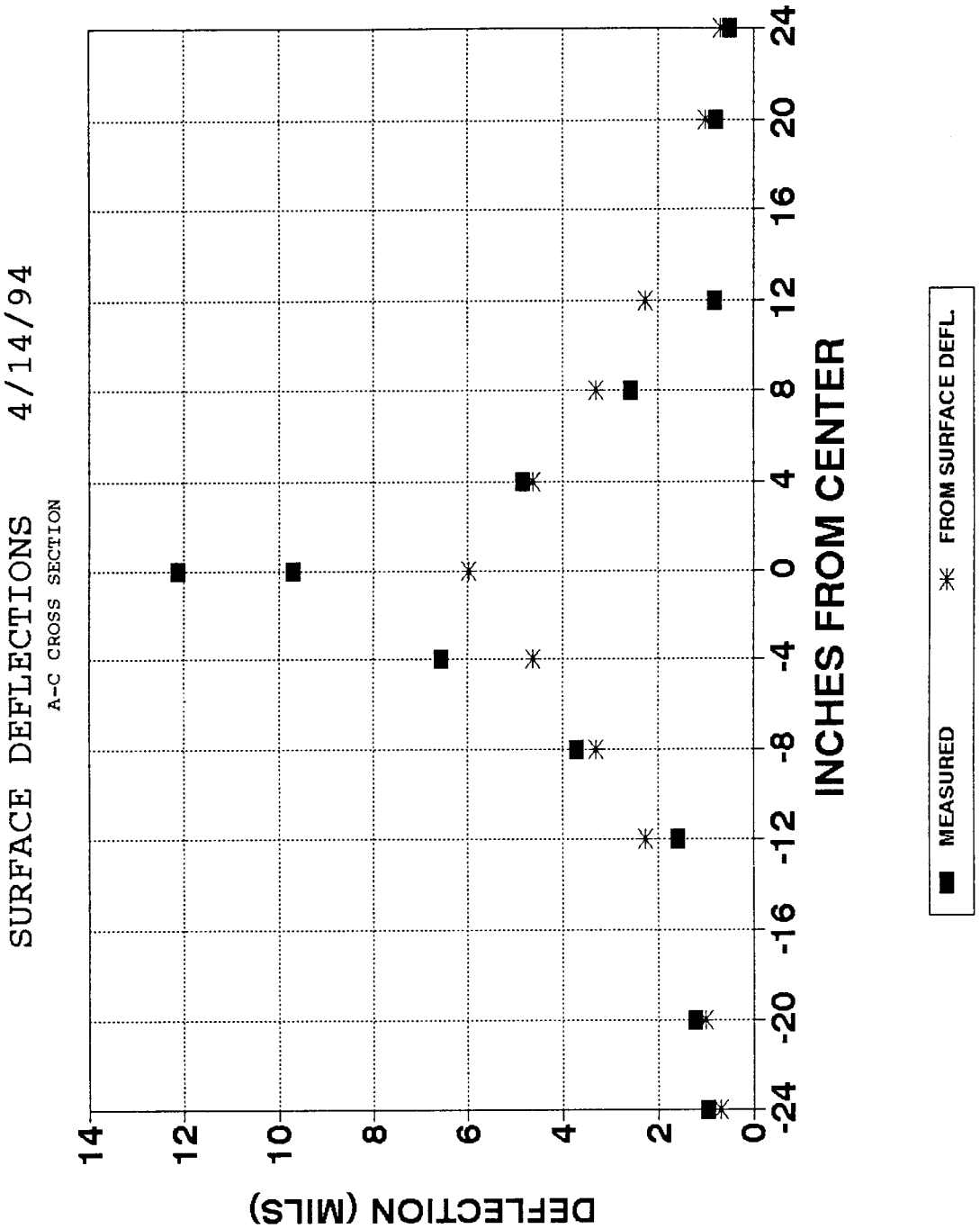
SURFACE DEFLECTIONS 4/14/94
A-C CROSS SECTION
DEFLECTION (MILS)
14
12
10
8
6
4
2
0
-24 -20 -16 -12 -8 -4 0 4 8 12 16 20 24
INCHES FROM CENTER
MEASURED
FROM SURFACE DEFL

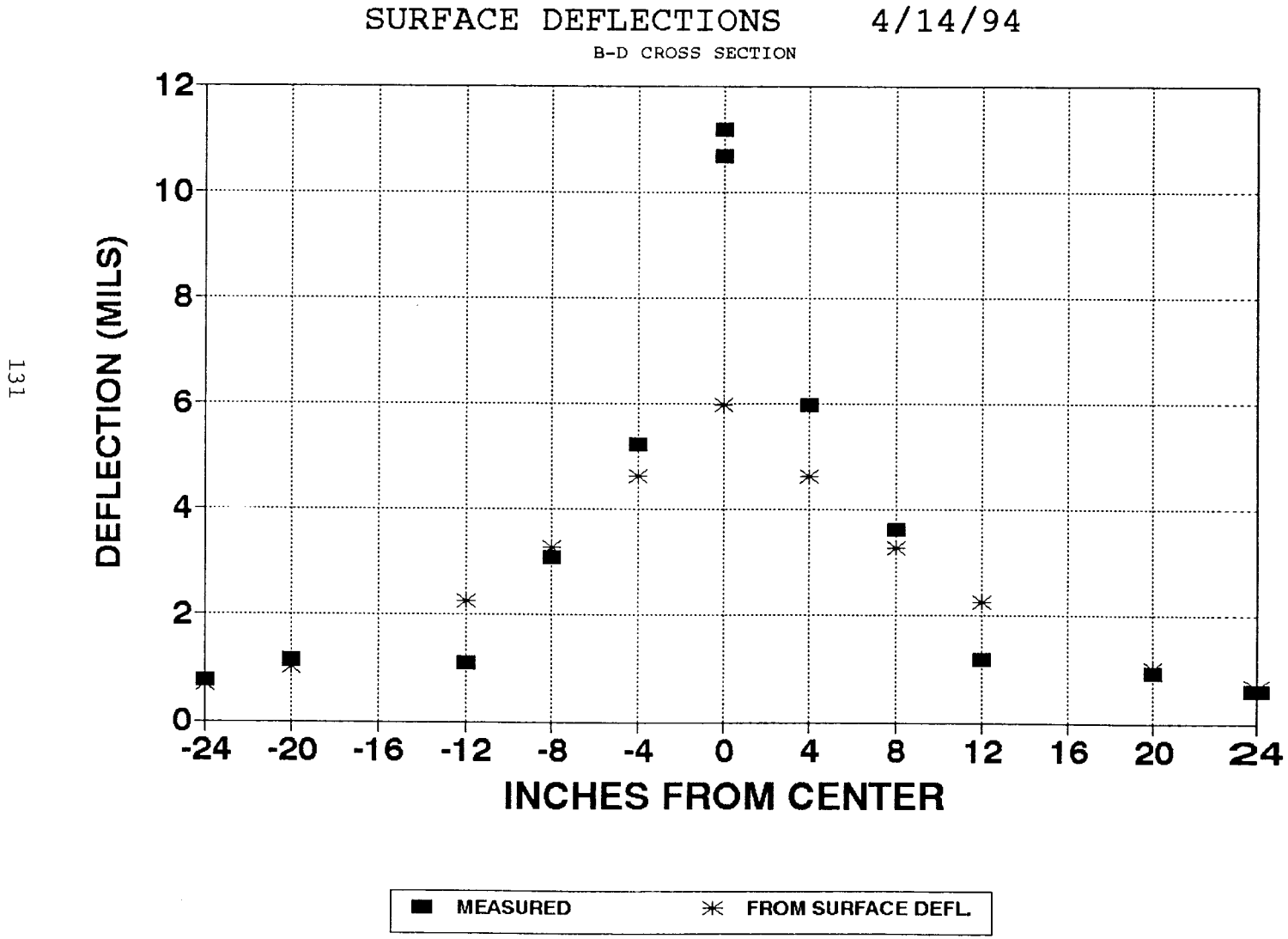
SURFACE DEFLECTIONS 4/14/94
B-D CROSS SECTION
DEFLECTION (MILS)
12
10
8
6
4
2
0
-24
-20
-16
-12
-8
-4
0
4
8
12
16
20
24
INCHES FROM CENTER
MEASURED
FROM SURFACE DEFL.

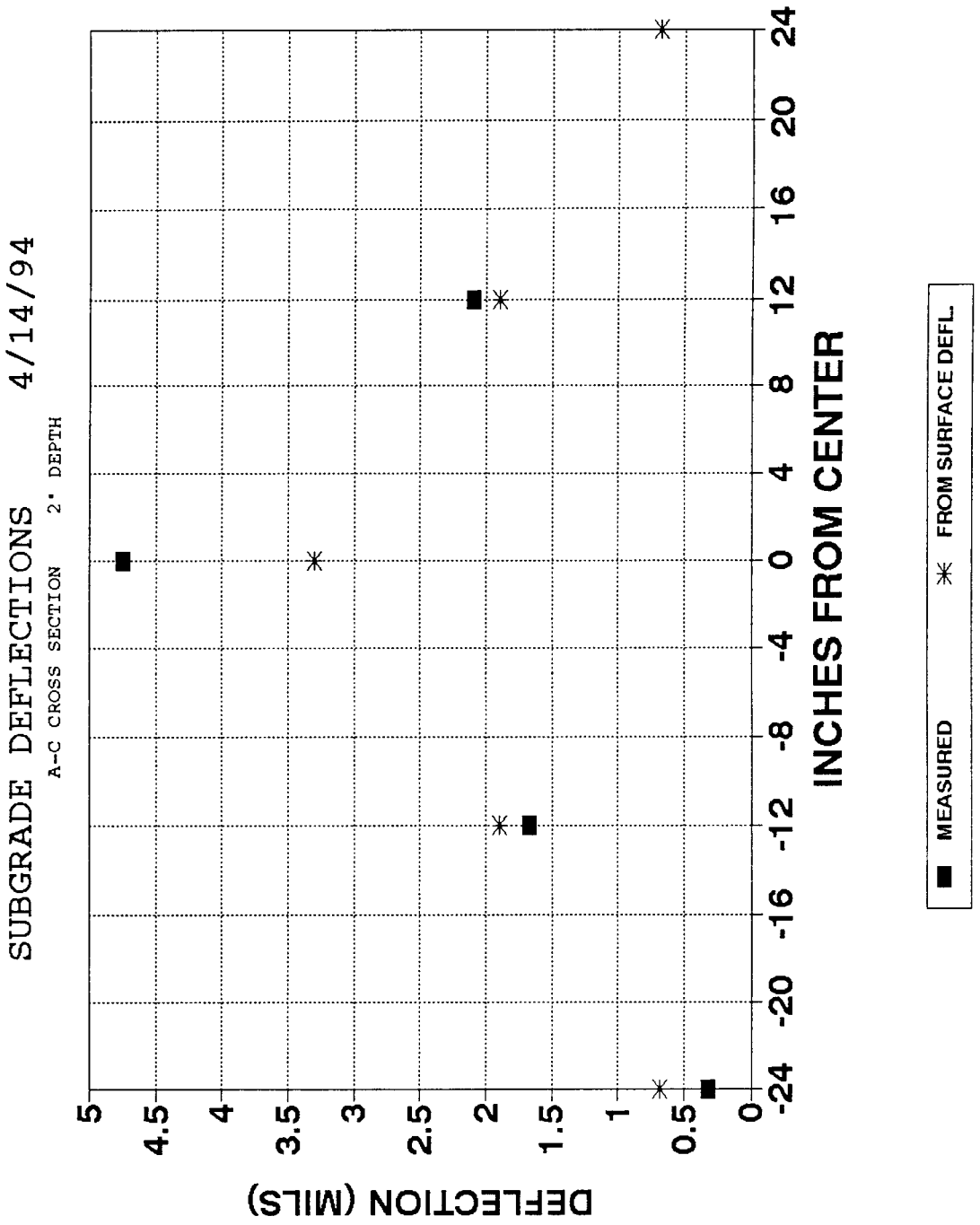
SUBGRADE DEFLECTIONS 4/14/94
A-C CROSS SECTION 2" DEPTH
DEFLECTION (MILS)
5
4.5
4
3.5
3
2.5
2
1.5
1
0.5
0
-24 -20 -16 -12 -8 -4 0 4 8 12 16 20 24
INCHES FROM CENTER
MEASURED
FROM SURFACE DEFL.

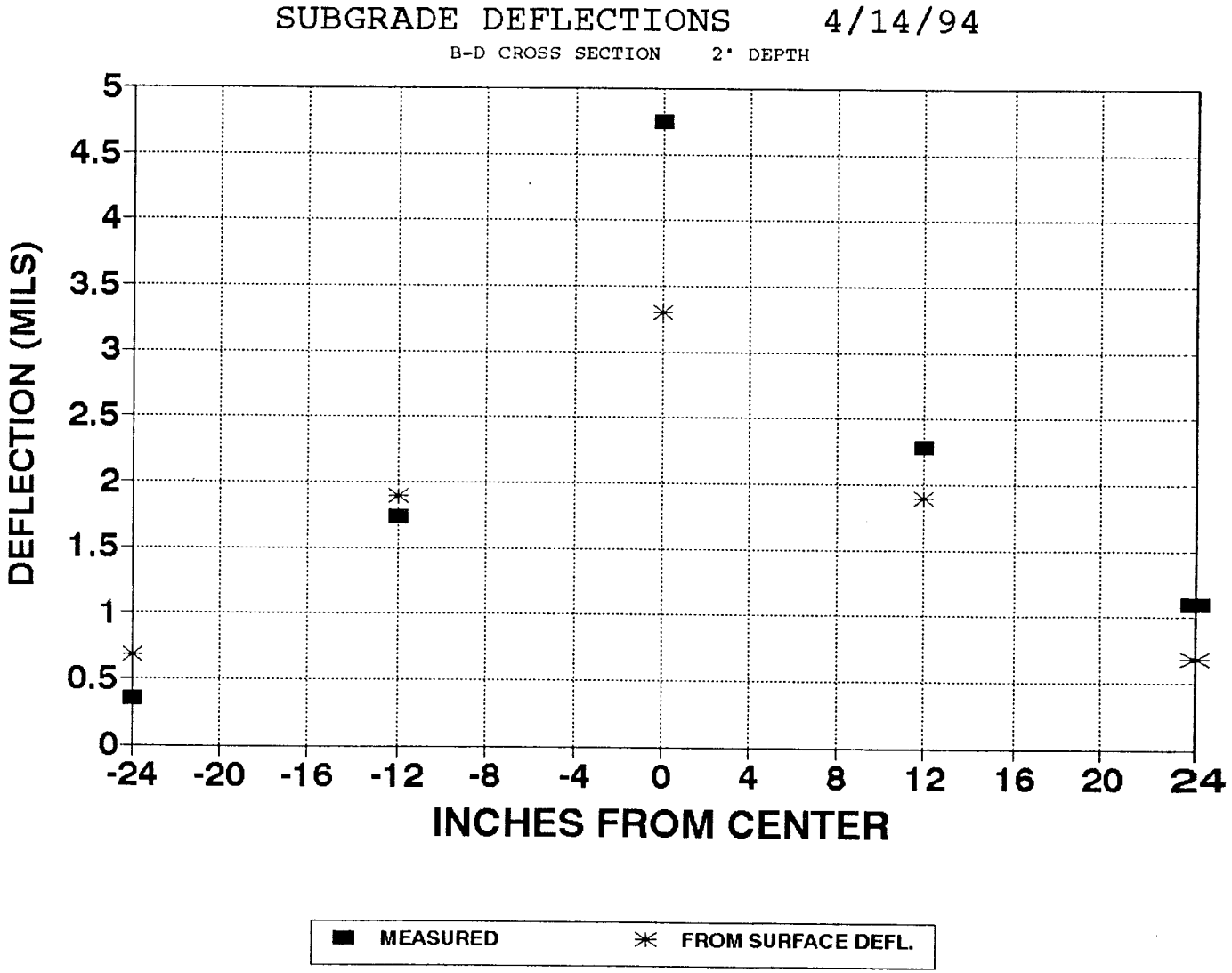
SUBGRADE DEFLECTIONS 4/14/94
B-D CROSS SECTION 2' DEPTH
DEFLECTION (MILS)
5
4.5
4
3.5
3
2.5
2
1.5
1
0.5
0
-24 -20 -16 -12 -8 -4 0 4 8 12 16 20 24
INCHES FROM CENTER
MEASURED
FROM SURFACE DEFL.

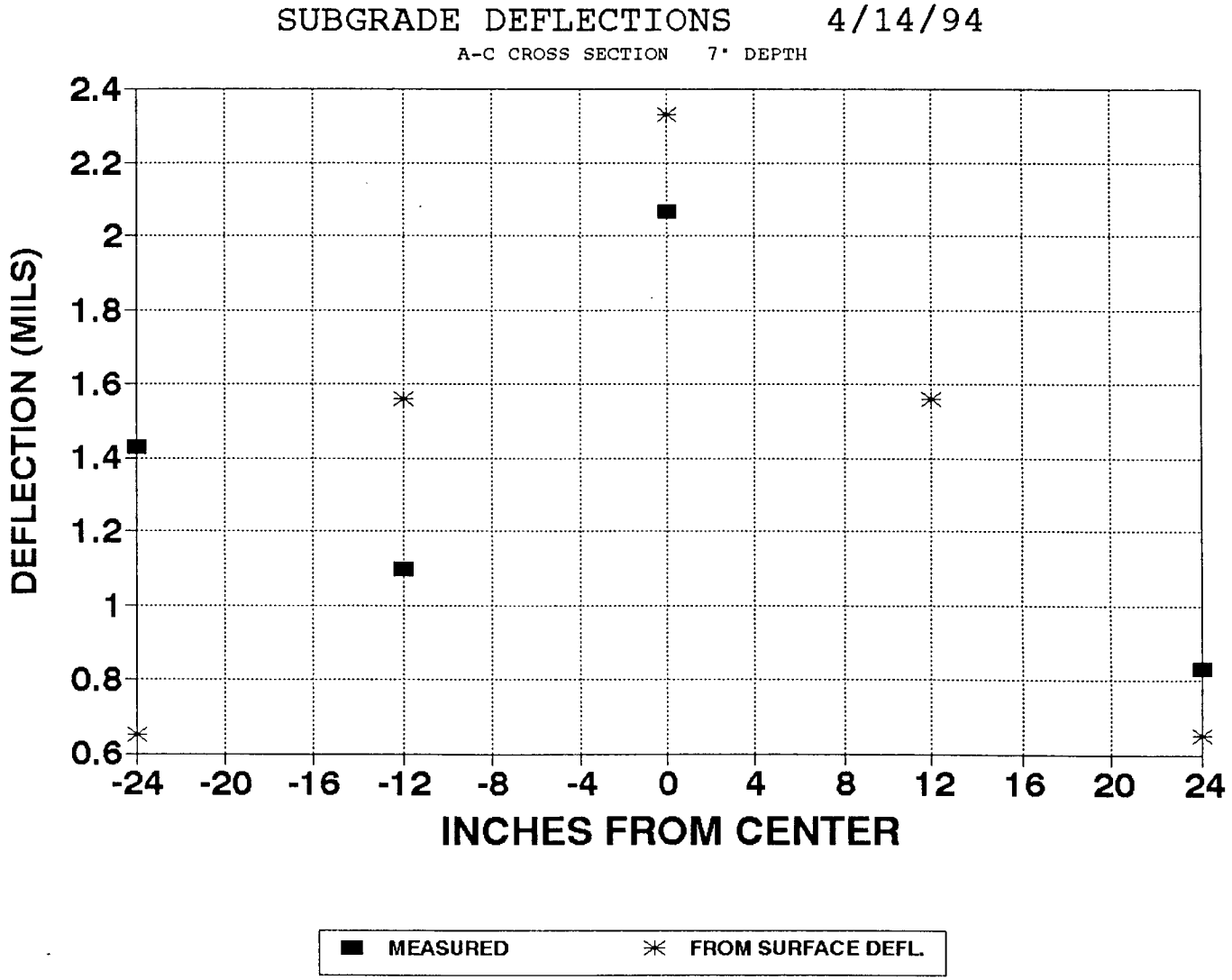
SUBGRADE DEFLECTIONS 4/14/94
A-C CROSS SECTION 7" DEPTH
DEFLECTION (MILS)
2.4
2.2
2
1.8
1.6
1.4
1.2
1
0.8
0.6
-24 -20 -16 -12 -8 -4 0 4 8 12 16 20 24
INCHES FROM CENTER
MEASURED
FROM SURFACE DEFL.

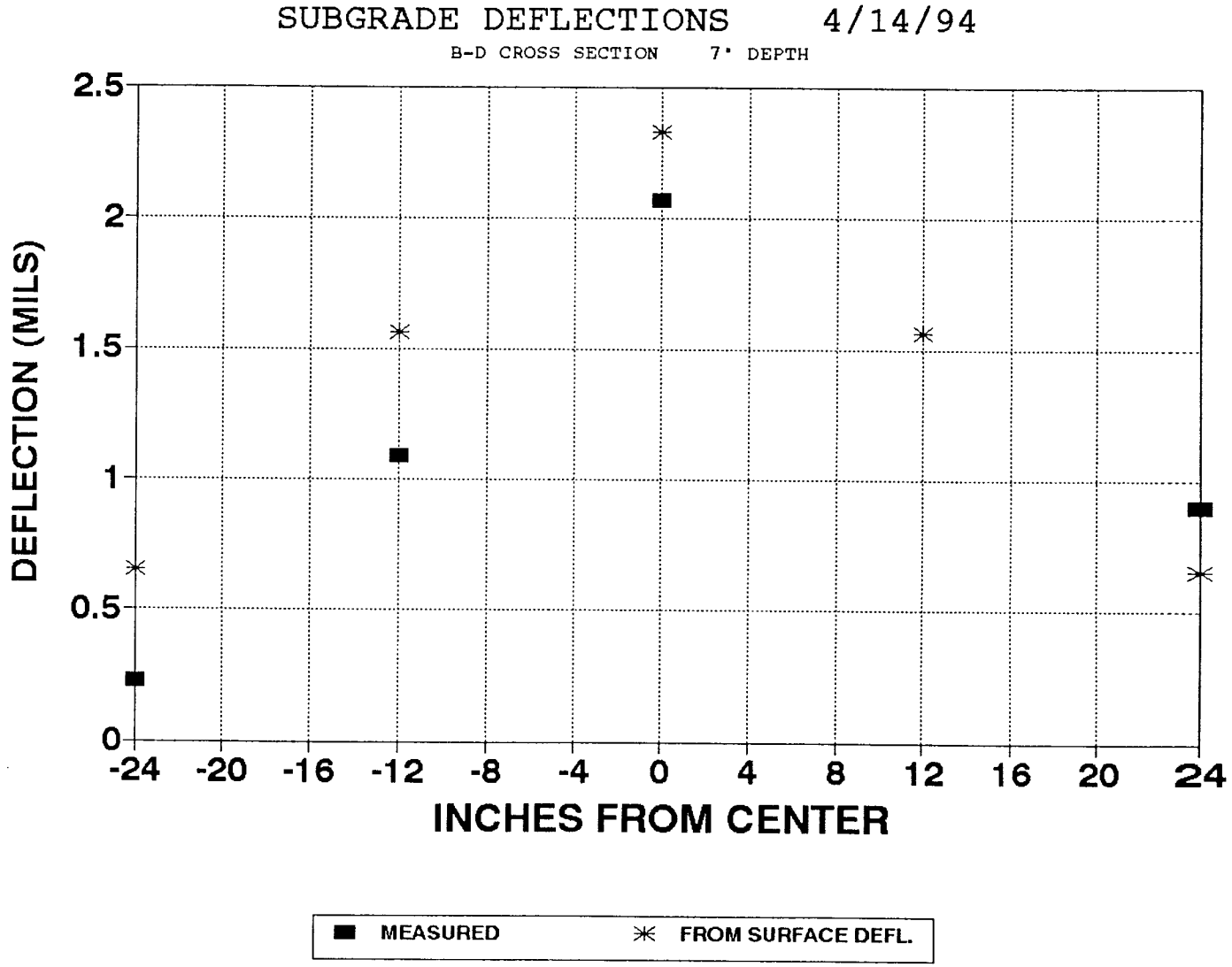
SUBGRADE DEFLECTIONS 4/14/94
B-D CROSS SECTION 7" DEPTH
DEFLECTION (MILS)
2.5
2
1.5
1
0.5
0
-24 -20 -16 -12 -8 -4 0 4 8 12 16 20 24
INCHES FROM CENTER
MEASURED
FROM SURFACE DEFL.

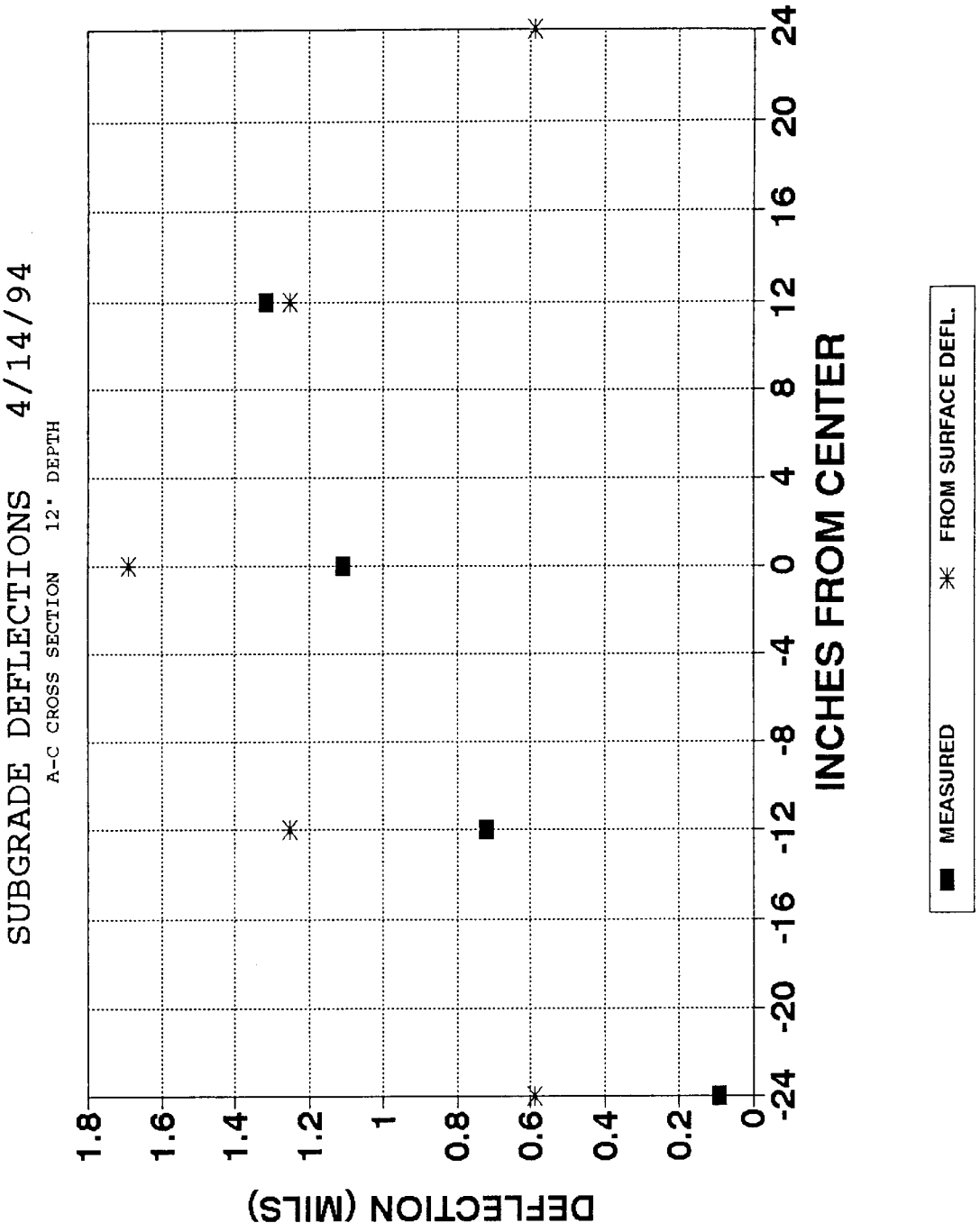
SUBGRADE DEFLECTIONS 4/14/94
A-C CROSS SECTION 12" DEPTH
DEFLECTION (MILS)
1.8
1.6
1.4
1.2
1
0.8
0.6
0.4
0.2
0
-24 -20 -16 -12 -8 -4 0 4 8 12 16 20 24
INCHES FROM CENTER
MEASURED
FROM SURFACE DEFL.

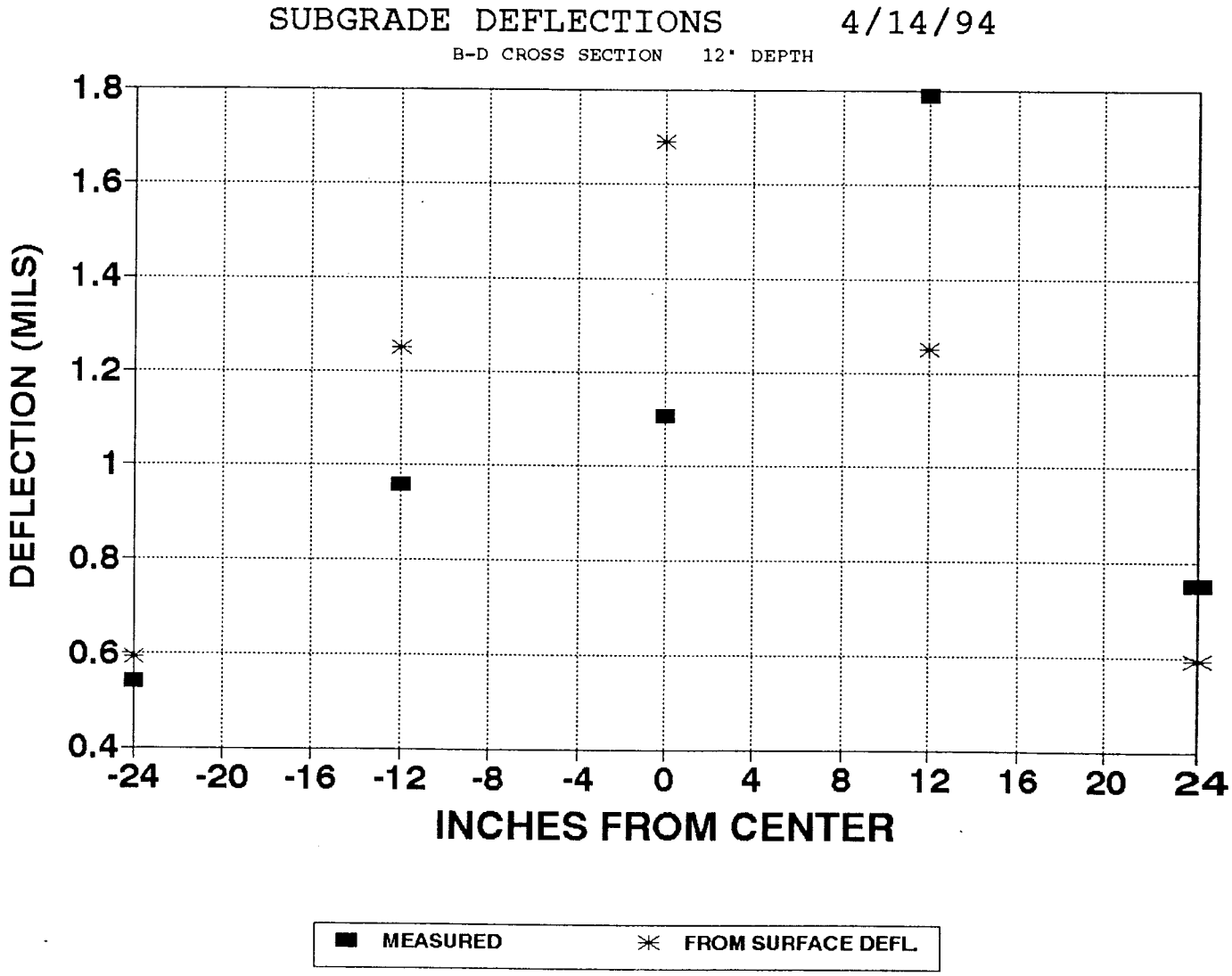
SUBGRADE DEFLECTIONS 4/14/94
B-D CROSS SECTION 12" DEPTH
DEFLECTION (MILS)
1.8
1.6
1.4
1.2
1
0.8
0.6
0.4
-24 -20 -16 -12 -8 -4 0 4 8 12 16 20 24
INCHES FROM CENTER
MEASURED
FROM SURFACE DEFL.

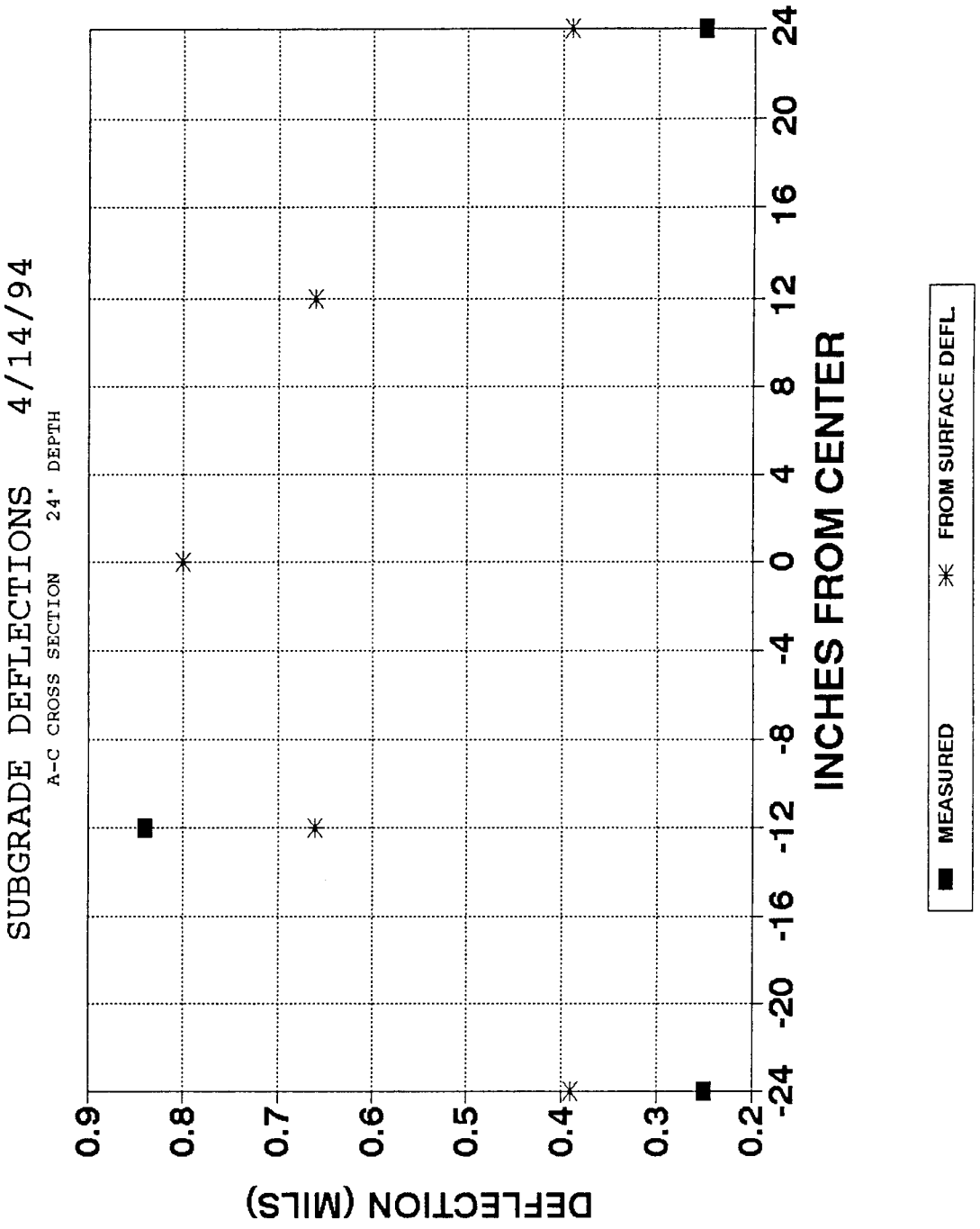
SUBGRADE DEFLECTIONS 4/14/94
A-C CROSS SECTION 24" DEPTH
DEFLECTION (MILS)
0.9
0.8
0.7
0.6
0.5
0.4
0.3
0.2
-24 -20 -16 -12 -8 -4 0 4 8 12 16 20 24
INCHES FROM CENTER
MEASURED
FROM SURFACE DEFL

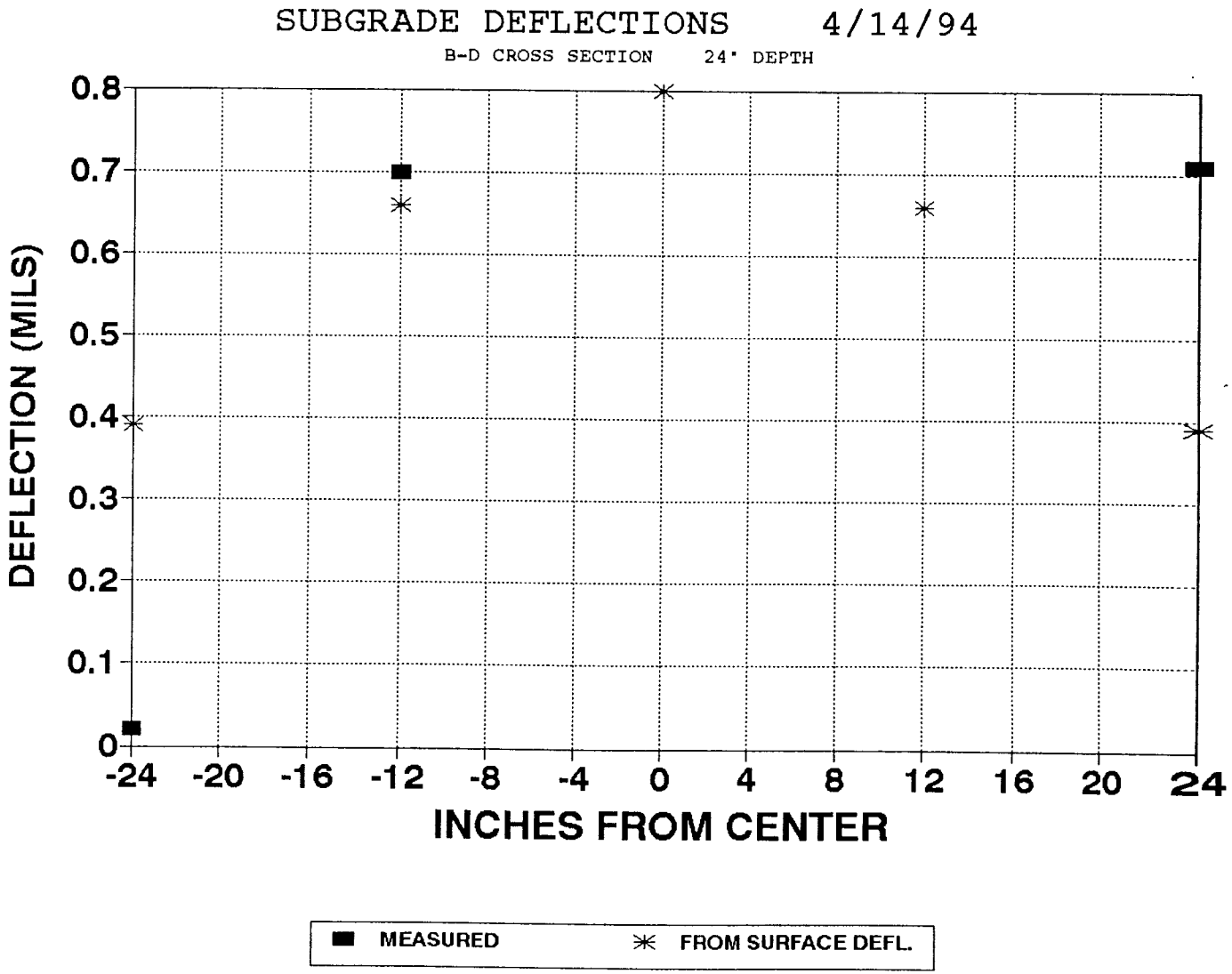
SUBGRADE DEFLECTIONS 4/14/94
B-D CROSS SECTION 24" DEPTH
DEFLECTION (MILS)
0.8
0.7
0.6
0.5
0.4
0.3
0.2
0.1
0
-24 -20 -16 -12 -8 -4 0 4 8 12 16 20 24
INCHES FROM CENTER
MEASURED
FROM SURFACE DEFL.

Appendix F

COPIES OF EXISTING/PROPOSED PUBLICATIONS

1993 FALL MEETING

American Geophysical Union

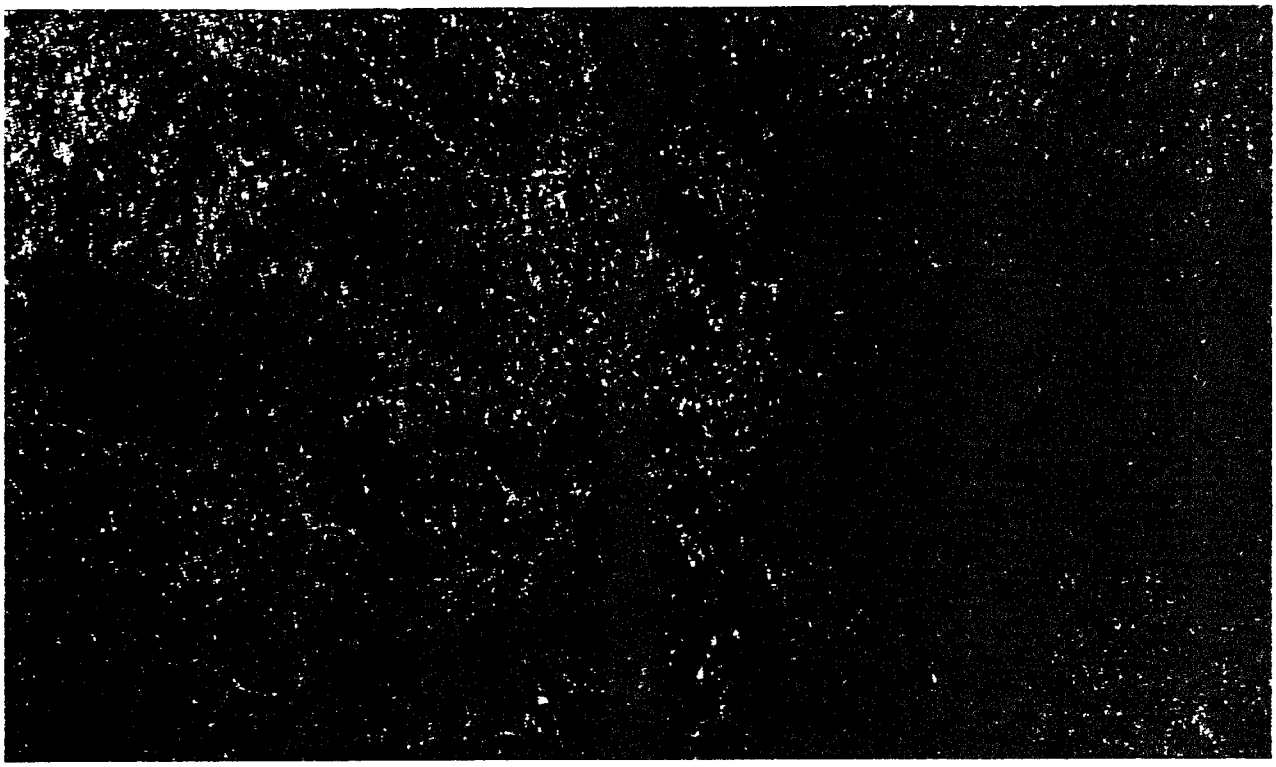

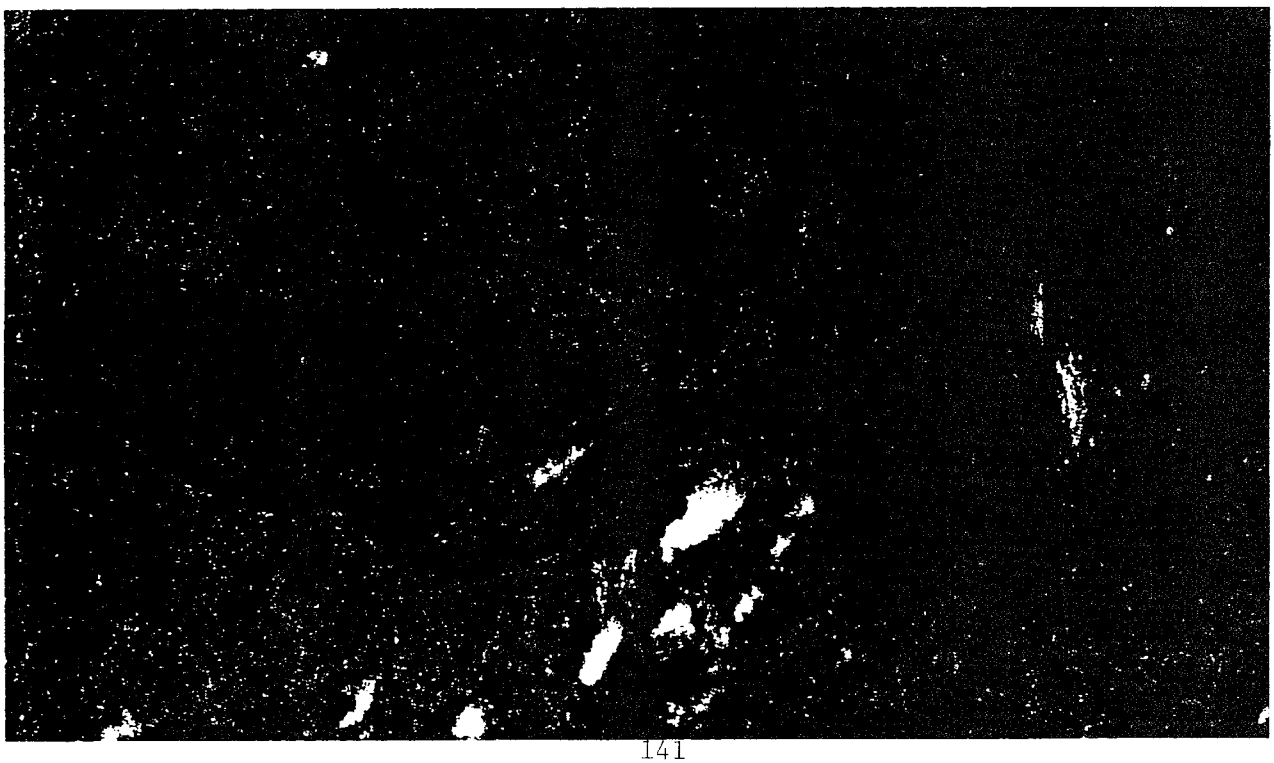

Published as a supplement to *Eos*, October 26, 1993

S21B-15 0830h POSTER

Seismic Tomography of Freezing and Thawing Soil

J L Williams, D I Doser, and M Baker (Department of Geological Sciences, University of Texas at El Paso, 79968-0555; 915-747-5501; e-mail: jwilliam@dillon.geo.ep.utexas.edu)
S Nazarian (Center for Geotechnical and Highway Materials Research, Department of Civil Engineering, University of Texas at El Paso, 79968-0516; 915-747-5464)

Seismic tomography is being applied in the laboratory to evaluate the extent of frozen soil layer formation. An instrumented 2.8 m^3 soil-filled tank is undergoing controlled freeze-thaw cycles, building a sequence of frozen and near-saturated layers within a characterized soil profile. The Center for Geotechnical and Highway Materials Research at the University of Texas at El Paso is studying the interaction of these variably frozen layers in order to determine soil response to dynamic loads.

The soil profile, similar to that present in areas affected by seasonal frost, can be modelled as a multi-layered system consisting of frozen, partially-frozen, and unfrozen water-saturated intervals. The tank is instrumented with forty-eight subsurface geophones, three electrical resistance probe columns, and fifteen thermocouples. Electrical resistance and temperature data are being collected as a means of assessing the tomographic results. A small, downhole seismic source produces both P and S waves. First-arrival times for varying source depths are determined for each geophone and are tomographically inverted using *apriori* slowness information to obtain the slowness distribution within the soil volume.

The resulting slowness distribution allows inference of frozen/thawed soil layering. The response of this system to dynamic loads is complicated due to extreme differences in rigidity of the various soil layers. Accurate determination of frozen layer thickness is critical to proper back-calculation of soil elastic moduli by multi-layer modelling programs.

BOISE STATE UNIVERSITY • 1910 UNIVERSITY DRIVE • BOISE, IDAHO 83725

CENTER FOR GEOPHYSICAL INVESTIGATION OF THE SHALLOW SUBSURFACE

TELEPHONE (208) 385-1419
FAX (208) 385-4061

17 January 1995

Dr. Soheil Nazarian
University of Texas
El Paso, TX 79968

Dear Dr. Nazarian,

This is letter is to confirm that we have received your abstract for the 1996 ASCE Geophysical Case Histories Session scheduled for Washington D.C.

We will be sending you instructions for authors later this year (March, 1995). The format will probably be similar to that of the Journal for Geotechnical Engineering. Papers will be due at the end of the summer, 1995. Peer review and final revisions will be completed by the end of June, 1996, to allow time for publication of the paperback proceedings volume.

Thank you for contributing an abstract. I look forward to seeing your paper later this year.

Respectfully yours,

Paul Michaels
Assistant Professor, BSU

Pavement Evaluation with Seismic Tomographic Imaging

S. Nazarian, D.I. Doser and K. Dhanasekharan
Center for Geotechnical and Highway Materials Research
The University of Texas at El Paso
El Paso, TX 79968

A desirable pavement design methodology should be based on an appropriate theoretical model which accurately predicts the behavior of a pavement structure. Even though numerous approaches are proposed, solutions based upon the elastic theory are generally adopted. Monitoring changes in material properties of different layers is also quite important. The most important parameters used in the design and monitoring of pavements are the elastic moduli of different layers. Nondestructive testing (NDT) techniques are typically utilized to determine the moduli.

The most common techniques used to determine pavement moduli are the deflection-based NDT methods. These methods typically encounter problems with predicting the moduli of pavement layers (i.e. base and asphalt layers), especially when they are thin.

The main objectives of the case study presented here are (1) to verify the accuracy of a deflection-based NDT device in predicting the deformations within a pavement section, and (2) to evaluate the feasibility of seismic tomographic imaging as a pavement evaluation tool.

A series of velocity transducers (geophones) were embedded within an existing pavement section to a depth of 1.6 m. For tomographic imaging, seismic records were collected using a borehole located 0.9 m from the receiver boreholes. Data were collected at 50-mm intervals to a depth of 1.6 m.

A Falling-Weight Deflectometer (FWD) was also used to determine the deformation of the pavement at different distances from the load, using the same buried geophones. Moduli were also determined using the SASW, downhole seismic, and crosshole seismic methods.

In the paper, the accuracy of the deflection-based NDT device, the feasibility of the tomographic method, and the adequacy of the other seismic methods are discussed. The advantages and disadvantages of each method are also included. The paper may provide a practical guideline for the use of each method.